THE CONSTRUCTION OF A LARGE MACH - ZEHNDER INTERFEROMETER AND ITS APPLICATION TO THE STUDY OF GAS / LIQUID TRANSFER PROCESSES.

A thesis submitted to the University of London for the Degree of Ph.D. in the Faculty of Engineering (Chemical Engineering)

by

ROGER KENNETH MAXWELL JOHNSTONE B.Sc.(Eng.), A.C.G.I..

Department of Chemical Engineering,

Imperial College of Science and Technology,

London, S.W.7.

February, 1964

ERRATA

p.37. Line 29 for 'increases' read 'decreases'

p.50 line 24 for 'cell' read 'fluid'

p.94 line 26 read trace speed in 'cms/sec' .

p.111 equation 8.1 the integral should contain the term

$$e^{-x^2/4k\tau}$$

p.114 line 13 insert 'coefficient' after 'condensation'

p.116 line 18. insert 'with increase in mass transfer rate and when the rate began to decrease' after 'decreased' .

ABSTRACT.

A Mach - Zehnder interferometer with 200 mm. mirrors has been designed and constructed for the study of refractive index fields. The instrument can accommodate large test-sections and is mounted on a sprung cradle to isolate it from any external vibration.

Transient heat transfer phenomena occuring during evaporation and condensation in liquid vapour systems were studied, using the inferometer to measure the temperature gradients existing adjacent to the surface. From these results values of the condensation coefficient were calculated for propyl alcohol, pure water and water with involatile contaminants. For all systems studied the calculated values of the coefficient were found to decrease as the rate of condensation increases and it was considered that this effect cannot wholly be attributed to the small quantities of air sometimes present near the liquid surface.

Coefficients obtained for water during condensation were of the same order as those measured by other workers studying evaporation. Traces of sodium lauryl sulphate, a surface active agent, reduced the coefficient by a factor of about 3; a similar reduction was found for a normal solution of sodium chloride. Coefficients for propyl alcohol were less than those for water by a factor of 20. Evaporation and condensation yielded similar coefficients for all systems.

ACKNOWLEDGEMENTS.

The author wishes to thank Professor D.M. Newitt and Dr. W. Smith for their supervision of this work; especially to Dr. Smith for his criticisms and continual encouragement.

Numerous helpful discussions with my friends at college are gratefully acknowledged.

Thanks are also due to Mr. J. Oakley and the workshop staff who aided in the construction of the apparatus.

The author would like to thank D.S.I.R. for a maintenance grant and an equipment grant for the construction of the interferometer.

CONTENTS.

NOMENCLATURE.

PART A. INTERFEROMETERY.

b = fringe spacing (cms.).

d = deflection of a vibration isolator (feet).

D = geometric length of cell (cms).

f = exciting frequency (cps).

f_n = natural frequency (cps).

F = focal length of the collimating element (cms).

l = optical path difference (cms).

M = number of fringes.

M_1, M_2 = interferometer mirrors.

P = difference in glass thickness (cms).

r' = equivalent source radius (cms).

S_1, S_2 = interferometer splitters.

T_f = Force transmissibility.

T_d = Displacement transmissibility

$u,v,w.$ = co-ordinate system axes.

x = image diameter (cms).

$x,y,z.$; $x',y',z'.$ = co-ordinates of points in space.

α = angle of intersection of two light rays (radians).

ϑ = included angle of M - Z interferometer parallelogram.

λ = wavelength of light.

μ = refractive index.

ϕ = angle between the light beam and liquid surface.

PART B. MASS TRANSFER.

a_n = a constant in the half power series.

b_n = a constant in the half power series.

c = specific heat (cals/gram. ^{o}K).

$\bar{c}$ = average velocity of vapour molecules (cms/sec).

D = geometrical length of cell (cms).

f_n = a constant as defined by equation 6.18..

F = surface area of the sample (cm^2)

H = heat given up per mole of condensed vapour (cals/mole).

I = a constant in the equation $x = 2I\sqrt{K\vartheta}$.

K = $k/c.\rho$ for the liquid phase.

L = latent heat of vapour (cals/gram).

M = molecular weight (grams/gram mole).

n = molecular density of gas phase (moles/cm^3).

r_s = molecular density of gas phase at equilibrium conditions (moles/cm^3).

N = mass transfer (moles/cm^2.sec).

$\bar{N}$ = net rate of mass transfer (moles/cm^2.sec).

p = pressure in the vapour space.

p_s = equilibrium vapour pressure at the surface temperature.

R = gas constant (ergs/mole. ^{o}K).

R' = $K^{\frac{1}{2}}.\gamma.\pi^{-\frac{1}{2}}$.

T_s = liquid surface temperature (^{o}C).

T_v = temperature of the vapour (^{o}C).

T' = change in temperature from time zero $(T - T_o)$ ^{o}C.

T^{*} = temperature of the vapour at which the saturation pressure is equal to p (^{o}C).

V = vapour volume (cm^3).

x = distance from the interface (cms).

y = $(\vartheta - \tau)$ secs.

α = condensation coefficient.

$\dot{\alpha}$ = point value of the condensation coefficient at time $\vartheta = \vartheta$.

$\bar{\alpha}$ = average value of the condensation coefficient over the time interval $\vartheta = 0$ to $\vartheta = \vartheta$.

β' = gradient of the vapour pressure temperature curve.

γ = $\alpha . \phi . \beta . H / k$.

ϵ = a small time interval (secs).

ϑ = time (secs).

λ = wave length (cms).

μ = refractive index.

ρ = density (grams/cm^3).

τ = time (secs).

ϕ = $(2 . \pi . R . M . T)^{-\frac{1}{2}}$

ψ = $\Delta T(y) . (\vartheta - y)^{-\frac{1}{2}}$

Subscripts.

e = evaporation.

c = condensation.

v = vapour.

L = liquid.

o = value at zero time.

n = corresponding to the nth term of the series.

CHAPTER 1.

INTRODUCTION.

The work described in this thesis had two objects. First, it was desired to construct a general purpose instrument by means of which the interfacial behaviour of heat and mass transfer processes could be studied in detail with quantitative accuracy. For this purpose, a Mach - Zehnder interferometer with a high sensitivity, a wide field of view and adequate working space was designed and built.

Changes in chemical and physical properties of fluids are frequently accompanied by proportionate changes in refractive index. The extensive application of refractive index measurement has, until recent years, been restricted to purity determinations and to the evaluation of density fields in aerodynamics. Optical measuring techniques are indirect and produce contour maps of refractive index over a field of view in a plane perpendicular to the light beam. No physical probes are required and measurements can be made close to an interface.

Three optical phenomena, which are dependent upon refractive index variation, have been used to study variations in system properties of gases and liquids:

1. Schlieren.
2. Shadow effects.
3. Interference.

of these interferometery is the least sensitive, and shadow effects the most sensitive, to changes in refractive index.

Weinberg[80] and Holder and North[36] have discussed the relative importance of these techniques and their applications in the fields of combustion and aerodynamics, but only infrequent references occur to their use in the study of heat or mass transfer. Schlieren and shadow effects are primarily intended to

present a visualization of the refractive index gradients but do not readily permit quantitative studies. The simplest Schlieren system, a knife edge placed at the focal point of a beam after passage through a refractive index field, has been used by Goltz and Sawistowski[25] to study interfacial turbulence during liquid - liquid mass transfer. The structure of flames and shock waves has been investigated using Schlieren and shadowgraphy[22,55]. In shadowgraphs patterns are produced by redistribution of light intensity in a refractive index field, owing to ray deflections. The essential feature of shadowgraphy, as distinct from schlieren methods, is that the receptor is not optically conjugate with the test section.

Interferometery is the only optical technique which is directly quantitative, but the optical equipment is usually more complex. The number of fringe shifts on the interferogram is related directly to the refractive index change along the light path. It should be emphasised that all measurements made by interferometery are of changes in system properties and must be related to an independent determination at one point if absolute values are required.

In any experiment it is preferable that the refractive index variations can be attributed to the change in only a single property, or that the effects of two properties differ in magnitude (e.g. for water the refractive index coefficients are $82.5 \times 10^{-6}/^{\circ}C$ and 14.65×10^{-6}/atm. for temperature and pressure respectively.)

In particular cases the effect of one variable may be determined independently (a blank determination) and the appropriate corrections made when variations of both properties occur simultaneously; this technique is seldom practicable.

Three properties which have been measured by interferometery are:

1. pressure - in the study of flow past aerofoils and turbine blades[71].

2. temperature - in combustion processes and heat transfer problems[56,67].
3. concentration - in the determination of diffusion coefficients and solute concentrations adjacent to crystal faces[70].

Many different interferometers have been used in these studies and their comparative merits are discussed in art. 2.6..

It is desirable for the purpose of investigating heat and mass transfer that the interferometer is capable of measuring time - transient, refractive index gradients; in particular, those occuring during the evaporation and condensation of fluids. The refractive index variation caused by the pressure changes in the vapour will be negligible for pure fluids, or fluids with relatively involatile solutes; the interferograms will be directly temperature profiles. The rate of mass transfer across the interface will be proportional to the rate of heat transfer in to the liquid and, from a consideration of driving force, a mass transfer coefficient may be calculated which is called the 'condensation coefficient'. This coefficient has been measured by many workers[44] for evaporation in liquid - vapour systems but only Harvey[29] has studied condensation. In his apparatus variable air-water vapour ratios were used and no account was taken of temperature changes in the air caused by adiabatic pressure changes. The coefficient for water evaporation has been measured by many workers[44], it has been related to the ambient temperature by Delaney[16] but its dependence upon the rate of mass transfer as noticed in the present work has not been recognized.

CHAPTER 2.
THEORY OF INTERFEROMETRY

2.1. Formation of Interference Patterns.

Light interference patterns are readily interpreted in the terms of the wave theory of light. Briefly, the theory is as follows.

If two wave trains, of equal wavelength and amplitude, intersect at an angle α as shown in fig. 2.1., the net intensity of light observed will be the algebraic sum of the intensities caused by each separate wave. At points along BB' the peaks of the waves reinforce giving a region of high intensity, whilst along AA' a maximum in one wave corresponds to a minimum in the other giving a region of zero intensity. This system repeats itself at regular intervals across the place of intersection, the size of the interval being a function of the angle of intersection. The intensity profile which results is shown below fig 2.1. In three dimensions, if there are no refractive index gradients in either beam prior to the plane of intersection, the pattern observed will be a series of bright, parallel, straight lines on a dark background; these are called wedge fringes. The intensity of light in the plane of the fringes varies sinusoidally in a direction normal to the fringes. Thus the dark fringes appear narrower than the light because the intensity can never be less than zero. The term 'interference' is misleading, for this phenomena depends upon superposition and implies the absolute independence of the two wave trains which together form an interference pattern. The experiments of Ebert[19] showed that one bright beam, however intense, has no effect on another crossing its path.

2.2. Conditions for Interference

There are several conditions which must be satisfied by an experimental apparatus for it to produce observable interference.

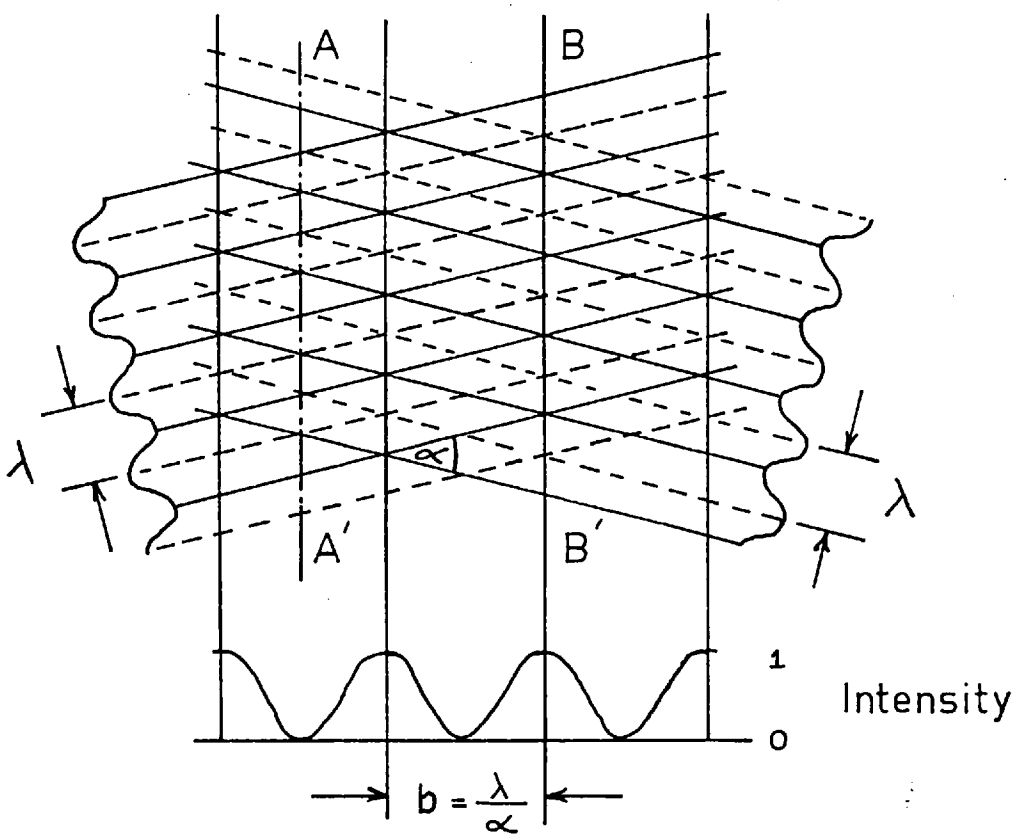

FIG 2.1. FRINGE FORMATION AND SPACING

These are:-

1) The light in the two wave trains, which combine to give interference, must come from the same source.
2) Unless the light is monochromatic, the optical path difference between the beams must be small.
3) The angle of intersection between the emergent beams must be small.
4) If the light is polarised, the emergent beams must be in the same plane of polarization.

The first condition is a practical consequence of the nature of light; most nearly monochromatic sources radiate an unbroken train of waves for about 10^{-8} secs. after which another train will be emitted which will bear no definite phase relationship to the former. The probability of any other atom or molecule giving rise to an identical wave train is very small. In view of the comparitively long period required to record experimental effects, interference may be observed only when the beams originate from a common source.

The second condition is a result of the destructive interference which occurs between the various wavelengths present in light sources which are not monochromatic. Consider two wave trains W_1 and W_2 from the same source, each consisting of two wave lengths λ_1 and λ_2 intersecting at a small angle α and advancing towards the right as in fig. 2.2. The optical path difference from the source to the position A is zero, and at position A reinforcement will take place for all wave lengths, as illustrated by the dotted and continuous waves in fig. 2.2. At a position B, where there is a path difference of $\frac{\lambda_1}{2}$, the continuous waves are exactly out of phase, whereas the dotted waves are seen to reinforce each other to a limited extent. At position C the dotted waves are almost out of phase whereas the continuous waves reinforce; this corresponds to a path difference of λ_1. As may be seen fringes caused by more than one wavelength mask the clarity of those caused by a single wavelength. Two cases of masking are worthy of note:-

FIG.No.2.2. FRINGE MASKING.

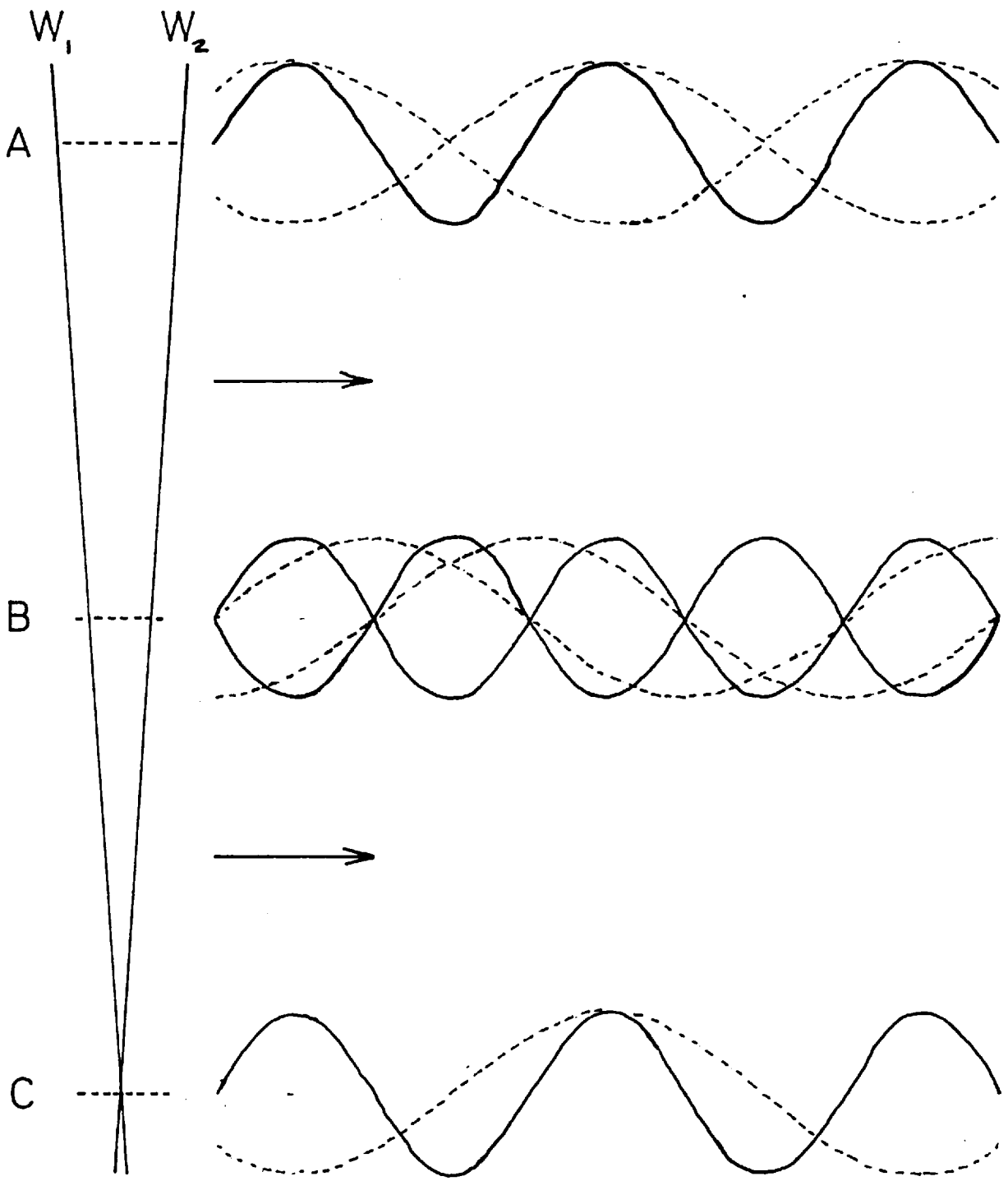

1) If the spectrum of the source contains two or three predominant wavelengths, the fringes will be of a maximum contrast at the position of zero path difference and at all other positions where the path difference is an integral number of each of the major wavelengths. In the fringe pattern for mercury light this phenomena is especially noticable; it gives rise to 'beats'.
2) The extreme case of masking occurs in the fringe pattern for white light in which only one high contrast fringe is visible. The remainder are coloured, and the degree of dispersion increases with distance from the central fringe. Masking is so acute that only about 10 fringes can be detected.

The third condition applies rather to the observation than to the production of the fringes and is illustrated by fig 2.3.. Two plane wave trains from the same source cross each other at angles α_1 in fig. 2.3.a. and α_2 in fig 2.3.b. (the convention the same as in fig 2.1.). It is seen that the fringe spacing decreases with increase in α. If α is large the fringe spacing will be too small for the fringes to be detected, even under high magnification e.g. for the meroury green line in air a fringe spacing of only 0.01 cm. is given for $\alpha = 0.31$. At the other limit, if α is zero, the fringe spacing will be infinite and one fringe will cover the field of view.

The fourth condition stipulates that, if the original beam is plane polarized and is passed through a doubly refracting medium, the emergent beam must be analysed on a common azimuth before interference patterns will be visible.

2.3. Relation Between Fringe Pattern and Path Difference Variation

Consider light from a source (co-ordinates x',y',z') travelling along two paths and intersecting at a point x,y,z. The optical path will, in general, depend upon all these co-ordinates. If the intensity from a source of unit volume

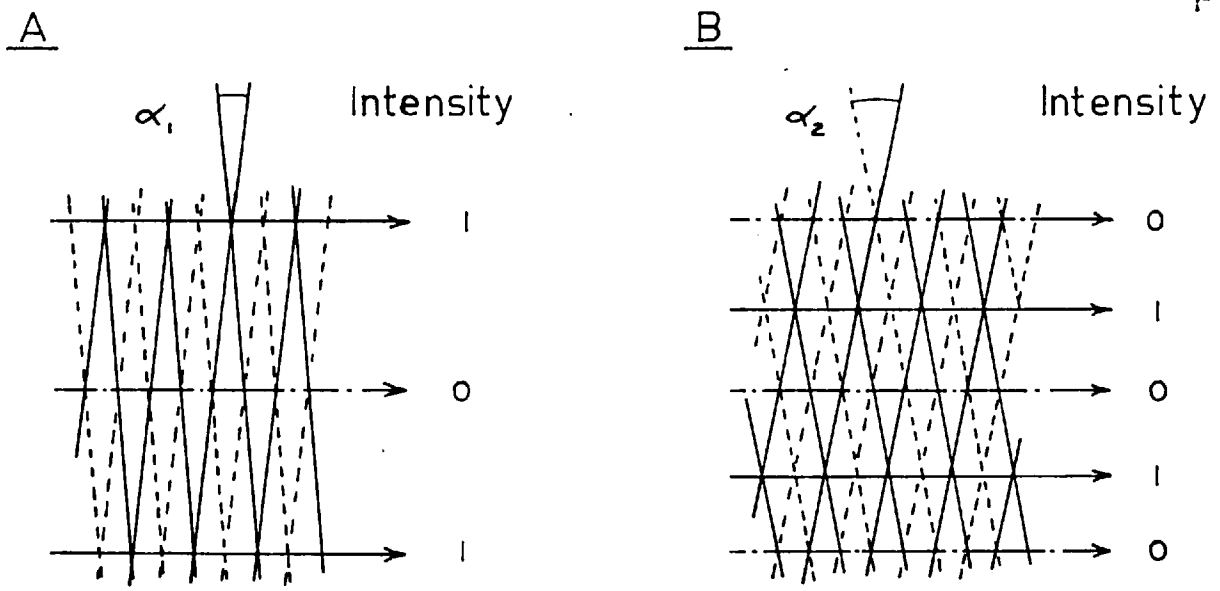

FIG.2.3.RELATION BETWEEN ANGLE OF INTERSECTION AND FRINGE SPACING.

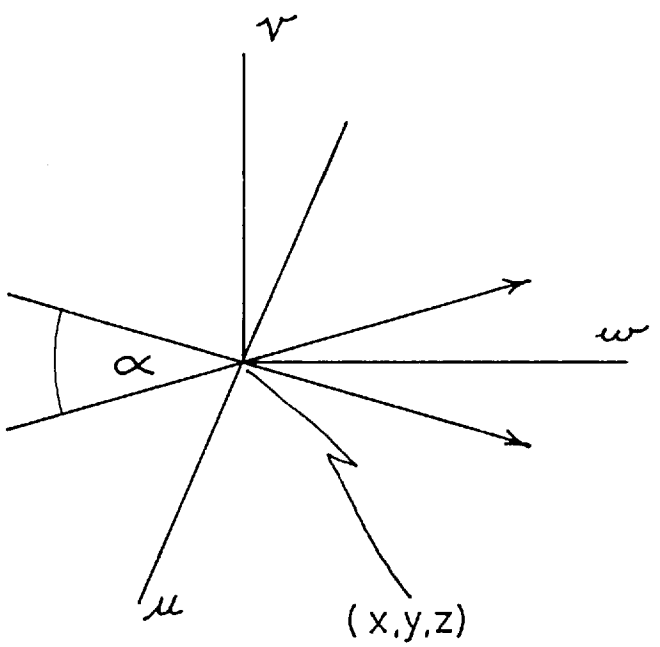

FIG.2.4. RECTANGULAR AXES.

arriving at x,y,z, via each path is 'i', the total intensity is

$$I(x,y,z) = \int 4i \cos^2 \frac{\pi l}{\lambda} \, dx'dy'dz' \qquad (2.1.)$$

With a small source of dimensions $\delta x', \delta y', \delta z'$, such that

$$\frac{\delta l}{\delta x'} \cdot \delta x' \ll \lambda$$

and if the total intensity via each path separately is I_o,

$$I(x,y,z) = 4 I_o \cos^2 \frac{\pi l}{\lambda} \qquad (2.2.)$$

The intensity is a maximum on surfaceswhere the path difference is an integral number of wavelengths; these surfaces correspond to bright fringes. Similarly dark fringes occur where the path difference is an odd number of half wavelengths. Since the fringes are surfaces of constant path difference the gradient of the path difference l is normal to the fringes. Between two consecutive fringes the path difference changes by λ. Hence the spacing between two fringes b is given by

$$b.\text{grad } l = \lambda \qquad (2.3.)$$

2.4. Relationship Between Fringe Pattern and Inclination of Wave Fronts.

Consider two rays which intersect at an angle α at the point (x,y,z) as shown in fig. 2.4.. Draw rectangular axes through this point. Axis w to be along the bisector of angle α,and μ to be in the same plane but perpendicular to w. v is then normal to μ and w. The path lengths of the two rays are l_1 and l_2.

By inspection

$$\frac{\delta l_1}{\delta v} = \frac{\delta l_2}{\delta v} = 0 \qquad (2.4.)$$

$$\frac{\delta l_1}{\delta w} = \frac{\delta l_2}{\delta w} = \mu \cos \alpha/2 \qquad (2.5.)$$

$$\frac{\delta l_1}{\delta u} = -\frac{\delta l_2}{\delta u} = \mu \sin \alpha/2 \qquad (2.6.)$$

Hence as

$$l = l_1 - l_2 \qquad (2.7.)$$

$$\frac{\delta l}{\delta v} = \frac{\delta l}{\delta w} = 0 \qquad (2.8.)$$

$$\frac{\delta l}{\delta u} = \text{grad.} l = 2\mu \sin \alpha/2 \qquad (2.9.)$$

Equation (2.8.) shows that the fringe passing through (x,y,z) lies in a plane perpendicular to that of the two rays and that the rays are incident on the fringe at equal angles but on opposite sides. From equation (2.3.) and (2.9.)

$$2\mu\, b \sin \alpha/2 = \lambda \qquad (2.10.)$$

As α is small, $b = \frac{\lambda}{\mu\alpha}$

In a given application with a light source of known wavelength λ, the spacing depends solely upon the angle of intersection of the emergent beams.

2.5. Limitations Placed by Dispersion.

Tanner[72] gives a method of estimating the maximum difference in the thickness of glass plates, placed in each of the two beams, which can be allowed before dispersion markedly reduces the contrast of the central fringe. He states that a reasonable limit for dispersion is when the number of fringes caused by dispersion becomes comparable with the number obtained in the absence of dispersion; that is

$$M^2 = P.\lambda.\frac{\delta^2\mu}{\delta\lambda^2} \qquad (2.12.)$$

where M = number of fringes in the absence of dispersion, and
P = difference in glass thickness.

For crown optical glass at λ = 5461, the Mercury Green Line,

$$\frac{\delta^2\mu}{\delta\lambda^2} = 3.48 \times 10^7 \text{ cm}^{-2}$$

Hence $$P = 2.07 \times 10^{-4} \times M^2 \text{ in.} \qquad (2.13.)$$

Thus, if it is required to identify the unique central fringe for white light, for which M is about 5, the difference in glass thickness = 5.10^{-3} in.. This limit is easy to attain in practice, whereas that given by Tanner of $1.6\ 10^{-3}$ in. would require much closer tolerance in the size of splitters and of optical flats. If fluids with $\mu > 1$ are to be used in the cells it should be noted that it is the difference in thickness of the two glass plates with their fluid contents which must be less than the calculated limit.

2.6. Types of Interferometer.

All instruments which are designed to produce interference phenomena are called 'Interferometers' and they may be classified in two main groups, namely those which depend upon

a) Division of Wavefront,

b) Division of amplitude.

In both cases all the conditions for interference previously discussed must be satisfied.

a) Instruments in this group are those which, by any optical effect, change the direction of two parts of a wave front, so that they intersect at a small angle in the desired plane. All interferometers of this type require either a point source or a narrow slit parallel to the intersection of the two wave fronts. If too wide a slit is used the wave fronts will not be identical and a clear interference pattern will not be seen. The best known example of this class is the apparatus of Young[85] in which the division is achieved by two adjacent slits both receiving light from a single source. Other common examples are the Fresnel Biprism[23], Lloyds Mirror[49], and the Rayleigh interferometer[63].

b) Instruments of this type divide the primary beam into two secondery beams of approximately equal amplitude, which subsequently intersect at a small angle to form an interference pattern. In most cases splitting is achieved

by partial reflection at a half-silvered mirror. With this method of division of the beam the same portion of the wave front is split and hence any irregularities will occur in both of the secondary beams. There is, therefore, no restriction upon the size or shape of the source which can be used with this type of instrument and this allows an extended source to be used which will give much brighter interference patterns. This kind of interference is commonly seen in thin films, for example soap bubbles. Examples of this group of interferometers are those of Jamin[39], Mach[53] and Michelson[57]. A further example of this type of instrument is the four grating interferometer of Weinberg and Wood[79], which is geometrically similar to a Mach - Zehnder. The use of gratings instead of plates effects a large reduction in cost.

A further classification is sometimes made which subdivides these groups into those instruments with two and those with multiple secondary beams. Only two beam interferometers will be considered and the above examples are of this case.

It was decided to construct a Mach - Zehnder interferometer principally because it can be used to study a wide variety of problems involving both high and low speed phenomena. The main disadvantages of a Mach - Zehnder are its supposed difficulty in operation and its high initial cost. Previous experience has confirmed that in the past operating difficulties have been exagerated and cost was considerably reduced by constructing most of the instrument in the College workshops. The Weinberg - Wood interferometer is not suitable because of the limited available grating size and the wastage of light which would prevent high speed photography. The instrument is more suited to low speed phenomenon of small field of view.

2.7. A Mach - Zehnder Interferometer.

A Mach - Zehnder interferometer has four primary optical

components; the geometric arrangement is shown in fig. 2.5.. Two of the plates S_1 and S_2 are semi-reflecting whilst the others M_1 and M_2 reflect all the incident light. Light from a single source can pass through the instrument by two different paths, $S_1M_1S_2$ or $S_1M_2S_2$, and there will be two sets of emergent beams; one pair is along M_1S_2E which is termed the emergent beam and the other is along M_1S_2W which is termed the waste beam. Only the light in along M_1S_2E can be utilised and this reduces the efficiency of the system to a maximum of 50%, but the use of an extended source reduces this limitation. In most instruments the angle θ is taken as 60 or 90 degrees: further consideration is given to the choice of optimum angle in the design section on page 28.

Several analytical studies of the Mach - Zehnder optical system have been published since its increased use as a research tool in aerodynamics during and after the Second World War. Kinder[43] presented an historical survey of the development of the instrument together with a comprehensive biblography, but restricted his analytical studies to the conditions where $\vartheta = 45$ and for specific fringe orientations. Winkler[83] made the first complete survey of the subject and considered the effects of the various mirror movements and gave expressions for the limitations imposed by imperfections in the optical elements. Tanner[72] provides the most comprehensive of the analytical studies: he has collected together the results of many previous papers and has distinguished between those which are applicable to all two-beam systems and those which refer only to Mach - Zehnder instruments.

The principle optical properties of the Mach - Zehnder interferometer are:-

1) Only a small part of the source light is absorbed in the system and the emergent beam contains nearly 50% of the inlet light.
2) The dimensions of the parallelograms, at the corners of which the optical plates are arranged, can be chosen to give the required beam spacing, but must not be so large as

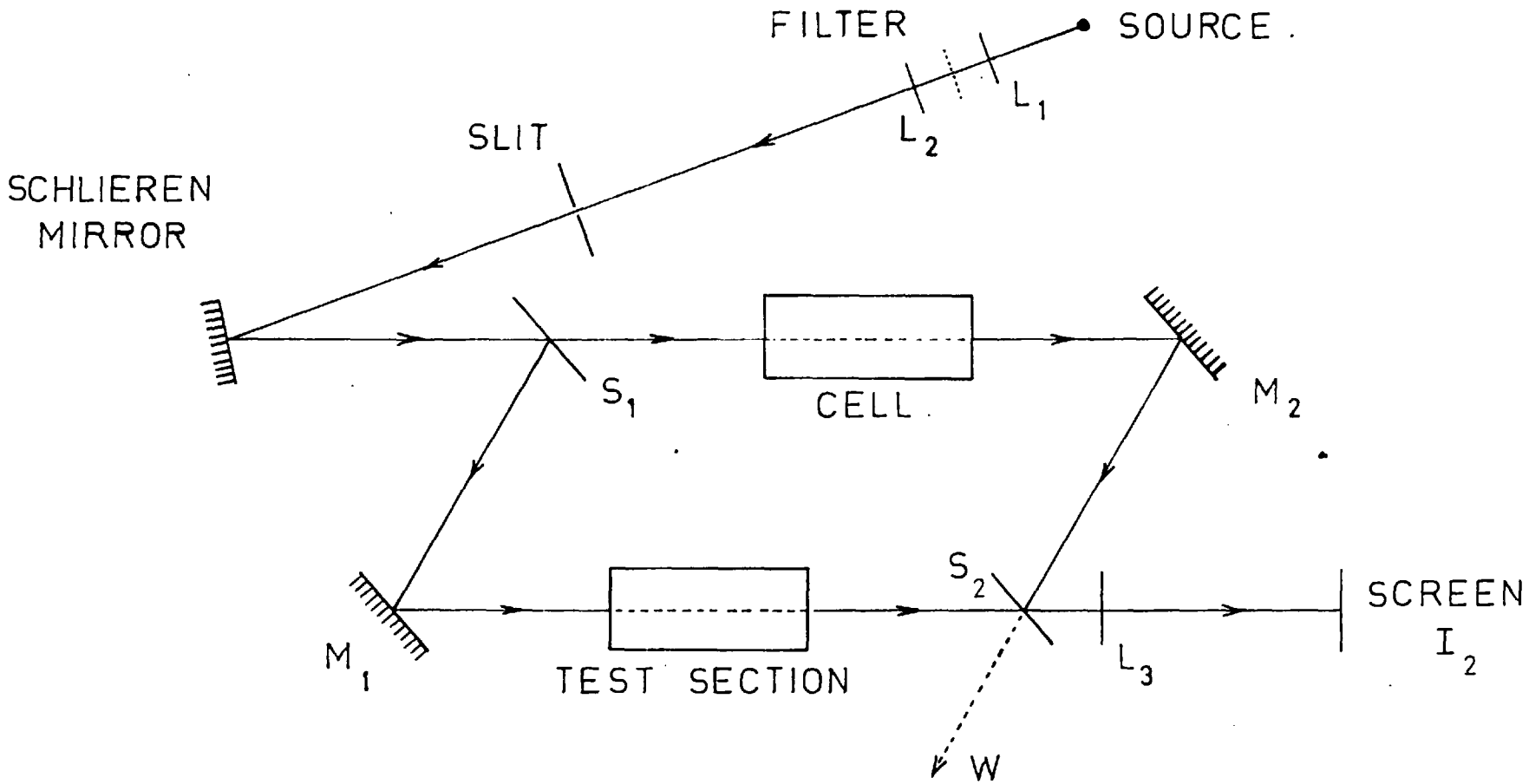

FIG. 2.5. THE MACH ZEHNDER INTERFEROMETER.

to reduce frame rigidity. Light passes only once through the test section and compensating cell.

3) The path difference may be adjusted to zero and therefore the number of fringes required can be a minimum and the intensity can be a maximum.

4) The instrument can be adjusted for usewith an extended source which can give sufficient light for the recording of high speed phenomena.

5) The instrument may be adjusted by altering the position of only the optical plates on the emergent side of the test-section and compensating cell, thus avoiding disturbing their alignment with the inlet beams.

It has been shown by Tanner[71] that for a parallelogram interferometer five fine adjustments are required. These are usually provided by

a) one plate being traversed, that is, moved perpendicular to itself.

b) the rotation of two of the optical plates about their horizontal axes.

c) the rotation of two of the optical plates about their vertical axes.

Alternatively two wedge-shaped compensating plates can be placed in one beam, as in the Lutz Interferometer, and these can be rotated relative to one another and tilted relative to the incident beam. This arrangement is sometimes favoured because it reduces the fine mirror adjustments required to one in the horizontal plane and one in the vertical plane plus a traversing motion. No compensating cell is needed but it requires an additional mechanism for fine adjustment and another pair of high quality optical components.

The interferometer is in correct adjustment when high contrast fringes of the desired spacing and location are in view. (A geometrical representation of the state of adjustment is given by Tanner[72].) This is equivalent to reducing the path difference

to zero for a particular wavelength and causing the beams to intersect virtually at an angle α in the plane of the cell.

As is seen from equation (2.10.) the fringe spacing is given by

$$b = \frac{\lambda}{\mu\alpha}$$

It is important when choosing the working mirrors, that is, those to which fine adjustments are fitted, to select those which alter angle of intersection and plane of intersection independently. If the working mirrors are chosen arbitarily it may be necessary to couple the adjustments of two mirrors in order to simplify the procedure.

CHAPTER 3.

INTERFEROMETER DESIGN.

The basic optical arrangement of the Mach - Zehnder interferometer, first devised in 1890 for studying air flow and ballistics[53,86], has remained unchanged, although in the details of design it is rare to find two instruments which are identical. Many designs are recorded[3,4,6,20,26,47], but there is little information on their relative merits or their cost. Although superior in many ways to other kinds of interferometer, a Mach - Zehnder is expensive to manufacture, and the instrument described here was for this reason designed so that it could be constructed by ourselves. As a result the cost of the instrument was much less than that of its commercial equivalent. Details are given in appendix A.6..

3.1. Selection of Working Mirrors and their Arrangement.

The detail design of the interferometer is determined by several criterea:-

1) Plane of parallelogram.
2) Angle of parallelogram.
3) Dimensions of mirrors.
4) Choice of working mirrors.
5) Size of parallelogram.

1) The plane of the interferometer is usually either vertical or horizontal. If the mirrors are arranged in the vertical plane, the floor space required is reduced but the control of the mirrors is complicated. The traversing mechanism must be designed so that the weight of the optical plate and its holder do not affect the movement in either direction; in addition the optical flats bend under their own weight and give curved fringes[26]. If the parallelogram is in the horizontal plane accessibility to all components is much improved and irregular shapes of cell can be accommodated more easily. A large instrument is more stable in this

plane and the mirrors do not distort under their own weight. It was decided to arrange the mirrors in the horizontal plane.

2) The apex angle of the parallelogram is equal to twice the angle of incidence of the light beams upon the optical plates. Tanner[71], in his analytical study, has calculated that the effect of imperfections in the optical flats decreases with decrease in angle of incidence. The severest restriction, that of the permissible wedge angles of the semi-reflecting plates, is relaxed by a factor of 1.86 with a decrease of angle of incidence from 45° to 30°. The ratio of useful field width to unit mirror width increases with decrease in angle of incidence but, for a given beam spacing, the path length increases with decrease in angle of incidence. It is important that the path length should not be too large because of the difficulty of designing a rigid structure: also the ease with which the instrument can be adjusted is inversely proportional to the path length. It was decided to use an angle of incidence of 30° which for a given minimum beam spacing of two feet gives a workable path length with not too strict optical tolerances.

3) For a circular mirror the field of view will be elliptical and the minor axis will be equal to 0.81 of the mirror width for an angle of incidence of 30°. Plates of 200 mm. diameter are used which after taking into account the area wasted by the plate retaining wing provide an elliptical field with a minor axis of 6". To ensure rigidity the plate thickness is 24 mm..

4) It was first noticed by Kinder[13] that if the distance from the focal plane of the test-section to S_2 is made the same as the distance from M_2 to S_2 (see fig. 2.5.), adjustment of the fringes is simplified. In this case, if the axes of rotation lie in the reflecting surface, rotation of M_2 varies the fringe spacing and orientation without changing the focal plane in which the fringes are localised. Fringe focussing is then

achieved by control of S_2 alone. Several other factors favour the choice of M_2 and S_2 for the working mirrors. If beam alignment with the test section and compensating cell is not to be upset when the instrument is adjusted the original settings of M_1 and S_1 must remain undisturbed. It was not considered that the complication and expense of fitting remote control to the mirrors was justified, hence all the adjustments must be within easy reach from a single position. Therefore the holders of M_2 and S_2 were designed so that each could be rotated about two perpendicular axes and a traversing mechanism was fitted to M_2.

5) The lengths of the parallelogram sides are chosen in the ratio of 2:1 in order to have the test section in the middle of the longer side. With a 2 foot separation of the beams and an angle of incidence of 30° this gives values of 4'6" and 2'3" for the parallelogram dimensions.

3.2. Specification of Optical Components.

It is essential that the fringes which are produced by the interferometer are of a sufficiently high contrast to facilitate accurate measurements from the photographic records obtained. Loss of contrast arises from three major causes:-

a) Masking by reflection of light from components of the apparatus and surrounding objects.
b) Inequality of light via the two paths.
c) Effects dependent upon the source size and optical component imperfections.

In addition, design of the plate adjustments must be such that lack of sensitivity does not restrict fringe contrast.

a) Reflections are reduced if the air-glass interfaces are coated. Adjustable irises in the inlet beam help to eliminate stray light and the light beams in the interferometer parallelogram are enclosed by tubes, coated internally

with optical black paint. These tubes serve also to exclude draughts and convection currents from the working beams: these may give shifts of the order of one fringe.

b) The effect of reflection ratio (the ratio of the light intensities of the two emergent beams from a splitter) upon fringe contrast has been investigated by Tanner[71]. He shows that if the beam splitters have the same reflection ratio there is little influence upon fringe contrast for ratio values of 0.25 - 0.75, but if the splitters have unequal reflection ratios the emergent beam intensities will differ and fringe contrast will be reduced. Normal optical procedures can ensure that the ratio will be 50 $\pm$ 2% and an identical coating on each splitter will give equal ratios.

c) The importance of optical component inperfections increases with increase in source size. Tanner[71] gives a method of estimating the effect of imperfections upon fringe contrast. He divides the imperfections into two groups; those which give a linear term and those which give a quadratic term in the source plane path variation.

The first group consists of wedge angles which exist in the light beams, that is, caused by the splitter faces and the cell windows not being parallel. These give rise to the most serious restrictions in the design and operation of the instrument; here we have allowed them to give a 5% reduction in fringe contrast. Using the following particular values:-

Angle of incidence of plates	60°
Refractive index of plates and windows	1.51
Thickness of plates	1.0 in.
Source wave length	5500° A
Source size	$2r'/F = 6.10^{-3}$

calculation shows that, for the pair of splitters, the optical thickness must not vary by more than $2.88\ 10^{-4}$ in. For the cell windows the tolerance is $1.05\ 10^{-3}$ in.. The tolerance placed upon beam splitter thickness is easily achieved by

standard optical workshop methods. The permissible restriction upon wedge angle of the cell optical plates is more difficult to satisfy and will be achieved in the present apparatus by making one optical flat in each of the cells adjustable with respect to the incident light beams (cell design art. 7.2.a.). The method of adjustment is described in art. 4.2.d..

The second group involve less severe restrictions and we have permitted a 2% reduction in fringe contrast. Using the same dimensions as above:-

The thickness of glass in the semi reflecting plates must not differ by more than 0.15 in. nor must their refractive indexes differ by more than 0.105. Likewise the sum of the glass thicknesses in the windows must not differ by more than 0.159 in. nor must their refractive indexes differ by more than 0.103.

The tolerances given here are much wider than those required to give a negligible dispersion as calculated in art. 2.5.a. and are therefore of no practical significance. The interferometer optical plates are of crown optical glass, manufactured by Bernhard Halle Hachft, of Berlin, and were specified to be plane parallel to within $\lambda/10$ in order to give straight parallel fringes. The surface coatings are of aluminium covered with a hard quartz layer to prevent abrasion of the surface.

3.3. Mirror Mounts and Adjustments.

The dimensions of the optical plates were fixed at 200 mm. dia. and 24 mm. thick; each weighs three kilograms. This load and the degree of rigidity required influence the choice of mount design. The traversing mechanism must be capable of adjustment to within one wavelength of light. For the sodium, mercury and white light sources which will be used with this instrument one

PLATE 3.1.. OVERALL VIEW OF THE MACH - ZEHNDER INTERFEROMETER.

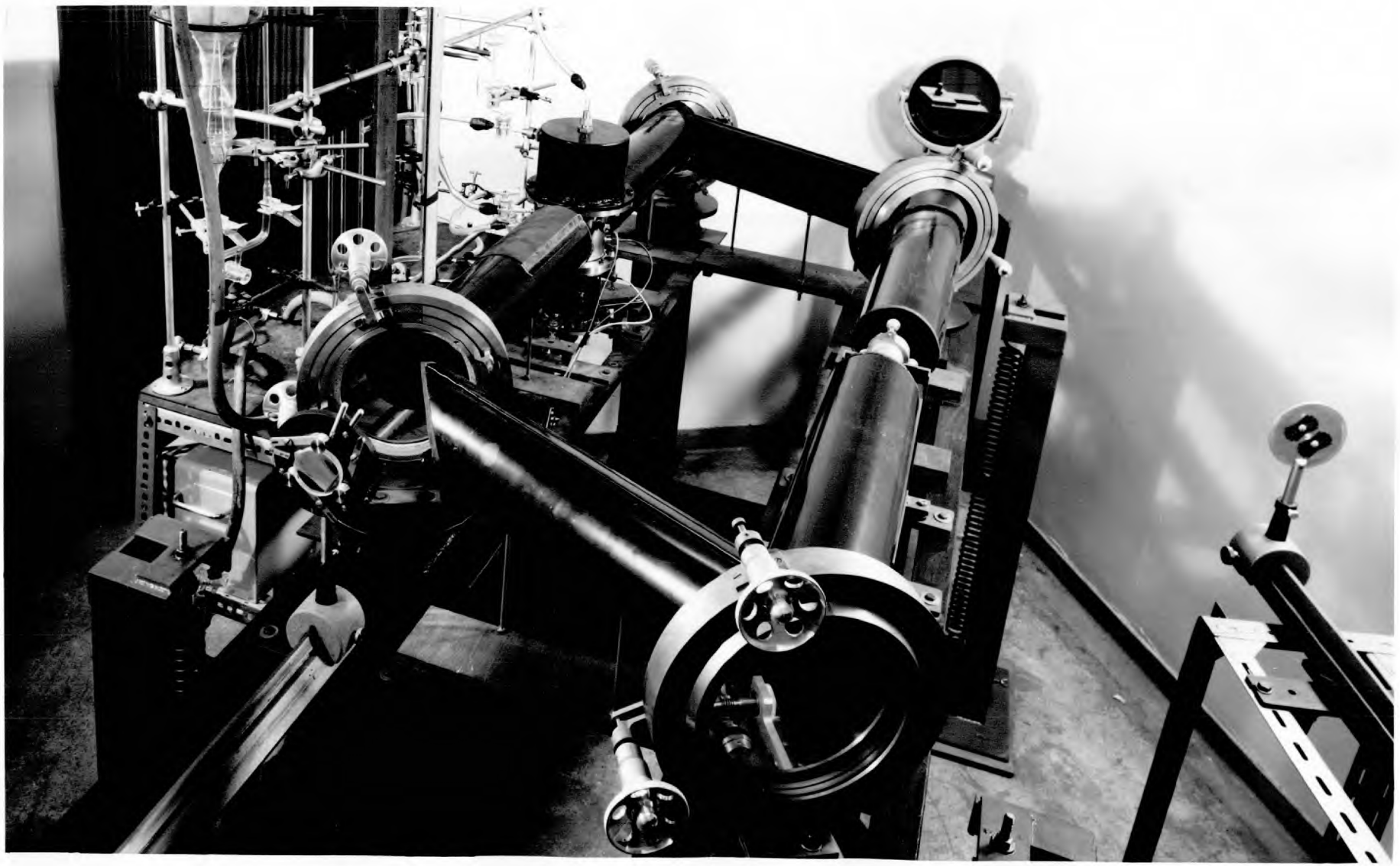

PLATE 3.2.. INTERFEROMETER PLATE HOLDER M_2.

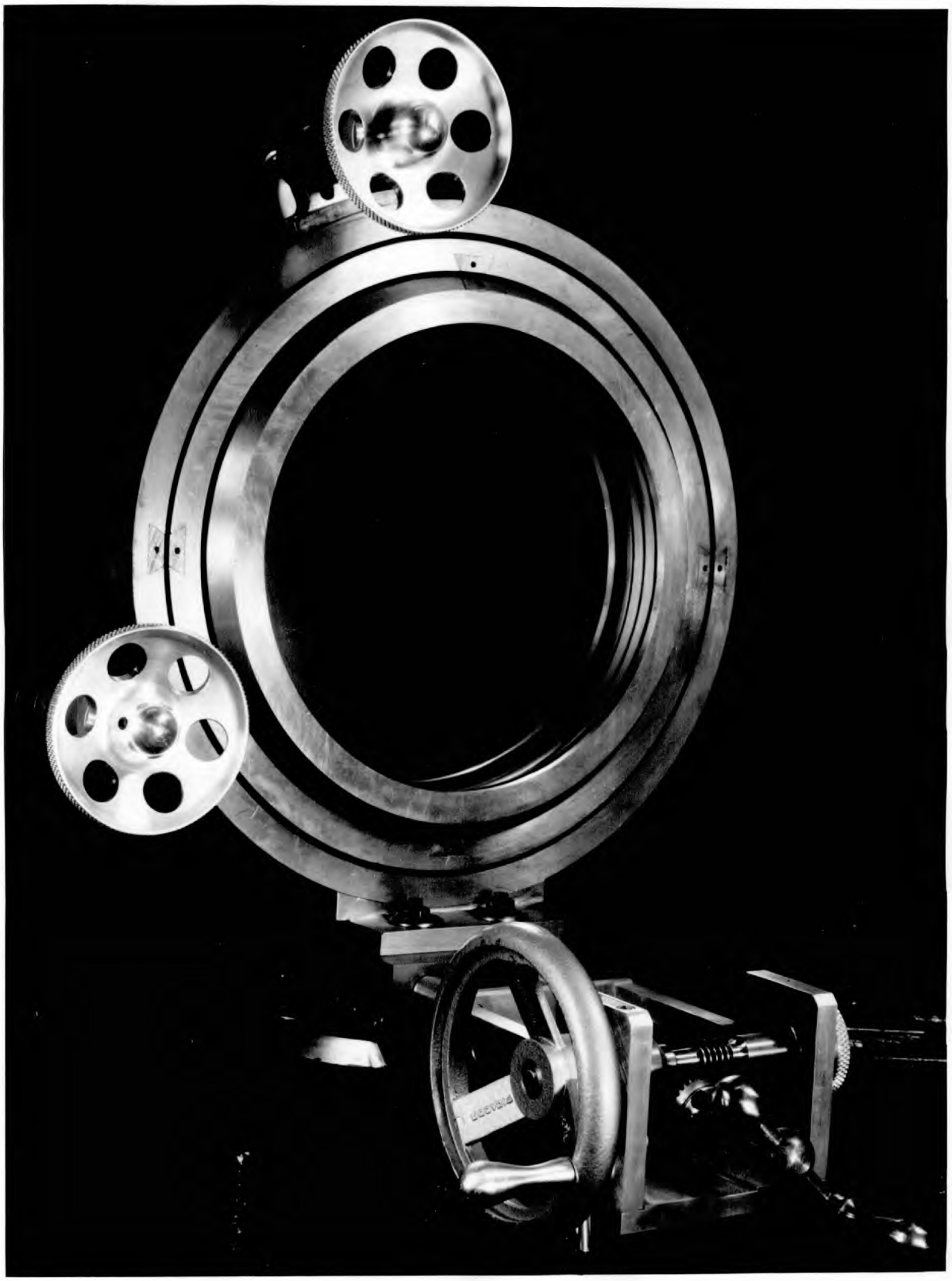

wavelength is 1.8 - 2.5 10^{-5} in.. For the rotational movement of the mirrors a similar sensitivity will be required. This degree of sensitivity in adjustment may be achieved in several ways and different methods were adopted for the rotation and traverse. It is important that in all adjustments backlash (free movement) is entirely eliminated or a lack of 'feel' will be present in the adjustments which will make setting-up difficult. In addition to the fine rotation adjustments which are to be fitted to M_2 and S_2 , all the mirrors must have coarse adjustments which will be used during the initial setting-up. In order to reduce manufacturing costs the four mountings were made identical, fine adjustment being achieved merely by fitting a large size of handwheel to the micrometers. Plates 3.1. and 3.2. show the mountings of mirrors M_1, M_2, S_2; detailed drawings are given in the appendix A:7..

The optical plate is retained within its gunmetal holder by a threaded ring. Flat cork gaskets are fitted in front of and behind the plate to prevent direct contact with the metal holder and the plate is supported around its edge by a soft rubber cord located within a grove in the holder. The cork and rubber gaskets take up any differential expansion between glass and gunmetal thus preventing temperature stresses in the glass.

For ease of adjustment, it is desirable that the plates rotate about an axis which lies as near as possible in the surface of reflection. The mirror holder is supported by two pairs of gimbals inside two concentric rings. The axis of the rings can be adjusted so as to coincide with the face of the optical plate. The gimbals and 1/4 in. dia. stainless steel rod and are run in mild steel housings. The spacers between the rings are of phosphor bronze. The bearing assembly was made with a minimum of clearance and was thoroughly lubricated with oil-based molybdenum disulphide before assembly. Plate movement is controlled by standard micrometer heads acting a distance of 7" from the gimbal axis and bearing against coil compression springs as shown in plate 3.2..

Free movement is eliminated by this system and the end load on the micrometer threads is not sufficient to cause excessive wear or distortion. The end thrust can be adjusted by using different springs or by preloading the spring. Micrometers are used since they provide a cheap, accurate smooth-acting screw thread; and any readings which are taken are an indication of the position of the adjustment, but these readings are not essential because fine adjustment is carried out with reference to the observed fringe pattern. Three inch diameter aluminium handwheels are fitted to the micrometer heads on M_2 and S_2 in order to give the required sensitivity. Locknuts are fitted to all the micrometers, and those fitted on the coarse adjustments of M_1 and S_1 were tightened after the preliminary stages of setting up with no noticeable alteration to the state of adjustment.

Owing to the considerable weight of the optical plate and its gimbal assembly (30 lbs.) it was decided to use a standard lathe top-slide to provide the basic runners for the traversing mechanism. Other designers have recommended that the lathe slide should be avoided on the grounds that it is not usually able to move exactly parallel to itself. The characteristic has not been overcome, but provided the two light paths are equated early in the setting-up procedure the slight misalignment resulting causes no inconvenience and is easily compensated at a later stage in the adjustment. However backlash has not been satisfactorily eliminated by this design and in the discussion in art. 4.4., an alternative design is given.

The traversing mechanism is shown in plate 3.2. As originally constructed the lathe slide gave an advance of 0.10 in. per turn: this being further geared down by 50:1 using a worm and pinion. The worm is spring loaded in mesh to remove backlash and the gears may be disengaged by the operation of a simple cam, allowing the coarse original lathe slide movement to be used for the initial setting-up. The backlash of the lathe slide is largely

overcome by the two coil compression springs seen in plate 3.1., but these must exert a considerable axial force to eliminate free movement, and this makes operation of the lathe slide difficult when working in opposition to the springs.

Remote control is usually effected either by flexible Bowden cables or by electric motors connected to the micrometers by flexible couplings. It was decided not to install remote control to the instrument as first set up, but to make provision in the design for its addition if found necessary. This would be done by fitting Bowden cables to the micrometer spindles. In practice, it was found that the fringe pattern could be observed whilst manual adjustments were being made, and therefore the cables were not used.

3.4. Vibration Isolation.

All interferometers are highly sensitive to external vibration and vibrometers are sometimes calibrated by interferometery[14]. In normal applications a movement of one tenth of the fringe spacing is easily recorded and this corresponds to a relative displacement of the optical plates of about one millionth of an inch.

At present the interferometer is installed on the fourth floor of a building adjacent to a road carrying considerable traffic including Omnibuses. The building is of platform floor construction and the instrument is situated at a corner adjacent to two load bearing walls, in order to utilise the maximum obtainable wall stiffness. The building contains many pumps and compressors and other machines most of which are mounted on ineffective anti-vibration matting; in particular on the third floor are several wind tunnels and their ancillary equipment. All of these contribute towards the high level of vibration existing in the building. (Recent measurements made with a Hilger and Watts Seismometer in the older part of the building on the second floor showed frequencies of 2-5 cps. and amplitudes of

1.4 - 4 microns peak to peak[54]. The different construction of the newer part of the building gives a lower natural frequency but larger amplitude.)

Previous designers have attempted to achieve freedom from vibration by many different techniques. Tanner[72] mounted an instrument on pneumatic-tired castors and these in conjunction with 'Silentbloc' rubber brushes gave satisfactory isolation. Hall[26] and Lee[47] used a similar suspension. Ashkenas and Bryson[4] used a system of rubber bands in tension together with a foot of foam rubber in compression. Binnersley[8] found that a one inch thick sheet of foam rubber gave adequate isolation, but he used a heavy framework of great rigidity. Sufficient rigidity would be difficult to obtain with the 200 mm. plates arranged in a parallelogram of 4'6"x 2'3".

Literature references to a comprehensive design procedure for isolators are rare. Crede[14] and Den Hartog[28] give theoretical treatments whilst Macinate[52] gives a bibliography together with practical design data on the suitability of various isolators. To achieve a low vibration transmissibility (the ratio of the force communicated to the object with and without the isolator being present), the natural frequency of the system should be many times lower than the fundamental exciting frequency. For a system with one degree of freedom (vertical) and zero damping the force transmissibility (T_f) and the displacement transmissibility (T_d) are both equal:

$$T_f = T_d = \frac{1}{1 - \left(\frac{f}{f_n}\right)^2} \qquad (3.1.)$$

where f = fundamental exciting frequency

f_n = natural frequency of the system.

Damping decreases the amplitude magnification at resonance but increases the transmissibility at frequencies $> \sqrt{2} f_n$. Therefore in the operational range of frequencies the effect of damping

is always to lessen the degree of isolation.

At first a rubber in compression system of 'Tico' anti-vibration matting was used but this did not prove satisfactory. The static deflection was 0.25" under load and gave a natural frequency of about 6 cps. It was decided to design a system with a natural frequency less than 1 cps. For a static deflection 'd' in. of an isolator, the natural frequency is given by

$$f_n = 3.13 \sqrt{\frac{1}{d}} \qquad (3.2.)$$

Therefore to achieve an f_n less than 1 cps. a static deflection of greater than 10" is required. The only practical way to obtain this extension is by means of metal coil springs. In order to simplify the installation, two sprung cradles were used each with a pair of tension springs, all of identical specification:

Number of turns	46
Wire size	3 S.W.G.
Outside diameter of coil	2"
Unextended length	18"
Extension under a load of 330 lbs.	$12 \pm \frac{1}{2}$"
Natural frequency	0.90 cps.

Sponge rubber mats, 0.625" thick, were placed under the bases of the cradles in order to eliminate spring resonance and to accommodate floor and base plate irregularities. It was decided not to incorporate dampers in the system until they were proved necessary in practice. The amplitude of vibrations induced during optical plate adjustment was found to be small and the fringes were always visible.

3.5. Framework Design.

The interferometer framework can either be constructed so rigidly that any vibration which excites the instrument produces no vibration of importance, or it can have a lighter construction so effectively isolated from vibration that no measurable disturbance of the fringe pattern takes place. The large size of the interferometer parallelogram (4'6" x 2'3") makes it difficult to design a rigid enough structure to adopt the first method and the high level of vibration present makes it doubtful whether the second would be successful. Therefore the framework was designed to give moderate rigidity but with a fairly high mass to act as an inertia block. As discussed above, it was at first mounted on 'Tico' anti-vibration pads but these did not prove satisfactory, and a suspension system incorporating coil springs under tension was installed instead. The location and the narrow doorway of the room in which the instrument is placed limited the size and weight of any one part of the apparatus. Therefore it was decided to construct the framework of two all-welded components which could be bolted together on installation. This limitation precluded an all welded structure which would have given maximum rigidity. The framework is shown in plate no. 3.1.

The two main framework members are of 6" x 6" R.S.J. and to these are welded the 5" x 4½" R.S.J. which carry the mirror assemblies and mirror bench supports. The platforms for the mirror assemblies are of ½" mild steel plate, 3½" diameter, and are welded to the tops of the uprights. The cell support runners are of 1½" M.S.A., which are extended at the inlet end to carry the collimating element, an 8" diameter Schlieren Mirror. Along the axis of the emergent beam provision is made for a 1½ metre optical bench which is supported on 1½" M.S.A.. This bench carries the optical elements necessary to give the required magnification of the fringe pattern. If the instrument is used

in single shot photography the camera is placed on this bench, but a cine camera must be mounted separately in order to isolate its vibration. The framework cross members of 4" x 3" R.S.J. and 2" x 3/8" strip are secured in place with 5/16" BSF high tensile bolts. The total weight of the framework, less mirror assemblies, is about 1100 lbs.

It was decided to install the coil spring suspension after the anti-vibration had proved unsatisfactory; hence two sprung cradles were designed to accept the existing framework. Each spring support, shown in plates 3.1. and 3.2., consists of a vertical length of 5" x 2½" steel channel welded to a mild steel base plate 12" square and 3/8" thick. The top bracket is made from 2" M.S.A. and of 2" X 3/8" strip. The load bearing sections of the cradle are of 3" x 2½" steel channel and are clamped to the main R.S.J.s by two pieces of channel gripping the inside edges of the R.S.J. Each is fitted at both ends with 3/8" Whit. eyebolts, the upper being made with three inches of thread to give a fine adjustment in frame attitude.

The framework as constructed is unsymmetrical and was preloaded with steel blanks to ensure that the centre of gravity coincided approximately with the geometric centre of the structure. The springs were all manufactured to an identical specification but the tolerances were relatively high, ±½" on the specified extension, and the eyebolts were adjusted to place the cell optical axis in the horizontal plane. Providing that the thrust faces of the washers under the eyebolt nuts are well greased, the manual effort required to adjust the attitude is small despite the load per bolt being 2½ cwt. Stops are fitted at the cradle ends to prevent excessive movement in any direction, both for safety and to reduce the possible amplitude of any vibration induced accidentally or by manual adjustments. By restricting amplitude, the stops decrease the time taken for oscillations to damp out.

3.6. Light Sources and the Inlet Optical System.

The two important properties of a light source to be used in interferometery are its intensity and spectral band width. Usually the higher the intensity the higher the band width. Sources may be classified in three groups:-

1) Low intensity and narrow band width - a sodium lamp.
2) Medium intensity and wide spectral band width - a high pressure mercury lamp.
3) High intensity and wide band width - a spark source.

The use of sources in the first group is restricted to the initial setting-up of the instrument. A laboratory sodium lamp gives about 10,000 fringes which increase in contrast towards the centre of the field, and its use in setting-up is described in art. 4.2. The spectral band width of a mercury vapour lamp increases as it heats up. When cold it is a member of the first group but as the operating temperature is attained the number of visible fringes is greatly reduced and it is then an example of the second group.

Sources of the second group provide sufficient light for the photography of low speed phenomena, where exposures of the order of milliseconds can be tolerated. Usually a filter is used with this type of source to decrease the width of the spectral band but this also reduces the available light, often by as much as 60%. A white light source, with its unique central fringe, gives absolute fringe numbering by which refractive index changes can be traced across a section where the fringe pattern is too complex to be resolved.

Sources of the third group are used for the study of the ultra high speed phenomena encountered in aerodynamics, where an exposure of the order of microseconds is essential. This is achieved by the discharge of a large capacitor across a gap between two electrodes, usually made of steel. The light from the spark is not monochromatic and must pass through either an interference

filter of a prism monochromator before reaching the camera.

For the purposes of this investigation it was decided to provide three types of source, a sodium lamp, a high pressure mercury lamp and a 1000 cp Pointalite (a white light source). The same collimating system was adopted for each light source in turn, the lamp being placed in the source position as shown in fig.2.5. The collimating element is an 8" Schlieren mirror M which permits the inlet optical bench to be placed at an angle of 20° to the interferometer axis with little spherical aberration. Light from the source S is collected by lens L_1, an 8" RAF camera lens, and is condensed by lens L_2, focal length 60", onto the slit T. When necessary a filter is placed between L_1 and L_2. The edges of the slit are defined by four razor blades which can be adjusted to give a slit of the desired size and proportions. The inlet optical bench is mounted on a framework made from Dexion. No attempt is made to isolate the bench from vibration but it is bolted to the floor to prevent accidental movement.

3.7. Emergent Beam Optical System and Camera Arrangement.

When the interferometer is adjusted so that the plane of localization of the fringes is within the length of the test-section, the gas-liquid interface and the fringe pattern will be in focus together. Even if the camera were to be placed directly behind S_2 the focal plane would be 2'4" from the camera and the field of view would be larger than required, giving a small image of the fringe pattern on the emulsion. A 20" ex W.D. lens was placed adjacent to S_2 (fig. 2.5.) and formed an inverted image of the fringe pattern at I_2 with a magnification of 1.30.

The choice of photographic technique was governed by the desired magnification. If the magnification given by L_3 was adequate no further lenses were used and photographs were taken with the film plane at I_2. If further magnification was required the camera was fitted with a 25 mm. Yvar f1.8 lens together with

extension tubes. The maximum magnification of 3.9:1 was obtained using a 75 mm. extension tube with an object - image distance (film plane - I_2) of 133 mm.. The depth of focus at this magnification is very small 0.2 - 0.6 mm., but reduction of image definition within 5 mm. of I_2 was hardly perceptible and therefore, the accurate location of I_2 was not important. The camera is mounted on a dexion frame independent of the interferometer framework.

CHAPTER 4.

ADJUSTMENT AND USE OF INTERFEROMETER.

4.1. Objects of Interferometer Adjustment.

An interferometer is said to be in adjustment when:-

a) The test-section windows are aligned perpendicular to the beams and the plates are adjusted to give maximum field size for the chosen beam spacing.

b) Fringes of the correct spacing and orientation are localised in a particular plane of the test-section. This is equivalent to adjusting the beams to intersect virtually at a chosen angle in the plane of the test-section.

c) The zero fringe (the fringe of maximum contrast) of the wavelength to be used is at the centre of the field of view. This is equivalent to reducing the path difference of the two beams to zero.

d) The fringe contrast is a maximum for the source size and fringe spacing to be used. This is equivalent to reducing the source plane path variations to a minimum.

4.2. Adjustment Procedure.

The procedure is divided into five stages:-

a) Positioning of plate holders on the framework.
b) Location of visible fringes by geometric optics.
c) Fine adjustment by interference optics.
d) Insertion of cells and alignment of cell flats.
e) Final adjustment for photography.

4.2.a. Positioning of plate holders on framework.

The framework was assembled and installed in the laboratory prior to positioning the plate holders. Thick steel discs were welded to the tops of the uprights and in bolting the framework together, care was taken that the discs were all on the same level (a spacer was placed at M_2 of height equivalent to the traversing

mechanism); this ensured that the mirror centres were in the same plane. Steel spigots were placed in the centre of each disc. Standard lengths corresponding to the sides S_1M_1 and M_1S_2 were constructed by drilling holes in a length of aluminium channel; the separation of the holes being equal to the standard lengths. The centre point of M_2 was established by drawing loci of the point from S_1 and S_2 using a pointed spigot in the end hole of the channel as a scriber.

The value of the parallelogram apex angle is not critical to within a few degrees, and although the positions and lengths of framework components were calculated on the basis of an apex angle of 60°, no attempt was made to establish this angle accurately during assembly. Each mirror mount base (saddle) is secured to its steel table by four 1/4" BSF set screws passing through 1/2" clearance holes in the saddle in order to accommodate any inaccuracy in the hole location.

Prior to making any optical adjustments, the components of the collimating system were arranged on their optical bench. The slit was positioned by finding the focus of the mirror M (fig. 2.5.) using a telescope focussed at infinity. Lens L_1 was placed at a distance equal to its focal length from the source and L_2 was arranged to give an image of the source in the plane of the slit. The mirrors were then adjusted to give maximum field size. The axis of the inlet optical system and the attitude of the Schlieren mirror were arranged such that the collimated beam, which exactly filled S_1, fell directly onto M_2. S_1 was then adjusted such that that the reflected beam filled M_1; then M_1 so that the beam filled S_2; then M_2 so that the beam filled S_2.

4.2.b. Location of visible fringes by geometric optics.

The optical plates were made nearly parallel using a modification of the method given by Tanner[71]. As a consequence of having chosen the parallelogram sides in the ratio of 2:1

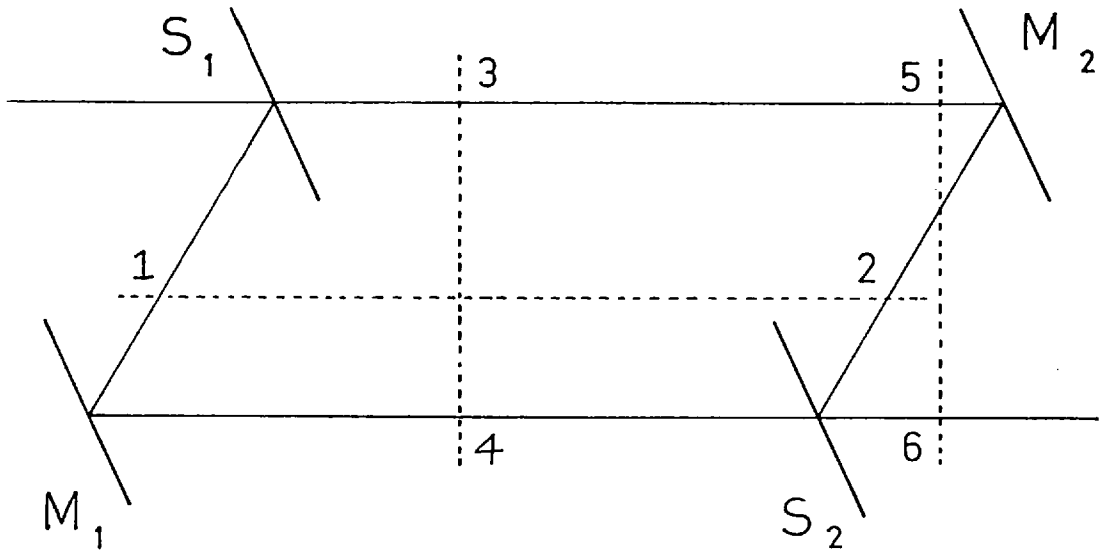

FIG. 4.1. AUXILARY OPTICAL BENCH POSITIONS.

together with an apex angle of 60, it was not possible to use a sheet of plane glass as the mirror in beams M_1S_1 and M_2S_2 (fig. 4.1.) as in the original method. Instead a small mirror, held in a saddle on an optical bench, was used. The procedure was as follows:-

1) Direct a narrow beam of collimated light along M_1S_1.
2) Bench in position 1 - 2, saddle in position 1, adjust mirror such that reflected images are coincident.
3) Saddle in position 2 adjust mirror M_2 to make image coincide with source, M_2 is then parallel to S_1.
4) Bench in position 3 - 4, set mirror with saddle in position 3 and then with saddle in position 4 adjust M_1 to be parallel to S_1.
5) Bench in position 5 - 6, set mirror with saddle in position 5 and then with saddle in position 6 adjust S_2 to be parallel to M_2.

Little difficulty was experienced in aligning the images to less than 1/64"; and providing that a standard technique was followed when setting the saddle clamping screw, and that the distance of the source S_1 was greater than six feet, sodium lamp fringes were usually located on traversing M_2. For this purpose a sodium lamp was placed on the inlet arm of the framework so as to illuminate a ground glass screen situated just before S_1. This method proved simple and reliable in practice and required only a minimum of auxiliary equipment. As all subsequent adjustments were made to M_2 and S_2, the micrometer locknuts were tightened on M_1 and S_1.

4.2.c. Fine adjustment by interference optics.

The fringes located by the previous method were usually of low contrast and before they were shifted to the desired plane it was necessary to improve their contrast. Firstly the fringes were swung so as to be approximately in the vertical plane by

rotating M_2 about its horizontal axis (henceforth called the vertical adjustment) and then M_2 was traversed towards the fringe of highest contrast. The increase in contrast of sodium fringes around the fringe of highest contrast is low and the adjustment was simplified if the diffuse screen was illuminated half by sodium and half by mercury light. The mercury fringes increase in contrast more rapidly but as their number is far less than the sodium fringes they are not visible until approaching the limit of adjustment of the sodium lamp. The worm drive on the traversing mechanism was used only when the mercury fringes had been located. The sodium lamp was then removed.

The procedure adopted to improve the fringe contrast was a modification of the 'Source-plane fringe' method proposed by Tanner[71]. A filter to isolate the 5461^{o}A mercury line was placed in position between L_1 and L_2 on the inlet optical bench. The technique was as follows :-

1) Splitter S_2 was rotated about its vertical axis so as to improve the fringe contrast.
2) Mirror M_2 was then rotated about its vertical axis in order to restore the fringe spacing which was usually reduced by stage 1 .
3) This sequence was repeated two or three times.
4) Splitter S_2 was rotated about its horizontal axis to improve the fringe contrast.
5) Mirror M_2 was rotated about its horizontal axis to restore the attitude and spacing of the fringes normally changed by stage 4 .
6) Stages 4 and 5 were repeated until no further improvement was obtained.
7) Mirror M_2 was traversed to bring the central fringe back into the middle of the fiel d of view.

During these operations the fringe plane was brought into the central plane of the test section. The plane was located either by checking for parallax with an object inserted in the beam or

by using a telescope with a short depth of focus.

The ground glass screen was then removed and the aperture of the source slit reduced to 1/16" square. The lens L_3 was placed in position adjacent to S_2 and a screen located in the plane I_2. The low contrast fringe pattern seen on the screen was then improved using the 'Source size - fringe contrast' method of Tanner. This is essentially the same as the previous method but before each pair of adjustments the source slit is elongated in a direction perpendicular to the axis about which the plate is to be rotated. During this stage the advantage of the Kinder[43] arrangement became apparent. When the fringe plane was in the region of the test-section it was noticed that horizontal adjustment of S_2 altered the fringe plane without appreciably changing the fringe spacing or attitude. Vertical adjustment of M_2 changed the fringe attitude and horizontal adjustment the fringe spacing, neither affecting the position of the fringe plane. This stage was completed when the aperture was 3/8" square and the fringe pattern was of maximum contrast.

4.2.d. Insertion of cells and alignment of flats.

Before the cells were placed in position on the interferometer framework the separation of the pairs of optical flats was set to within 0.001" using a comparator. This instrument is designed to compare lengths to within 5.10^{-5}" and the accuracy required to satisfy the criterion for negligible dispersion as calculated in art. 2.5. was easily attained. One flat of each pair is mounted in a three point holder (see design art. 7.2.a.) and may be set at any angle within $\pm 3^{\circ}$ of the fixed flat. A vacuum tight closure is ensured at all times by using an O-ring as the gasket. The comparator readings were taken adjacent to one arm of each holder and any subsequent changes in holder attitude were made using the other two knurled adjusters.

The mountings of both cells are fully adjustable and the

longitudinal axis of each may be swung in a horizontal or vertical plane in order to align the optical flats perpendicular to the light beam. The aperture of the slit on the inlet bench was reduced to about 1/32" square and the cells arranged so that the images of the aperture as reflected by the cell flats were seen on the aperture plate. Firstly the test-section was blocked off from the light beam and the compensating cell was set so that the image reflected from the fixed flat coincided with the aperture in the plate. The locknuts on the mountings were tightened and the adjustable flat set so that its image also coincided with the aperture on the plate. It was estimated that the images could be made coincident to within 1/3 of their diameter which equals 10^{-2}". As shown in fig 4.2. with a collimating element focal length of 60" the flats will be parallel to within ϑ where

$$\vartheta = \frac{x}{2f}$$

$$= \frac{10^{-2}}{120} = 0.83\ 10^{-5} \text{ rad.}$$

The width of the optical flats is 1.5".
Maximum wedge thickness of glass and water plate is $1.5\ 10^{-4}$".
This is less than the theoretical limit as calculated in section 3.2. The same procedure was followed for the test-section optical flats. Both sets of flats were then parallel to each other and perpendicular to the light beam. The compensating cell was completely filled with the ~~water~~ fluid under investigation and the test-section half filled so that the interface was at the centre of the optical flat.

4.2.e. Final adjustment for photography.

On the insertion of the cells the fringe contrast was always markedly reduced but fringes were always visible with an aperture

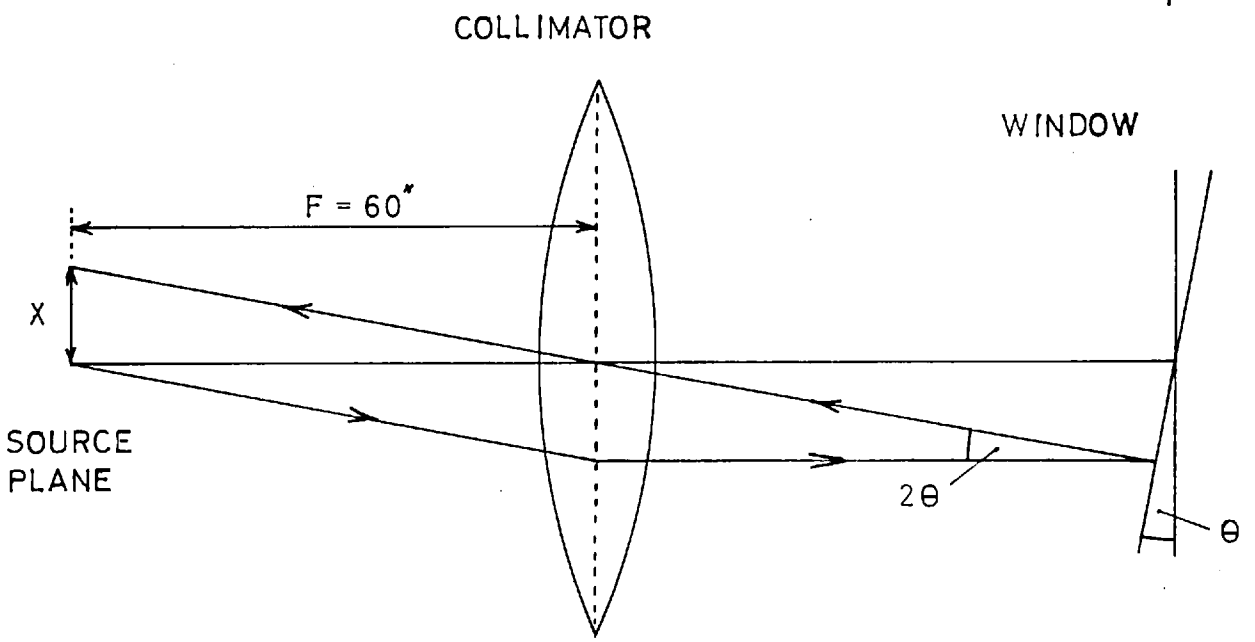

FIG.4.2.WINDOW ALIGNMENT.

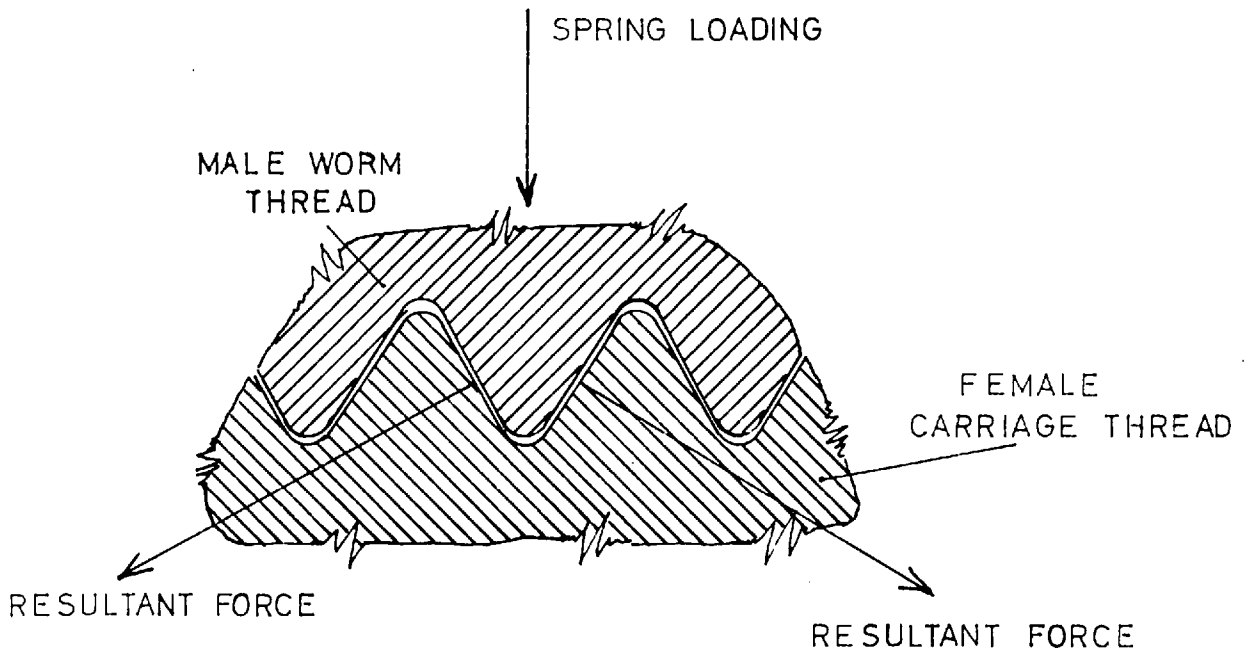

FIG.4.3. LATHE SLIDE DETAIL

of 1/16". Mirror M_2 was traversed to restore the central fringe to the centre of the field of view. The source size fringe contrast method of Tanner was repeated to restore the fringe contrast.

If the gas-liquid interface was not aligned parallel to the light beam spurious fringes were observed. Howes and Buchle[37] give photographs showing the change in shape of the spurious fringes as a function of the angle between the axis of the light beam and the model surface which was an optically-flat, face aluminised mirror. In the case of a cell containing liquid and vapour the meniscus at the glass interface further complicates the problem by giving diffraction patterns. These take the form of a series of horizontal lines parallel to the interface on the liquid side; in most cases these are of low contrast when compared with the Mach - Zehnder fringes.

If the appearance of the spurious fringes indicated that ϕ was little different from zero (the extreme cases of Howes and Buchle were not found unless artificially produced) the horizontal axis of the test cell was tilted slightly on the framework by adjusting the rear screw of the three point mounting. The collimating mirror was then rotated about its horizontal axis to restore the coincidence of source aperture and images thus making the light beam perpendicular to the cell flats; the reference cell was also readjusted perpendicular to the light beam. On re-examining the spurious fringe pattern it was apparent whether ϕ had been increased or decreased. The cycle was continued until the fringe tops had a 'picket fence' appearance which occurs when $\phi = 0$. It is important that all observations occur in the same plane, that of the camera film, because the appearance of the spurious fringes changes on either side of the focal plane.

Final adjustments were made for photography whilst the cell was under vacuum. Venkatarman[76] measured the piezo-optical coefficients for water at 23°C and gives average values for pressures around one atmosphere of 14.65 10^{-6}/atm. Harvey[29]

found the coefficient to be 22.07 10^{-6}/atm. at 14°C for pressure in the range 0 - 1 atmosphere. The change in optical path length of the cell which results from the decrease in refractive index gives a fringe shirt of $S = d\mu.L/\lambda$

where $d\mu$ = change in refractive index.

L = geometric length

λ = wave length of light.

Therefore Fringe shift = $\frac{22.07 \times 10^{-6} \times 4.5 \times 2.54}{5461 \times 10^{-8}}$

= 4.5

On evacuation a shift of ten fringes was observed which suggests that the separation of the optical flats decreases slightly under vacuum. A decrease of only 2.10^{-4}" would give a shift of five fringes. The attitude and spacing of the fringes did not change during evacuation indicating that the optical flats remained plane parallel. Finally M_2 was traversed to restore the central fringe to the middle of the field of view.

4.3. Photography.

A 16 mm. Paillard Bolex cine camera, model H 16 T, was used for photographing interferograms. The camera has an indicated speed range of 12 - 64 f.p.s. and exposes 16.5 ft. of film per cycle of the clockwork motor. At 64 f.p.s. the exposure is 1/60 sec. per frame. The normal camera lens was used only for run captions and it was removed for all fringe photography. An image of the fringe plane was projected directly onto the photographic emulsion by L_3. Exposure control of the film was achieved either by stopping down L_1 or by adjusting the slit size. A Chance glass finter was used to isolate the Mercury Green line

at 5461°A in the spectrum from the high pressure Mercury lamp. The filter gave sufficient light transmission for the correct exposure of Ilford HP3 film at 64 f.p.s. with L_1 at f 2.9 and the slit at its maximum aperture of 5/16" dia.. The image size on 16 mm. film of 10.45 x 7.40 mm was only 5% of the total interferogram area and hence the light intensity on the emulsion could have been increased many times by changing the focal length of lens L_2. The film was developed commercially by Kay Laboratories Ltd. using Kodak D 76 developer to give the standard speed rating of 400 ASA:

4.4. Discussion of Design.

The interferometer proved easy to operate and bring to the required state of adjustment. The following are only minor criticsms of the detail design:-

1) As previously mentioned the inequality in ease of movement of the lathe slide in opposite directions, owing to the springs acting along its axis, proved irksome in giving a 'lack of feel' to this adjustment. If the back-lash in the slide had been removed by forcing the male screw thread of the shaft either to top or bottom of the female thread in the carriage block by spring loading as is shown in fig. 4.3., the torque required to move the carriage would have been the same in either direction. In addition this force would have removed any free movement in the dovetail slideways. The carriage traverses only a small proportion of its design range and hence the spring loading could have been designed to act under the middle of the carriage, but this arrangement would require a bearing on the floating end of the shaft to take the upthrust. Alternatively the spring could be placed under the floating end of the worm and the consequent distortion of the thread tolerated.
2) The lathe slide traverse, when using the reduction gear, was

a little too rapid. A worm and pinion giving 100:1 reduction rather than 50:1 as designed would have given greater control.

3) The attitude of the framework changed slightly from day to day owing to the effect of temperature upon the tension springs, in addition the springs tended to sag over a long period of time suggesting that they were underdesigned for a standing load of this magnitude. Both these effects are characteristic of the type of suspension chosen and could not be eliminated.

4) The mirror-mount design proved satisfactory, but the usage made of the fine adjustments available on M_1 and S_1 did not warrant having their components made of similar accuracy to those of M_2 and S_2.

5) Remote control would have been of assistance only when the plane in which the fringes were being viewed was further than arms-length away from M_2 and S_2.

CHAPTER 5.
LITERATURE SURVEY.

5.1. Introduction.

In 1893 Hertz[33] published his paper on the evaporation of mercury into a vacuum; this was the first quantitative study of the evaporation phenomena of a single component system. He postulated from the kinetic theory of gases that for any substance at a given temperature there exists a maximum rate of evaporation which is equal to the number of molecules which strike a surface placed anywhere in the vapour phase and is also equal to the number of molecules which strike the surface of the condensed phase under equilibrium conditions. Therefore the upper limit on the rate of evaporation or condensation is

$$N = 1/4\ n_s \cdot \bar{c} \qquad \text{moles/cm}^2\text{.sec.} \qquad (5.1.)$$

where n_s = molecular density of gas phase at equilibrium conditions. moles/cm^3.

$\bar{c}$ = average velocity of vapour molecules. cm/sec.

In his experimental work on mercury Hertz obtained values for the rate of evaporation which were only 10% of the theoretical rate.

In 1915 Knudsen[45], using a more accurate experimental technique, obtained rates of evaporation equal to the theoretical maximum from the surface of mercury which had been carefully purified, but only 30% of these rates from impure mercury. He introduced a parameter 'α' ≤ 1, variously called the 'Mass accommodation coefficient or the 'Condensation coefficient' defined for the general case, where the gas phase shows a pressure at the interface, by the equation

$$\bar{N} = \frac{\alpha \cdot \bar{c} \cdot (n_s - n)}{4} \qquad (5.2.)$$

where $\bar{N}$ = net rate of evaporation. moles/cm^2.sec.

n = molecular density of gas phase. moles/cm^3.

This is called the Hertz - Knudsen equation which has been a basic relationship for all subsequent work on mass transfer in a single component system. Alternatively this equation may be derived by considering individual coefficients.

$$\text{Rate of evaporation} = \alpha_e \cdot \frac{\bar{c}}{4} \cdot n_s .$$

$$\text{Rate of condensation} = \alpha_c \cdot \frac{\bar{c}}{4} \cdot n .$$

$$\text{Net rate of evaporation} = \frac{\bar{c}}{4} \cdot (\alpha_e n_s - \alpha_c n) .$$

At equilibrium $n_s = n$, and the net rate of transfer is zero. Thus assuming α_c and α_e are independent of pressure and temperature, $\alpha_c = \alpha_e$.

Hence

$$\bar{N} = \alpha \cdot \frac{\bar{c}}{4} \cdot (n_s - n) .$$

This coefficient should not be confused with the energy accommodation coefficient, which is the ratio of sensible heat transferred by molecules striking the surface to the theoretical maximum of sensible heat transfer: the energy accommodation coefficient is generally close to unity.

Knacke and Stranski[44] give a comprehensive survey of the literature on evaporation and condensation coefficients. Other bibliographies include those of Courtney[13], Stever[59] and Rideal[65]. Paul[88] has compiled a list of evaporation coefficients. A large variety of experimental techniques have been used and we shall classify them as follows:-

A. Evaporation from a quiescent surface.

1) Evaporation into high vacuum of substances with vapour pressures less than 0.1 mm. of mercury.

2) Evaporation of substances with vapour pressures higher than 0.1 mm. of mercury.

3) Condensation experiments.

B. Evaporation from a moving surface.

5.2.a. Evaporation into High Vacuum.

For evaporation into high vacuum n = 0 in the Hertz - Knudsen equation and hence a knowledge of the vapour pressure of the substance together with its rate of evaporation into vacuum is sufficient to determine its condensation coefficient. In order to maintain n at zero, the probability of evaporating molecules being reflected back into the surface, after molecular collisions, must be small. In most techniques this is achieved by operating at high vacuums and making the separation of the evaporating surface and the condenser much smaller than the mean free path of the molecules.

Using this method Wyllie[84] determined the condensation coefficient of glycerol at 18°C as 0.052. He measured the loss in weight of a sample of known surface area placed under vacuum for periods of up to 35 hours. The sample holder was withdrawn from the thermostated cell for weighing. The vapour pressure of the sample was found by measuring the rate of effusion of vapour through a hole in platinum foil, the hole having a diameter less than the mean free path of the evaporating molecules. Wyllie also discusses the relationship between 'free angle ratio' (the ratio of the partition function for the rotation of the molecules in the liquid to that for molecules in the vapour), as calculated by Eyring and Kincard[21] and the values of the coefficients which had been measured by Alty[1] and Baraneav'[7]. Condensation coefficients and free angle ratios for CCl_4, C_6H_6, CH_3OH, C_2H_5OH and water are almost equal, but for $CHCl_3$ which does not form hydrogen bonds, the measured condensation coefficient is less than one-third of the calculated free angle ratio.

A mechanical torsion balance was used by Wessel[81] to measure the 'evaporation pressure' (the recoil of the evaporating molecules

against the condensate) for cadmium and silver at temperature near to their melting points. From a knowledge of vapour pressure and molecular weight he calculated $\alpha = 0.996$ for cadmium and $\alpha = 0.920$ for silver. Rideal and Wiggins[64] used a similar arrangement for the evaporation of napthalene and sulphur crystals: they found that rhombic and monoclinic sulphur showed different evaporation pressures. Tschudin[75], Kramers and Stemerding[46] found the coefficient for sublimation of ice at -60 to -80°C to be greater than 0.94.

5.2.b. Evaporation at Higher Pressures.

For substances of higher vapour pressures than 0.1 mm. it is not possible to maintain n = 0 and the term in equation 5.2. caused by condensation must be included. As shown in 6.5. the equation may be expressed as

$$\overline{N} = \alpha . \sqrt{\frac{}{}} (p_s - p) \qquad (5.3.)$$

The equilibrium vapour pressure p_s can be determined only indirectly, by measurement of T_s the surface temperature. For low mass transfer rates the difference $(p_s - p)$ is small and the accuracy of this measurement is critical.

In a series of papers from 1931 - 1936 Alty and his co-workers[1] measured the condensation coefficient for water. They determined α to be 0.036 and although the accuracy of their experiments has often been criticised, in view of the absence of more reliable figures this value is still widely accepted. Alty used several experimental methods, the most accurate technique being a modification of the Knudsen drop method, in which the surface temperature was estimated by measuring the radius of curvature and hence the surface temperature of the drop. The pressure in the gas phase was measured with a mercury manometer, 1 mm. from the evaporating surface. Evaporation of the droplets which had detached from the nozzle, was prevented by a layer of

oil placed in each of the collecting vessels. Heidger has suggested that impurities vaporizing from the oil may have contaminated the drop surface. Schrage[68] has objected to the assumption that the vapour pressure and temperature at the surface are constants throughout the evaporation process and also the assumption that gas and liquid temperatures are always equal. Pruger[60] has stated that in order to know the temperature within 1°C the capillary constant of the pipette must be known to within 0.5% Delaney[16] has criticised the data on the grounds that measurements at high and low temperatures are inconsistant and has pointed out that the method of calculation ignores any possible dependence of the condensation coefficient upon temperature.

Baraneav[7] measured the rate of evaporation of benzene, chloroform and of the lower alcohols. He used a steady state process in which the temperature of the evaporating fluid and the small degree of under-saturation in the vapour were recorded. The total pressure in the system was measured on a mercury manometer and the temperature was recorded by a 0.2 mm. diameter copper-constantan thermocouple as the junction passed through the falling liquid surface. In view of the probable inaccuracies of the experimental technique the results show surprising agreement.

In similar experiments Pruger[60] used a copper-constantan thermocouple in the shape of a spade, 0.04 mm. thick and 0.7 mm. long. The low degree of undersaturation of the vapour required to maintain the rate of evaporation was controlled by fitting a reflux cooler at the neck of the vessel. For CCl_4 he found that the liquid was superheated by 3°C almost up to the surface. The thickness of the surface layer across which the temperature fell to the vapour temperature was about 0.66 mm., this value varying with the rate of evaporation. For water he calculated that $\alpha = 0.02$ at 100°C and stated that the surface temperature was higher than the boiling temperature by 0.01 - 0.05°C. Baraneav using a less elaborate but similar technique found $\alpha = 0.040$ at 30°C.

Jarvis and Kagarise[41] compared the accuracy of a thermister and an infra-red radiometer for the measurement of surface temperature. They concluded that the radiometer was insensitive to temperature changes less than 0.1°C, although it had the advantage that it gave the temperature of a layer at the surface of the liquid only 0.1 mm. thick. The thermister measured the temperature of a layer 2 - 3 mm. thick and was slower to respond to rapid temperature changes but was sensitive to temperature variations of 0.05°C. Jarvis et al [40] have shown that a monolayer which reduces the rate of evaporation may increase the surface temperature by as much as 5 - 6°C.

Hammeke and Kappler[27] measured the condensation coefficient of water evaporating at a steady rate by determining the surface temperature with a radiometer and the under-saturation with a mercury manometer. The vapour was condensed in a cold trap and the rate of evaporation controlled by the speed with which vapour was pumped out.

They stated that owing to a large coefficient of extinction the radiation falling on the radiometer came from a layer 0.01 mm. thick. Temperature measurement was accurate to 0.05°C and they calculated the coefficient for water to be 0.045 at 20°C, this being independent of the rate of vaporisation. These authors concluded that most of the heat is carried to the surface by convection currents and Delaney suggests that lag in the responses of the barometer may have introduced appreciable errors. The sensitivity quoted for the radiometer differs markedly from that given by Jarvis and Kagarise.

Several investigators have measured rates of evaporation in a closed system under non-steady conditions. In the experiments of Bucka[11] a sample of 5 ccs of ethyl alcohol were allowed to evaporate from a depression in the face of an aluminium block, which acted as a heat sink. The block was enclosed in a large bell-jar which was evacuated and then isolated from the pump.

The rise in pressure was measured on a mercury manometer and the temperature of the sample was determined by a copper-constantan thermocouple placed at the bottom of the sample. He determined α from equation 5.3. which, if the pressure in the gas phase is uniform, may be written

$$\frac{dp}{d\vartheta} = \alpha . \frac{F}{V} \left\{ \frac{KT}{2\pi M} \right\}^{\frac{1}{2}} \left[p_s - p \right] \qquad (5.4.)$$

where F = the surface area of the alcohol sample. (cm^2).

V = the volume of the bell-jar. (cm^3).

Although his techniques for measuring the rapidly changing variables were elementary, Bucka obtained good reproducibility, calculating $\alpha = 0.024$ for a sample having a temperature between 12 - 15°C.

Delaney[16] investigated the dependence of the condensation co-efficient for water upon temperature. The sample was placed on a thermostated block of copper and the rate of increase of pressure in a closed system was recorded using an Alphatron vacuum gauge. The temperature of the water sample was measured using a glass bead thermistor. Both instruments were linked directly to high speed recorders. He obtained the following values:-

Water	43°C	α = 0.0265
	0	0.0415
Ice	-13 to -2	0.0144

The diameter of the thermistor probe was 0.25 mm. hence in these experiments positioning of the probe must be critical because of the sharp temperature gradient reported by Pruger[60]. Furthermore, it is probable that a probe of this size would alter the physical situation at the interface and affect the rate of evaporation. In order to avoid condensation on the pressure probe it was heated above the vapour temperature and this may have increased the recorded pressure.

Delaney correlated his results for water with those of Alty and Pruger in an equation of the form $\alpha = Ae^{-E/RT}$, and calculated E, the activation energy, to be - 1,523 cal/mole. The value of

the coefficient he quoted for ice, $\alpha = 0.0144$, cannot be compared directly with any other work although Tschudin has found $\alpha = 0.94$ at $-40^{\circ}C$.

Bogdandy et al[9] measured the coefficient for ethyl alcohol evaporating at a constant temperature in a closed system. The results were interpreted by using the integrated form of equation 5.4.

$$\ln (p_s - p) = - \alpha . \frac{F}{V} \left(\frac{KT}{2\pi M} \right)^{\frac{1}{2}} \vartheta + \text{constant.} \qquad (5.5.)$$

and was found to be 0.036. The liquid was contained in a copper tube placed in a water thermostat and it was assumed that both the surface and the bulk liquid were at a uniform temperature.

Harvey[29] used an interferometer to measure the surface temperature when studying the evaporation and condensation of water vapour in the presence of air. A mixture of air and saturated water vapour in the cell were allowed to change in pressure whilst the rate of mass transfer was determined from the temperature gradient in the liquid. No attempt was made to measure the form of the pressure rise at the interface, nor was allowance made for the effect of adiabatic expansion or compression of the air. Temperature changes of the order of $0.002^{\circ}C$ were measured by the interferometric technique.

5.2.c. Condensation Experiments.

Few investigators have measured rates of condensation of vapours onto solid or liquid surfaces. Volmer and Estermann[77] determined the rate of condensation of mercury at $-64^{\circ}C$ and calculated $\alpha = 0.85$. Haward[30] measured the rate of condensation of molecular beams of iodine and red mercuric iodide. He postulated the formation of an unstable layer of yellow mercuric iodide to account in the latter case for the low condensation coefficient found. No data, other than that of Harvey, has been published on the condensation of pure vapours onto the liquid phase.

5.3. Evaporation form a Moving Surface.

Hickman and Trevoy[34,35,74] in a series of papers have described the use of a flowing stream tensimeter (originally developed for measurements of surface tension) to measure the condensation coefficient for water and glycerol. This technique differs from all those previously mentioned in that the surface, from which evaporation takes place, is moving relative to the gas phase and is being continually replenished. A stream of liquid flows from the open lower end of a vertical glass tube and evaporation takes place from the cylindrical liquid surface. In the experiments of Hickman[34] on water the stream re-entered a second glass tube placed 1.2 - 1.7 cm. below the first The pressure in the gas phase was controlled by the rate of evacuation and was measured by a mercury manometer. The data were evaluated assuming that there was zero pressure in the gas phase and that the surface temperature was equal to that measured by a thermcouple adjacent to the stream. The condensation coefficient was calculated to be greater than 0.25, and if corrections were made for the gas pressure and the probable decrease in surface temperature, owing to evaporation, this value becomes greater than 0.65. Trevoy[74] in his work on glycerol evaporating into a high vacuum, in which there was little surface cooling, found α equal to unity.

Heidger and Boudart[31] investigated the effect of mild surface agitation on the evaporation of glycerol. Their method of calculation required no absolute pressure measurements to be made, since the coefficient was calculated from the ratio of the times to give a chosen pressure rise in a closed system for the two cases:

a) evaporation of glycerol from a pool of known surface area.

b) evaporation and effusion of glycerol through a small hole, of known diameter, in a copper diaphragm into the main vessel.

A magnetic sitrrer was placed in the liquid and tests were carried

out with and without the stirrer in operation. The condensation coefficient was calculated to be 0.05 at 19.2°C and no increase in α was reported during agitation even when the stirrer blades were cutting the surface. The authors state that the viscosity and surface tension of the sample were sufficiently high to prevent splashing on vigorous agitation. In fact, with glycerol, it is unlikely that fresh surface for evaporation is produced by this method of agitation.

5.4. Discussion.

Most previous workers have calculated values for the condensation coefficient from measurements of mass transfer across an interface; only Alty and Harvey have considered the heat flux during mass transfer. Many methods have been employed to measure the surface temperature but none can be regarded as accurate. All methods except those of Hammeke and Kappler and Harvey involve the insertion of either a thermocouple junction or a thermistor into the surface layers of liquid. The presence of these devices must affect physical and thermal conditions at the interface. Again the sensitivity of an infra-red radiometer, as used by Hammeke and Kappler, is low when compared with the accuracy of a thermocouple, although it gives the temperature of a layer only 0.05 mm. thick. The interferometric technique of of measuring interface temperature as used by Harvey is undoubtably the most accurate but the presence of air above the liquid during his measurements make the results of doubtful value, owing to the additional diffusion resistance in the gas phase. The advantages which make interferometers particularly suited to studying this problem are as follows:-

a) There is no disturbance of the physical and thermal environment at the interface.

b) The accuracy to which temperature changes can be measured is proportional to the length of the light path in the liquid

and this measurement can be made very sensitive.

c) The proximity to the surface at which the temperature can be measured is limited only by the available magnification and ability to define the surface.

d) Temperature is given directly as a function of the distance from the interface.

e) There is an instantaneous response to temperature change.

It is unfortunate that, owing to the impossibility of balancing light paths in the vapour at the same time as in the liquid, measurements of temperature may be made in one phase only at a time. Also this method may be applied only to a two dimensional system, because the fringe shift is proportional to the total change of refractive index along the light path.

It was decided to use the interferometric technique of Harvey and to apply it to the evaporation and condensation of pure substances with only vapour in the gas space. The only additives to the liquid would be relatively non-volatile surfactive agents or inorganic salts. The small degree of departure from equilibrium in the vapour phase, necessary to give a low heat flux at the surface, would be difficult to maintain for operation under a steady state. Therefore it was decided to use a non-steady method in which the pressure in the gas phase would be changed continuously, starting from its equilibrium value, by altering the cell volume occupied by the gas.

Two methods of calculating the condensation coefficient from the results will be used: the first will depend upon the accurate measurement of the surface temperature, whilst the second will utilise the temperature profile below the liquid surface. The latter will provide a check on the surface temperature measurement.

CHAPTER 6.
THEORY.

6.1. Progress of an Experiment.

Fig. 6.1.
Vapour p, Tv.

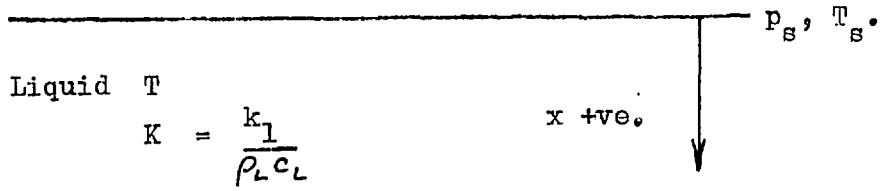

Initially pure vapour is in equilibrium with liquid having a quiescent surface. The pressure in the vapour (p) is then varied as a continuous function of time (ϑ) which causes condensation or evaporation of the vapour onto the liquid surface. The surface temperature (T_s) and the corresponding saturation vapour pressure (P_s) change at a rate governed by the kinetic rate of condensation, the pressure difference and the condensation coefficient at the interface. The temperature of the liquid (T) is controlled by conduction of heat from the interface and is measured as a function of time and distance from the interface (x) by the interferometric technique.

6.2. Evaluation of the Interface Boundary Condition.

The Hertz – Knudsen equation states that:

$$\overline{N} = \alpha . \frac{\overline{c}}{4} (n_s - n) \text{ moles/cm}^2\text{.sec.} \quad (6.1.)$$

We assume that:–

1) the ideal gas laws are obeyed then the pressure in the vapour space $p = nRT$
2) there is a Maxwellian distribution of velocities in the gas phase

$$\bar{c} = \left(\frac{8RT}{\pi M} \right)^{\frac{1}{2}}$$

where R = gas constant ergs/mole$^{\circ}$K

M = molecular weight grms/grm.mole

T = absolute temperature $^{\circ}$K.

Thus by equation 5.2.

$$\bar{N} = \alpha\phi(p_s - p) \qquad (6.2.)$$

where $\phi = (2\pi RMT)^{-\frac{1}{2}}$

Let ($T^{\ast}$) be the temperature at which the saturation vapour pressure is the pressure in the vapour space (p).
For the small pressure range over which the experiment is carried out it can be assumed that the vapour pressure curve is linear, and since the temperatures T_s and $T^{\ast}$ never differ by more than 0.2°C

$$p = \beta T^{\ast} + \eta \qquad (6.3.)$$

and $$p_s = \beta T_s + \eta \qquad (6.4.)$$

By substitution in equation 6.2.

$$\bar{N} = \alpha \phi \beta (T^{\ast} - T_s) \qquad (6.5.)$$

The heat given up by each mole of vapour which condenses onto the surface

$$H = M (L + C_v [T_v - T_s]) \text{ cals/mole.} \qquad (6.6.)$$

where L = latent heat of vapour cals/grm.

c_v = specific heat of vapour cals/grm.$^{\circ}$K

Thus total flux per unit area

$$Q = \alpha \phi \beta H (T^{\ast} - T_s) \text{ cals/sec.cm}^2. \qquad (6.7.)$$

This must be equal to the rate at which heat is conducted away

from the interface into the bulk of the liquid.

$$Q = -k \left|\frac{\delta T}{\delta x}\right|_S \text{ cals/sec.cm}^2. \qquad (6.8.)$$

where $\left|\frac{\delta T}{\delta x}\right|_S$ is the temperature gradient at the surface.
Hence

$$-k \left|\frac{\delta T}{\delta x}\right|_S = \alpha \phi \beta' H (T^* - T_s) \qquad (6.9.)$$

or

$$\left|\frac{\delta T}{\delta x}\right|_S = -\gamma (T^* - T_s) \qquad (6.10.)$$

where γ is a constant with respect to time and small temperature changes and k is the thermal conductivity of the liquid. (cals./cm.sec.^{o}K.)

6.3.a. Unsteady state heat conduction equation.

Here the liquid is stationary and not affected by convection currents even during evaporation when the liquid surface is cooler than the bulk. All the heat flux will be conducted away from the interface and the temperature distribution will be governed by a solution of

$$\frac{\delta T}{\delta \vartheta} = \frac{k}{\rho_L c_L} \cdot \frac{\delta^2 T}{\delta x^2} = K \frac{\delta^2 T}{\delta x^2} \qquad (6.11.)$$

where ρ_L = density of the liquid. (grm/cm^3.)

c_L = specific heat of the liquid. (cal/gram.^{o}K.)

The solution of equation 6.11. must obey two boundary conditions:

a) Initially the system is in equilibrium and there is no net transfer of heat or mass and hence no temperature gradient. Therefore when $\vartheta = 0$, $x \geqslant 0$ $\quad T = T_o$.

b) At the surface the temperature gradient $\left|\frac{\delta T}{\delta x}\right|_S$ is a known function of time governed by the condensation coefficient and the extent of departure from equilibrium conditions as shown in equation 6.10.

$$\left|\frac{\delta T}{\delta x}\right|_s = -\gamma (T^* - T_s) \qquad (6.10.)$$

When it is possible to express the temperature of the surface of the liquid (T_s) in the form of a series of half powers of the time:

$$T_s' = T_s - T_o = \sum_n b_n \vartheta^{n/2} \qquad (6.12.)$$

where b_n are constants,
Carslaw and Jaegar[12] show that the solution of equation 6.11. is

$$T' = b_n \Gamma\left(\frac{n}{2} + 1\right).(4\vartheta)^{n/2}.i^n \operatorname{erfc} \frac{x}{2\sqrt{K\vartheta}} \qquad (6.13.)$$

where $T' = T - T_o$

n is any positive integer

and i means $\int_x^\infty$

(i) Application of the first boundary condition.

When $\vartheta = 0$ and $x \geq 0$, $i^n . \operatorname{erfc} \infty = 0$ for all n.
Thus $T' = 0$ and hence $T = T_c$ as required.
Also in equation 6.11., when $\vartheta = 0$, $T_s' = b_o$.
But $T_s' = 0$, when $\vartheta = 0$ and therefore $b_o = 0$.

(ii) Application of second boundary condition.

By differentiating equation 6.13.

$$\frac{\delta T'}{\delta x} = \frac{\delta T}{\delta x} = \sum_n b_n \cdot \frac{\Gamma(n/2 + 1).(4\vartheta)^{n/2}}{2\sqrt{K\vartheta}} i^{n-1} \operatorname{erfc} \frac{x}{2\sqrt{K\vartheta}} \qquad (6.14.)$$

6.3.b. <u>Solution wher the surface temperature can be measured.</u>

At the surface $x = 0$, and $i^{n-1} \operatorname{erfc} 0 = \frac{1}{2^{n-1}\Gamma\left(\frac{n-1}{2} + 1\right)}$

Therefore $$\left(\frac{\partial T}{\partial x}\right)_s = -\sum_n b_n \cdot f_n \cdot \vartheta^{n/2 - 1/2} \qquad (6.16.)$$

where $$f_n = \frac{\Gamma(n/2 + 1)}{\sqrt{K}\,\Gamma(n/2 + 1/2)} \qquad (6.17.)$$

T^* is the temperature at which the vapour pressure of the liquid is equal to the pressure in the vapour space and is obtained as a function of time from the measured relationship between pressure and time.

Put $$T^{*\prime} = T^* - T_o^* = \sum_n a_n \cdot \vartheta^{n/2} \qquad (6.18.)$$

where a_n are constants.

At $\vartheta = 0$ there is equilibrium between the phases, then $T_o^* = T_o$, it follows that $a_o = 0$.
Substituting 6.13. and 6.18. into 6.10.

$$T^{*\prime} + T_o = T_s' + T_o - \frac{1}{\gamma} \Big/ \left(\frac{\partial T}{\partial x}\right)_s \qquad (6.19.)$$

$$\sum_n a_n \vartheta^{n/2} = \sum_n b_n \vartheta^{n/2} + \frac{1}{\gamma} \sum_n b_n f_n \cdot \vartheta^{n/2 - 1/2} \qquad (6.20)$$

Hence, comparing coefficients of like powers of ϑ

$$a_n = b_n + \frac{1}{\gamma} b_{n+1} \cdot f_{n+1} \qquad (6.21.)$$

and in general $$\gamma = \frac{b_{n+1} \cdot f_{n+1}}{a_n - b_n} \qquad (6.22.)$$

In particular $a_o = b_o - \frac{1}{\gamma} b_1 \cdot f_1$

and since $a_o = b_o = 0$ then as $f_1 \neq 0$, $b_1 = 0$.

From equations 6.19. and 6.22.

$$\alpha_n = \frac{k}{\phi H\beta} \left(\frac{b_{n+1} \cdot f_{n+1}}{a_n - b_n} \right) \qquad (6.23.)$$

All values of α_n should be the same and equal to α, provided that the series representation of T_s' and T' (equations 6.13. and 6.18. are correct.

6.3.c. Solution when the temperature profiles can be measured accurately.

The method above requires an accurate measurement of the temperature at the surface (T_s) in order to define the series given in equation 6.12. The coefficients of this series may also be calculated from the temperature profiles as follows:
Substitute $x = 2I\sqrt{K\vartheta}$ in equation 6.13.

$$T' = \sum_n b_n \Gamma(n/2 + 1).(4\vartheta)^{n/2}. \, i^n \operatorname{erfc} I \qquad (6.24.)$$

where I is a constant.

$$\text{Let } T' = T - T_o = \sum_n c_n \vartheta^{n/2} \qquad n \geqslant 2 \qquad (6.25.)$$

Thus by comparing powers of $\vartheta^{n/2}$

$$b_n = \frac{c_n}{\Gamma(n/2 + 1).2^n.i^n \operatorname{erfc} I} \qquad (6.26.)$$

I' can be chosen so that the relationship between x and ϑ can be easily and accurately measured from the interferograms.

6.4. Summary of the proposed method.

1) During an experiment the pressure at the liquid surface can be measured as a function of time. Then

$$T^{*'} = T^* - T_o = \left(\frac{p - \eta}{\beta} \right) - T_o \qquad (6.27.)$$

The values of the constant β and of may be found from the vapour pressure data using values in the region of T^* and T_s. Hence the values of a_n are found from $T^{*'} = \sum_n a_n \vartheta^{n/2}$
We generally restrict $n \geqslant 1$.

2) The temperature distribution in the liquid is measured directly from the interferograms as a function of time and distance.

   a) If the surface temperature can be measured directly b_n is found from

$$T_s' = T_s - T_o = \sum_n b_n \vartheta^{n/2} \qquad n \geqslant 2$$

b). If the measurement of surface temperature is not accurate, b_n can be determined instead by measuring T at points $x = 2I\sqrt{K\vartheta}$, where I is chosen to give convenient ranges of x and ϑ.

3) Knowing a_n, b_n and f_n we can calculate the values of the coefficient α_n from equation 6.23, if the experiments and analysis have been accurate, all α_n should be equal.

It is assumed in this analysis that the experimental data may be expressed accurately in the form of a half power series of a small number of terms.

CHAPTER 7.
EXPERIMENTAL.

7.1. Principles of the design of the Condensation Cell.

As is seen from the above theory in order to use the proposed method of calculation the following variables must be measured:

a) the pressure of the vapour at the surface as a function of time;

b) the temperature distribution in the liquid as a function of time and of distance below the surface.

In order to calculate the magnitude of the pressure and temperature changes a value of $\alpha = 0.01$ was assumed for the condensation coefficient.

Nothing was known of the probable form of the pressure rise at the surface and as an approximation, a step change in pressure was assumed at $\vartheta = 0$. The basic equation and boundary conditions were as before with the simplification that T^* is a constant and not a function of time.

Trial calculations showed that to produce a shift of three fringes in 0.25 secs. a pressure change of 0.1" would be required at the surface. In order to minimise end effects the cell should be as long as possible in the direction of the light beam consistent with the accuracy required.

a) The method chosen for pressure measurement must be applicable to a range of pressures because the trial calculations assuming a step change in pressure may introduce considerable error. In addition the value assumed for α in order to design the cell may have been in error by as much as a factor of ten. A rapid response is essential (0 - full scale in < 0.1 sec.) which requires an expensive mechanical recorder. It was decided that a pressure transducer in the form of a pressure sensitive diaphragm would be most suitable, since it may be placed so as to measure pressure in the liquid rather than

in the gas which may be at a different pressure owing to the net condensation. Conversion of the diaphragm deflection into variation of an electrical property can be effected in several ways:-

1) A probe is placed below the diaphragm and this unit is made one arm of a high frequency bridge. Variation in the diaphragm position changes the capacitance of this unit and alters the bridge balance.

2) An iron rod is attached to the diaphragm perpendicular to its surface. The rod is arranged along the axis of an induction coil and movement of the diaphragm will affect the rod position. The coil is part of a linear transformer and hence the output will be a function of the diaphragm deflection. The rod must be of a large diameter for high accuracy and the method is more suited to larger, more robust bellows and diaphragms[66].

3) A triode is marketed by RCA[61] in which the anode is a shaft mounted in a diaphragm which forms the base of the valve body. The shaft extends through the diaphragm and displacement of the shaft about the diaphragm as a pivot will affect the valve characteristics. In the present system it would be difficult to produce sufficient movement of the electrode and at the same time avoid high point loading on the very thin diaphragm necessary for the low pressure difference to be measured. The rotational compliance of the valve diaphragm is quoted as 0.075 degrees/gram.cm. and this method is more suited to vibration measurement[18,59].

It was decided to use the first technique of capitance variation, partly because a commercial bridge unit was available in the college which converted the small residual emf of the R.F. bridge into an amplitude modulation of a 1.5 kc/s signal. This output could be recorded from an osoilloscope using a drum camera.

b) The temperature distribution will be given directly by the interferograms recorded by the cine camera.

7.2. Apparatus.

7.2.a. Cell Design

The physical design of the cell was dictated by three main factors

a) Geometric path length greater than 4".
b) Achievement of a piston compression and expansion.
c) Measurement of a pressure difference of 0.1" wg. under low absolute pressures.

A drawing of the cell is given in the appendix A.7.2. and it is also shown in plate 7.1.

The optical flats 2" diameter and 0.5" thick are fitted into the sides of a stainless steel tube of wall thickness 0.25" and of bore 3.75". In order to avoid strains in the glass the holders are designed to give an even sealing pressure; the inside faces of the flats are sealed against soft O - rings, whilst the securing plates are faced by soft cork gaskets which distribute the load from the clamping screws. The holder of flat 'A' can be tilted by adjusting the nuts on the 0.25" x 40 TPI studs, thus permitting alignment of flat 'A' with the fixed flat 'B'. The O - ring 'C' maintains the vacuum seal and the locknuts on the studs take the load. In order that the assembly may be inserted in the comparator for the adjustment of the flats the flanges must be demountable. They are screwed onto the shell body and sealed with Klingerflow PTFE tape plus an O - ring. A stainless still plate 'D' 0.125" thick is clamped between the lower flange of the cell and the top flange of the transducer cover. The pressure sensitive diaphragm of copper - beryllium is sealed to this plate which forms the floor of the cell. Initially the diaphragm was fixed to the plate using AV 121 araldite and HY 951 hardener,

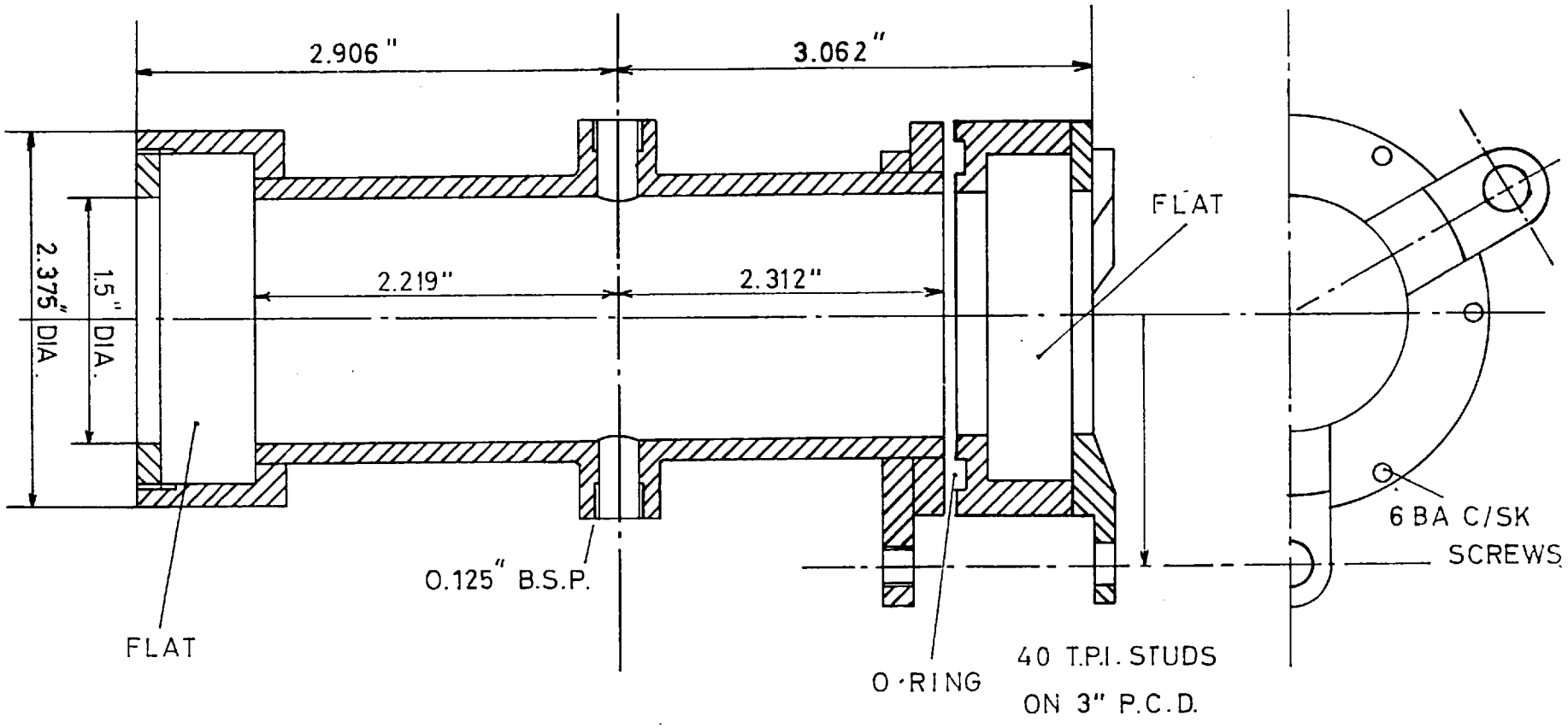

Scale: FULL SIZE. No. Off: 1. Material: BRASS.

FIG. 7.1. COMPENSATING CELL

both surfaces having been degreased and roughened. It was found that some of the liquids used slowly attacked the araldite, and it was decided to clamp the diaphragm in position using 1/32" Nebar as the gasket material. The pressure difference can never be greater than 25" wg. and the 6 BA clamping bolts provide adequate sealing pressures. By placing the diaphragm in direct contact with the earthed plate the sensitivity of the transducer is improved. Stainless steel bosses for vacuum pipe connections are welded into the cell walls and these are used for putting in and taking out fluids. Provision is also made for the insertion of two thermocouples - one in the liquid and one in the vapour space. For all components in contact with the test fluids EN 58 J stainless steel is used, where possible, because it has excellent corrosion resistance and can be machined.

Movement of the cover 'J', which is mounted on a PTFE bellows made from a 4" pipe expansion joint (manufactured by Crane Packing Ltd.), changes the cell volume. The bellows cover is made from mild steel and is sealed using O - rings. Movement of the bellows is controlled by the pressure difference across it, which may be up to a maximum of 12 psi. Although only small pressure differences are required to move the PTFE bellows (0.04" end movement/cm. Hg. pressure difference) in comparison with a stainless steel bellows of similar size, the PTFE bellows has the disadvantage that it takes on a permanent 'set' when subjected to a load for more than two or three minutes. This results in the bellows not giving the expected movement when the load is released. A tension spring is arranged as shown in Drawing no. 2 to support the weight of the cover 'J' and eliminate hysteresis.

7.2.b. Reference Cell Design.

The reference cell is inserted in the light path S_1M_2 as shown in fig. 2.5.. Its purpose is to maintain an optical balance with the test cell. The optical flat holders are of similar design to those of the test section except that flat cork

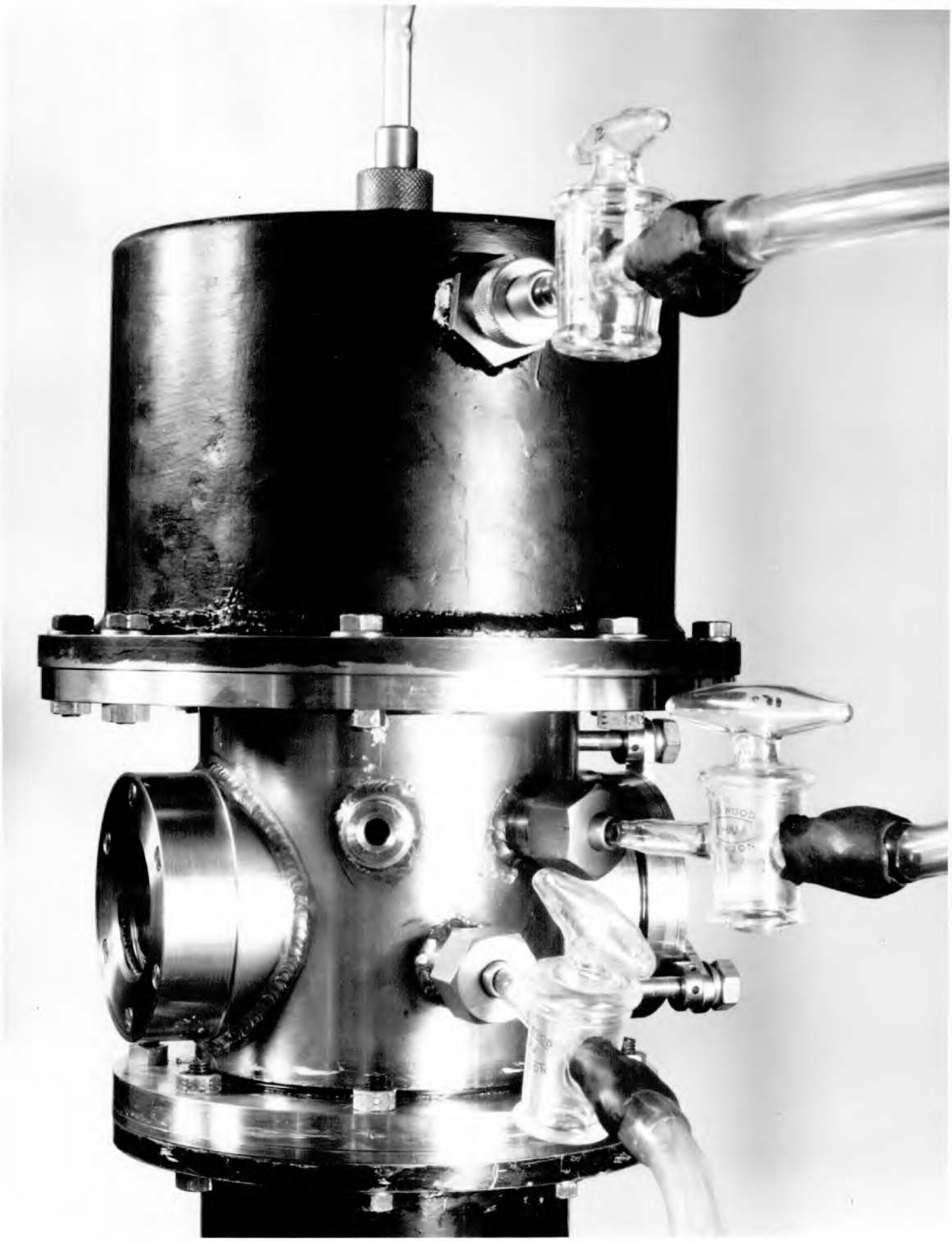

gaskets are used on both sides of the optical flats (fig 7.1.) rather than the more expensive O - ring type seals which are necessary for high vacuum work. The cell body is made from brass because non-corrosive fluids may be chosen to give equal optical path lengths.

7.2.c. Pressure Transducer.

The diaphragms used in this work were of beryllium copper, chosen because this alloy, when properly treated, has a high elastic limit combined with low hysteresis. If the work were to be extended to more corrosive liquids a diaphragm of stainless steel would be required which would be less sensitive and show greater hysteresis, making reproduceability more difficult. The diaphragms of 0.002" sheet were made by Kelvin and Hughes to a diameter of 2.625" ; two circular corrugations give the required sensitivity and six radial ribs give rigidity for handling.

The movement of the pressure sensitive diaphragm is detected by the change in capitance between it and a 0.5" diameter flat probe placed below it. This capitance C_2 is one of the arms of an R.F. bridge. The transducer design is shown in the appendix Drawing no. 2. The stainless steel probe 'L' is mounted in a brass bush which is bonded with araldite to a Distrene blank M. Distrene is the trade name of polystyrene, type 'Styron 666' as marketed by British Resin Products Ltd.. It is a polystyrene of low impact strength with excellent electrical properties: a power factor of 0.0004 and dielectric constant of 2.5, neither of which vary widely with frequency, make it suitable for use in the transducer components. The separation of the probe and diaphragm may be changed under vacuum by movement of the shaft 'N' which bears against a Distrene pad on the probe cap 'P'. A 16:1 reduction gear fitted below the cover plate Q combined with the micrometer thread of the shaft in the plate given an advance of the probe of 0.00156" per turn of the knurled adjuster. A Wilson

seal is used in the plate to allow rotation and linear movement of the shaft. The seal is made by passing the shaft of 0.156" diameter through a 0.0625" hole cut in neoprene sheet. The rubber disc 'R' lies against a conical metal seat and the shaft is lubricated with Apiezon N grease. Atmospheric pressure aids the rubber elasticity in making the seal. A brass guard ring 'S' is placed around the probe to restrict lines of force. Leads from this ring and the probe are taken out of the cell via two 4BA brass studs bonded with araldite into the distrene plug 'T'. This plug is bonded with araldite into a brass ring which is sealed into the boss by an O - ring.

7.2.d. Proximity Meter and Camera.

The Fielden PM.2. Proximity meter, used in conjunction with the pressure transducer, is basically a radio frequency A.C. bridge operating at 500 kc/s with its associated oscillator and detector circuits. The bridge is constructed so that the large inherent capacity of the probe and connecting cable is eliminated. The capacity of the probe diaphragm system is balanced against a variable capacity in the proximity meter and the null point is indicated as a minimum on the meter dial. Any variation of the pressure in the cell results in the bridge going out of balance by an amount proportional to the pressure change.

The output from the high impedance terminals of the proximity meter at 1.5 kc/s is fed into the Y plates of a Solartron CD 814 oscilloscope. Any change in the bridge balance modulates the amplitude of the signal on the oscilloscope. A drum camera, which has been modified to rotate at 19.4 rpm. is used with the oscilloscope to expand the vertical trace over a time axis. As the drum camera is moving slowly it is not possible to use the known frequency of the proximity meter output as a time calibration. A small torch bulb is used in front of the screen in circuit with a Master Contactor Unit (an ex WD clock with make and break

contacts) to give pulses at half second intervals. The 500 μF capacitor (fig.7.2.) gives a rapid build up of current in the bulb which ensures good definition at the beginning of the blip on the trace. The total pulse duration is about 0.04 sec..

The depth of focus on the camera lens was sufficient to bring the screen and bulb into focus at the same time. Ilford GK5, green-sensitive, recording paper proved adequate to record the trace at a peripheral speed of 16.5 cm/sec. Ilford Phentrace developer in a 4:1 dilution giving a developing time of 5 mins. at 16°C, followed by IF2 acid hypo fixer, was used. The brightness of the oscilloscope beam was chosen so as to give the optimum exposure between large and small wave amplitudes.

7.2.e. Temperature Measurement.

Three copper - constantan thermocouples are used to measure the temperatures in the transducer case and in the vapour and liquid present in the cell. The hot junction of the thermocouple protrudes 0.125" beyond its procelain insulator into which the two wires are separately araldited. This insulator is then bonded with araldite into a thin brass sleeve 0.125" dia. x 2" long which is sealed into the cell wall by an O - ring compression fitting. The e.m.f. of the thermocouples is measured on a Pye potentiometer used in conjunction with a Scalamp galvanometer.

7.2.f. Ancillary Apparatus.

The ancillary apparatus serves four main purposes:-

a) evacuation of the complete cell and other equipment without overstressing the diaphragm.
b) de-aeration and introduction of test fluids.
c) calibration of the diaphragm movement.
d) compression of the vapour in the cell.

A flow diagram is given in fig 7.3.. The ancillary apparatus

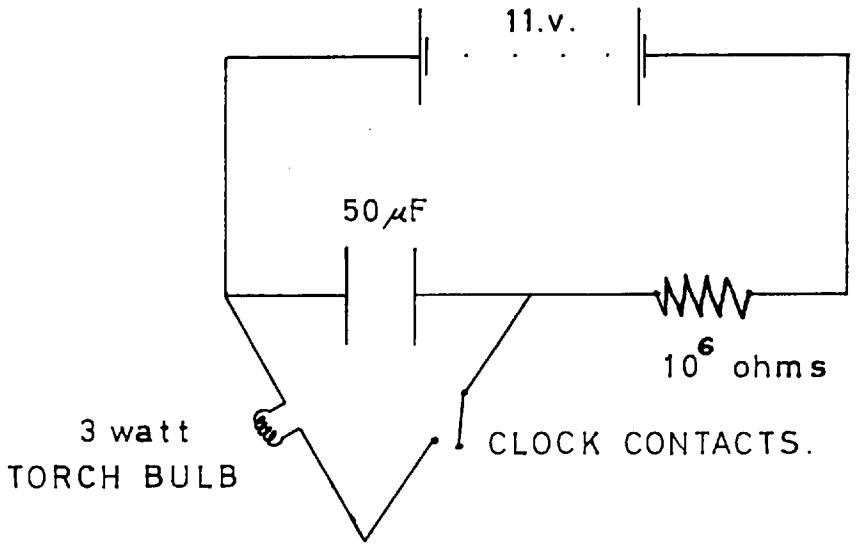

FIG.7.2. CONTACTOR CIRCUIT DIAGRAM.

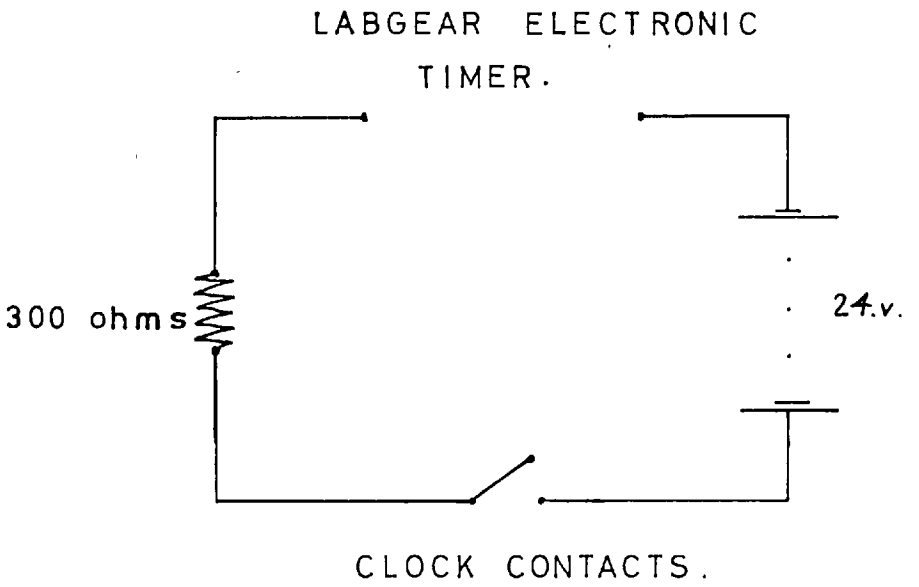

FIG7.7. CALIBRATION CIRCUIT DIAGRAM.

is mounted on a separate bench and all connections to the interferometer must embody a length of flexible tubing to prevent any vibration being transmitted to the interferometer. Thick walled 0.25" bore p.v.c. tubing was found to be satisfactory and joints of glass - p.v.c. were easily made by heating the p.v.c. to softening point in boiling water. The linkages were made a minimum length of 8", curved to approximately 5" radius, which gives sufficient flexibility to allow a very large amplitude of relative vibration of the interferometer and ancillary bench.

1) An Edwards Cenco - Hyvac pump, capable of pumping down to 0.001 mm. of Hg., is used to evacuate the system. A vapour trap cooled by liquid nitrogen or a freezing mixture of solid carbon dioxide, depending upon the freezing point of the vapour to be trapped, stops contamination of the pump oil. The rates of evacuation on the two sides of the diaphragm are controlled by the needle valves R_1 and R_2. The pressure difference existing across the diaphragm is indicated by the manometer 'L' which contains n-dibutyl phthallate. The vapour pressure of dibutyl phthallate at $25^{\circ}C$ is 4.10^{-5} mm. Hg.. The pressure balancing unit 'B' as shown in fig. 7.4. consists of a balloon to provide an extra capacity for gas, which may be taken up by either phase, thus slowing the rate of rise of pressure difference. The manometer fluid will blow over into the catchment bulb at a pressure difference greater than 25" wg. and act as a relief valve. The total pressure of the system is indicated by the mercury manometer M_1, but if accurate measurements of low pressures are required an Edwards 'Vacustat' with a range of 10 to 10^{-2} mm. Hg. can be fitted at R_4.

2) Fluids to be investigated enter the system via V_{23} into flask F_2 which is under vacuum. This effects a partial de-aeration. The fluid is then sucked up into flask F_1 at the top of the equipment where final de-aeration takes place;

FIG. No. 7.3.

ANCILLARY APPARATUS.

B - PRESSURE BALANCING UNIT.
F - FLASK.
L - DIFFERENTIAL MANOMETER.
M - MANOMETER.
R - VACUUM TRAP.
T - THREE - WAY COCK.
V - STOPCOCK.
W - BURRETTE.

——— GLASS LINE

------- PVC LINE

—·—·— FOR EVAPORATION RUNS THIS UNIT WAS REPLACED BY THAT SHOWN IN FIG. 7.5.

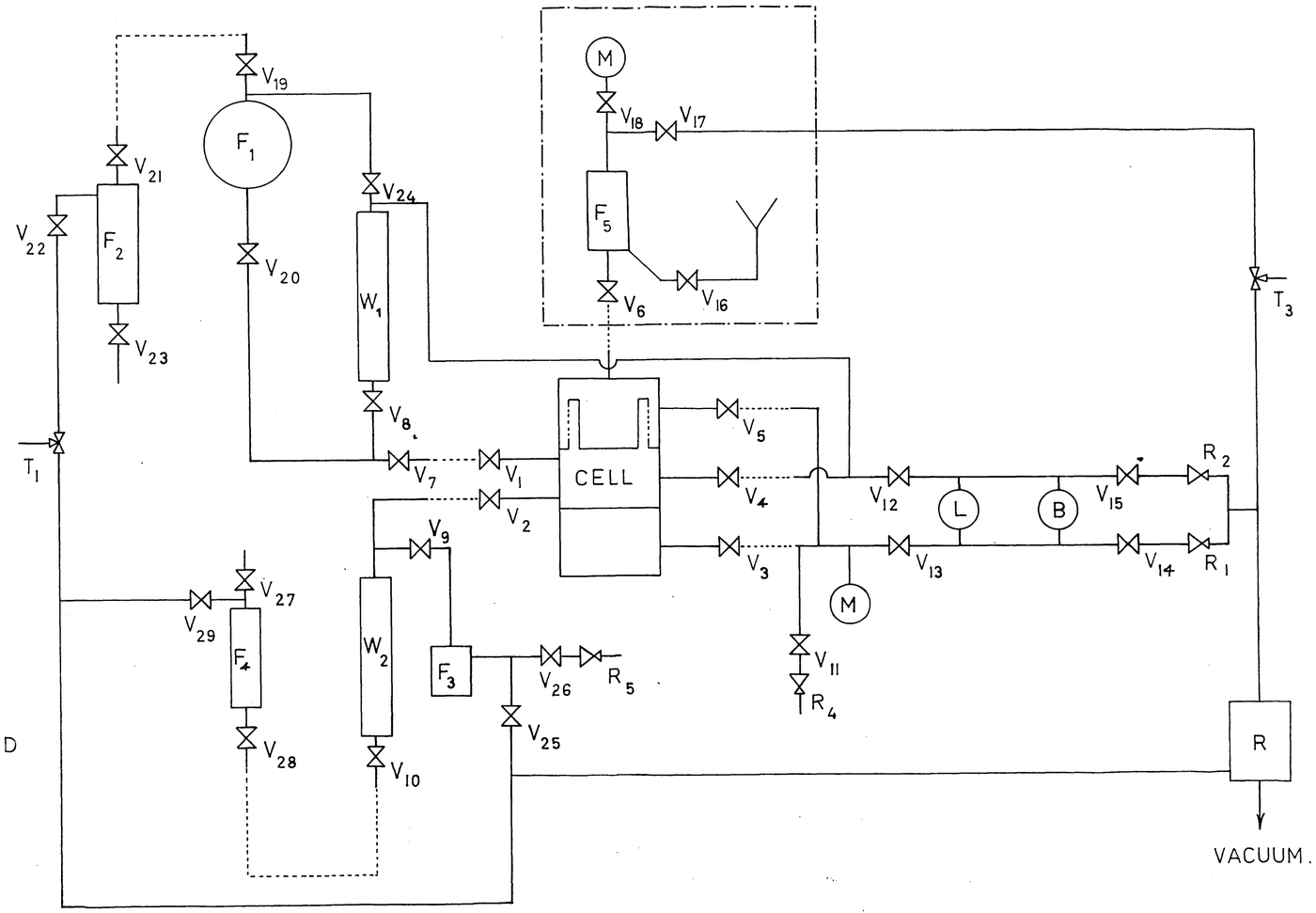

FIG. No. 7.5.

UNIT FOR EVAPORATION RUNS.

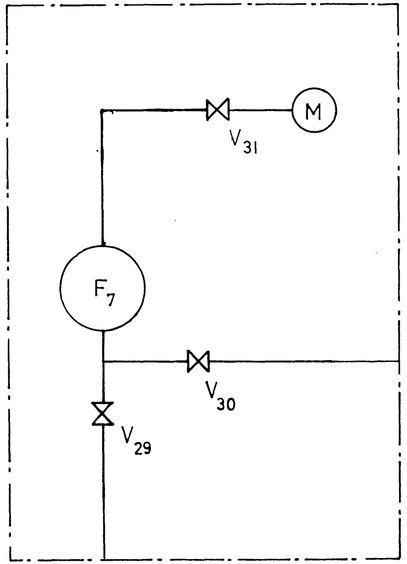

liquid is stored in this vessel and allowed to flow into the cell by gravity feed when required. In order that pressure differences may not occur when transferring liquids by the 5' head available, all vessels are vented back to the vapour space in the storage vessel via V_{24}.

3) The diaphragm is calibrated by measuring the deflection produced, on an arbitary scale for a known change in head of liquid. A volume addition of 25ml corresponds to an increase in head of 0.117". W_1 and W_2 are 25 ml burrettes graduated in 0.05 ml.. Liquids can be expelled from or introduced into W_2 by manipulating the mercury reservoir F_4, which is connected to W_2 by V_{28} and V_{10} with a length of flexible p.v.c. tubing. Liquid may be introduced into B_2 via V_9 from flask F_3 to eliminate vapour locks which sometimes occur in the line adjacent to V_2.

4) The apparatus as shown in fig. 7.3. is for condensation experiments. The effective volume of the flask F_5 may be varied by admitting or withdrawing vacuum oil via V_{16} using flask F_6 as an oil storage vessel. Thus both the pressure and the volume of air may be varied which, for a test, is allowed to compress the bellows suddenly by opening V_6.

For evaporation tests the unit shown in fig 7.5. replaces that enclosed by the dotted line in fig. 7.3. The bellows is preloaded with air and, for a test, the air is allowed to expand into F_7 which is maintained at a lower absolute pressure.

7.3. Procedure.

7.3.a. Cleaning and Assembling the Apparatus.

The optical flats of both cells were swabbed with absolute alcohol and then washed in a trough of distilled water to which a drop of Johnson's wetting agent had been added. They were then

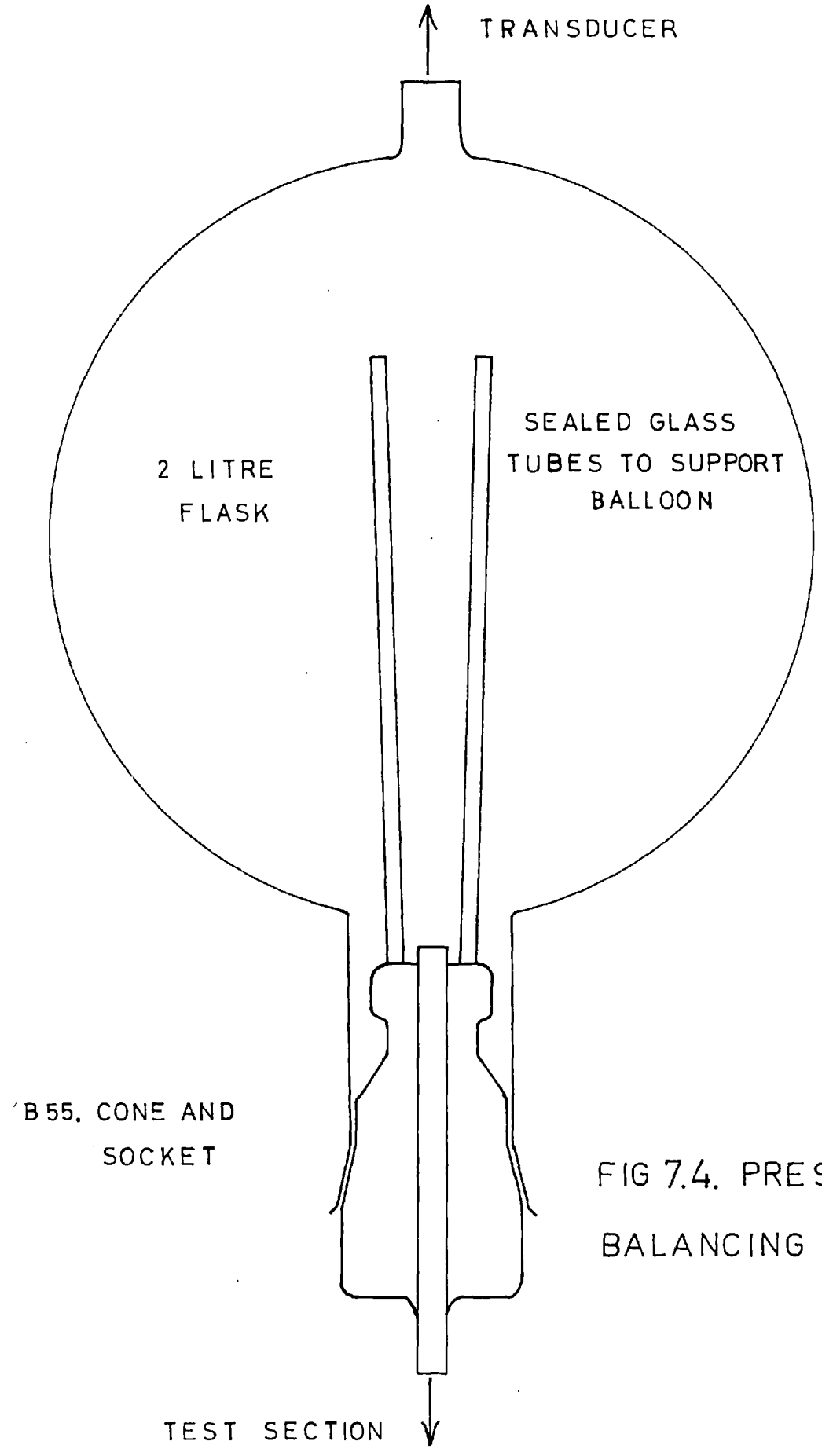

FIG 7.4. PRESSURE BALANCING UNIT.

washed in a stream of distilled water, dried and polished in soft lens tissue. All pyrex glassware was cleaned in hot chromic-sulphuric acid and after a thorough rinsing in distilled water dried in an oven. Stainless steel components were degreased in trichlorethylene and after etching in hot oxalic acid solution, were washed in distilled water and dried in an oven. The rubber O - rings and the transducer shaft seal were boiled in caustic soda solution and thoroughly rinsed in distilled water. The vapour pressure of neoprene synthetic rubber treated in this way is of the order of 10^{-4} mm. mainly from the release of hydrogen. The p.v.c. tubing was washed in chromic-sulphuric acid and rinsed in distilled water. Care was taken to avoid touching the inside surfaces of cell components during assembly.

All O - rings were used dry but Dow - Corning silicone high vacuum grease was used on the stopcocks and on ground glass seals. It has been reported that this grease is completely insoluble in water[2] and has no effect on the vapour pressure of the lower alcohols[3]. Glass - p.v.c. joints were made by softening the plastic in boiling water. As a further precaution all these joints were covered with Edwards Q compound (a substance like plasticine of low vapour pressure 10^{-4} mm. at 20°C consisting of graphite mixed with low vapour pressure residues of paraffin oil distillation) which adheres readily to degreased surfaces. Where this was not possible, the joint was painted with acetone - collodion solution from which the acetone quickly evaporates leaving a tenacious film.

7.3.b. Evacuation.

V_{19}, V_6, V_9, V_{10}, R_4 were closed. The cell was evacuated via V_4 and the relative rates of evacuation of the two sections of the cell were controlled by manipulation of the needle valves N_1 and N_2. It was found that the pressure difference across the diaphragm could be balanced to less than 0.5" wg. under the highest rates of

evacuation. If the valves were not used a large pressure difference built up rapidly owing to the inequality of the cell volumes and pressure drops in the pipe lines. It was not possible to heat the cell under vacuum to accelerate degassing because of risk of damage to the O- - rings and optical flats, and so a long degassing period was necessary. During this period a vacuum of better than 10^{-3} mm. was maintained. V_{14} and V_{15} were then closed and the remaining parts of the apparatus evacuated in the ordinary way via V_{22}, V_{25} and V_{29}.

7.3.c. Introduction and De-aeration of Test Fluids.

The water used for these experiments had been passed through a de-ionisation column and then triple distilled It was de-aerated during these operations but re-absorbed air on standing at room temperature. Vessel F_2 was isolated under vacuum by closing V_{21} and V_{22}, also V_{24} and V_{20} were closed and V_{19} opened. Water was sucked up into F_2 via V_{23} until the vessel was nearly full. Violent de-aeration took place as the water was let down to the pressure inside F_2: the vessel was connected to other components by long flexible links so that it could be shaken vigorously to assist evolution of the dissolved air. V_{21} was opened slowly and the pressure of the air in the space above the liquid was sufficient to transfer the liquid from F_2 to F_1 approximately 4' above it. V_{21} was closed before the liquid level fell below the level of the central tube. F_2 was then refilled and the process was repeated until F_1 was more than half full; usually two cycles were sufficient. Vessel F_2 was then brought up to atmospheric pressure via T_1 and the excess liquid was drained off via V_{23}. Vacuum was then applied to F_1 via V_{19} to remove any residual air, after ten minutes pumping the vessel was isolated. During these processes of transfer and de-aeration a large quantity of water vapour passed into the vacuum line and it was important that this was trapped before it reached the vacuum

pump. The same procedure was followed for the introduction of other test fluids and it was noted that the alcohols contained little dissolved air. The propyl alcohol used was Hopkin and Williams 'General Purpose Reagent' purity.

The pressure difference produced on sudden introduction of liquid into the cell would be equal to its vapour pressure at the operating temperature. In order to avoid this excessive pressure difference, air was admitted to the lower side of the diaphragm via $\overline{R}_4$ whilst vapour was admitted to the test section via V_{24}. By this method the maximum pressure difference was kept below 0.5" wg. When the pressures had been balanced V_{20} was opened and liquid allowed to flow into the cell. The level was observed in the image case on a screen by the interferometer beam and the vapour liquid interface was arranged to be approximately at the centre of the optical flat. Stopcock V_2 was left open during this process and usually after raising and lowering the mercury flask F_4 all vapour bubbles were eliminated from the line to the cell and from the burrette B_2. Occasionally this proved impossible owing to vapour lock. Liquid was stored in F_3 and could be passed into the cell via V_9 to displace any bubbles of vapour which would have destroyed the accuracy of the calibration.

7.3.d. Calibration of the Diaphragm.

It was decided to calibrate the diaphragm before each run because differences in static liquid head and initial probe to diaphragm separation change the calibration curve. During evacuation of the cell and introduction of test fluids the sensitivity control on the proximity meter was set to zero and the probe withdrawn at least 0.020" from the diaphragm. Before calibration the air and water vapour pressure were balanced approximately across the diaphragm as indicated on the butyl phthallate manometer. The three inch static head of liquid in the cell prestresses the diaphragm and removes any distortion

remaining after heat treatment. The mercury - water interface was set in the burrette B_2 to zero at V = 0 or 25 according to whether the calibration was for evaporation or condensation. The probe was pushed towards the diaphragm by rotating the control shaft below the transducer cover until it made contact with the diaphragm as indicated by the meter needle going hard off scale. The probe was withdrawn about 0.0015" by rotating the fine control one complete turn. The proximity meter was then balanced both for capacitance and resistance by manipulation of the bridge controls. The sensitivity control on the meter was set so as to give a reading of 60-70 on the meter scale for the maximum anticipated pressure change. The level of the mercury in burrette B_2 was recorded and the drum camera shutter opened for approximately one second whilst the drum was rotating at normal speed. The mercury level in the burrette was changed by raising or lowering flask F_4 and a further set of readings taken. This was repeated until the calibration curve was completely defined. If at the end of the calibration the meter reading given by the original burrette level was more than one scale division in error, the calibration was repeated. Any small difference in leak rate between the two parts of the cell made itself evident in a gradual drift of the meter needle. The leak rate of the transducer was always the greater and this was balanced by an adjustable leak to the vacuum line via R_4. The leak rate was constant and only occasional adjustments were necessary to maintain a constant meter reading.

7.3.c. Run Preparations.

For condensation runs V_5 was closed and the bellows cover evacuated via V_{17} and then isolated by closing V_6. Air pressure was built up in F_5 to the desired value by opening T_3 to atmosphere, V_{17} and V_{18} were then closed. For evaporation runs V_5 was closed and air admitted to the bellows cover via T_3 to

produce the required pressure. V_{29} was closed and the flask isolated after evacuation by closing V_{31} and V_{30}. Stopcock V_4 was closed and the leak to the vacuum line re-adjusted to give no drift of the proximity meter needle. After a new strip of film had been placed in the drum camera it was switched on to warm up and attain a constant speed. The Master Contactor unit was started and the torch bulb checked for position and brilliance. The fringe pattern was checked for orientation, spacing and for spurious fringes which, if present, would have indicated surface misalignment. The camera was fully wound and set at a nominal 64 fps. Finally the osoillosoope brightness was turned to a maximum and the room lights turned off

7.3.f. Run Procedure.

Time secs.

0	The cine camera was started by pressing the cable release.
2	The cine camera had attained constant speed. The drum camera shutter was opened.
3	Stopcock V_6 was opened.
6	The drum camera shutter was closed and the cine camera stopped quickly to conserve film.

The magnitude of the pressure change produced was recorded after a run from the proximity meter dial, but no similar check could be made on the fringe shift because all signs of the disturbance vanished within two or three seconds. For this reason results were usually taken in groups of two or three and the films developed and analysed before proceeding with further runs. Provided that the series of runs were carried out within four to six hours of the introduction of the test liquid, the amount of air leaking into the cell was negligibly small and therefore the cell was usually drained and completely dried out by evacuation only after each set of runs.

7.4. Run Programme.

RUN No.	LIQUID	TRANSFER PROCESS.
1.	Pure water	Condensation
5.		
8.		
11.		
33.		Evaporation
34.		
35.		
36.		
37.		
38.		
39.		
42.	Propyl alcohol	Condensation
43.		
44.		Evaporation
46.		
47.	N. Sodium chloride soln.	Condensation
48.		Evaporation
49.		
52.	Water + Sodium lauryl sulphate	Condensation
53.		
54.		Evaporation
55.		

7.5. Calibrations.

7.5.a. Calibration of cine camera speed.

The camera is driven by an electric motor and it was

considered essential that the speed of the film should be measured throughout the cycle of the spring. A group of four Decatron units of a Labgear time period counter, which indicates the passage of milliseconds up to a total of 9.999 secs., was photographed using H.P.3. film at a nominal speed of 64 fps.. The lens was used at maximum aperture of F 1.4 and an object distance of 1.75'. The work was carried out in the evening with the neon lamps as the only illumination and the exposure was more than adequate even for the millisecond unit which showed the total exposure for each frame. The graph of time vs. Frame No. is given in fig. 7.6. The average speed between frames 100 and frames 450, over which period measurements were recorded, was constant at 62.5 Frames/sec - 0.016 sec/frame. Over the total run of the film, 662 frames taking 11.06 secs., the speed was 59.8 frames/sec.

7.5.b. Calibration of drum camera speed.

In order to check the mechanism accuracy of the Master Contactor unit, the clock was arranged in circuit as shown in fig. 7.7. so as to supply pulses to the Labgear Timer on the make of the contacts. The counter was started and stopped at the beginning of successive pulses. The average time between pulses was found to be 0.5007 secs. with a maximum deviation of 0.0007 secs. The separation of blips on the trace was measured using a travelling microscope.

e.g. For run No. 1. Speed of trace $= \frac{8.28}{0.5007}$

$= 16.25$ secs. *

Thus 1mm on trace $= 0.00699$ secs.

* see ERRATA.

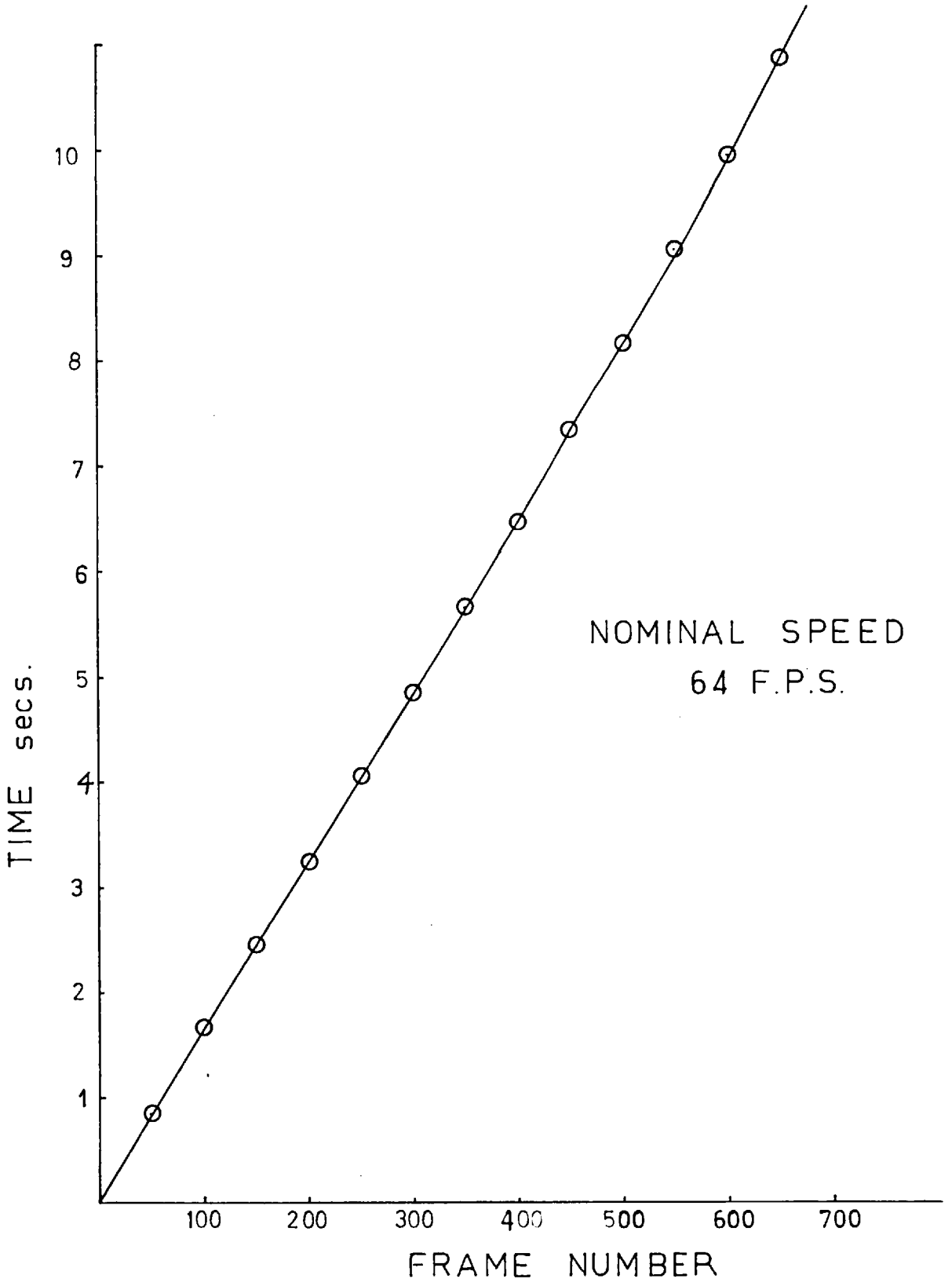

FIG.7.6. CINE CAMERA CALIBRATION.

7.5.c. Calibration of Magnification.

The magnification of the fringe pattern on the film emulsion was measured by photographing a slit of known width at the beginning of each series of runs The slit was placed in the fringe plane which was always adjusted to be at the centre of the test cell.

For run No. 1.

Overall magnification, cell to projector screen = 87.50

Primary magnification, cell to film emulsion = 1.303

7.5.d. Calibration of Fringe Shift.

For these experiments the fringes were adjusted so as to be orientated perpendicular to the liquid surface. Under equilibrium conditions no mass or heat transfer takes place and thus no refractive index gradients are present to distort the straight wedge fringes as seen in fig. 7.11.a.. During a run, temperature gradients exist and the fringe appearance is as seen in fig. 7.11.b.

An apparent shift of one fringe takes place when the optical path length changes by one wavelength of the light being used.

$$\text{No. of fringe shifts} = \frac{D.\Delta\mu}{\lambda}$$

$$= \frac{D.}{\lambda} \cdot \frac{\delta\mu}{\delta T} \cdot \Delta T$$

where $\frac{\delta\mu}{\delta t} = 82.5 \times 10^{-6}\ /^{\circ}C$ for water at $21.8^{\circ}C$.

$\lambda = 5461^{\circ}A$ $\qquad$ $D = 4.75"$

Thus a shift of one fringe represents a change in temperature of $0.0533^{\circ}C$. The fringe shift contributed by change in pressure is less than 10^{-4}, and over the temperature range considered

$\frac{d^2\mu}{dt^2} = 4.10^{-6}$ /°C and hence the fringe shift may be considered a linear function of temperature.

7.5.e. Calibration of Diaphragm movement.

During calibration, pressure on the diaphragm was determined from static head of liquid above it. The surface area of the liquid in the cell was 84.44 cm^2 and therefore the addition of 1 ml. of liquid gave an increase in static head of $4.67\ 10^{-3}$ " wg.. The burrette was graduated in 0.05 ml. and could be read accurately to 0.01 ml.. Typical calibration curves are given in fig. 7.8. and 7.9. which show the effect of changing plate spacing and meter sensitivity. For convenience these plots were taken at atmospheric pressure but similar results were obtained under vacuum. By using a combination of high sensitivity and small plate separation, high scale readings may be produced for small pressure differences. The maximum sensitivity was given by setting the control to S = 30 but for values of S > 24 the meter was sensitive to any outside noise or movement. The manufacturers quote a maximum deviation from scale linearity of less than 1.5% of full scale deflection at S = 25. It was noticed that after long periods of use the diaphragm lost some of its elasticity and higher sensitivities were required to produce comparable scale readings.

7.5.f. Calibration of Bellows movement.

It is necessary at first to know approximately the pressure differences required to move the bellows a chosen distance at a required speed. This information was obtained experimentally during some preliminary runs. A typical result, obtained for the evaporation of water, is given in fig. 7.10.. The maximum occurs because, although higher values of P (the pressure above the bellows) cause greater initial bellows deflection, an opening

METER SENSITIVITY S = 4

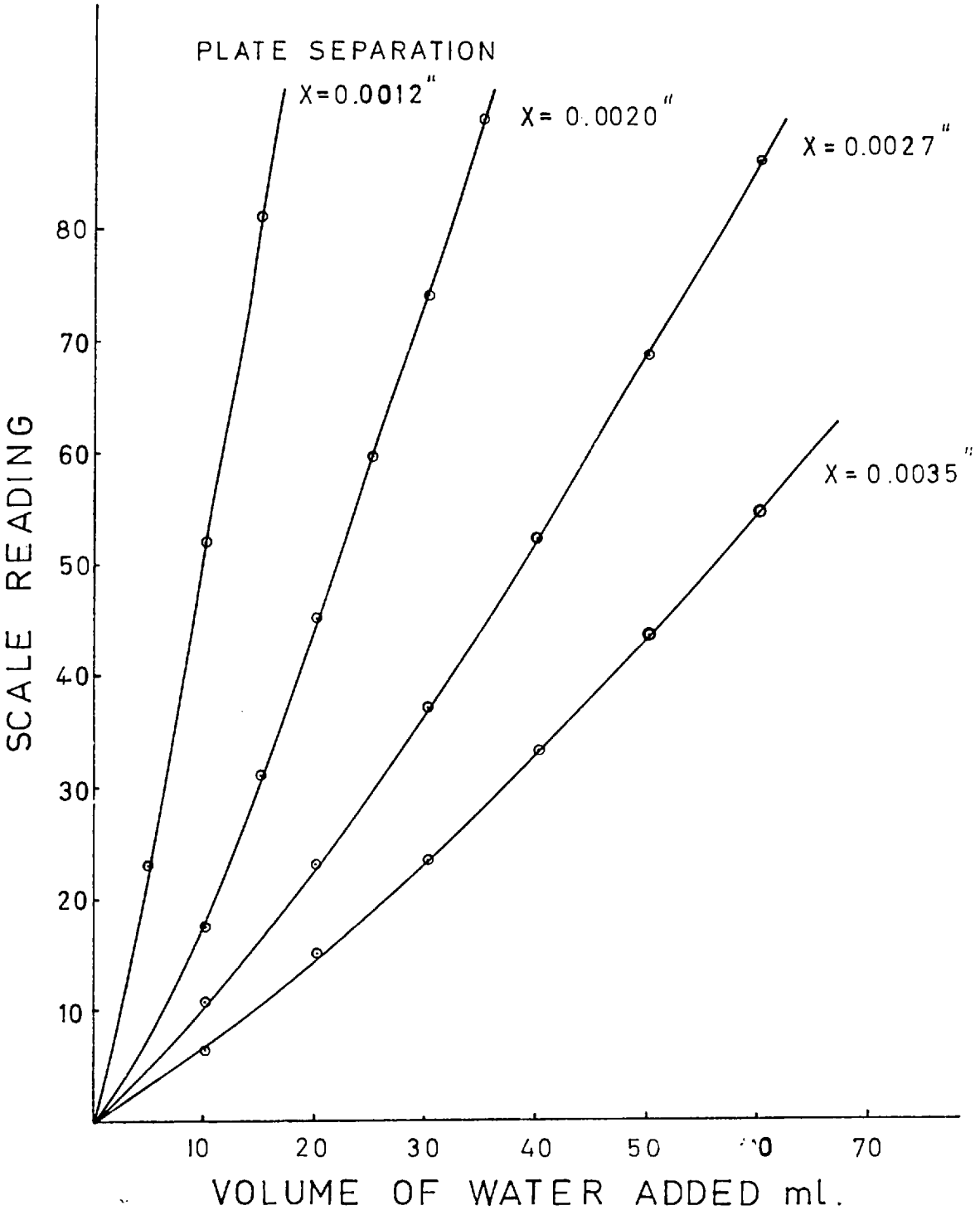

FIG.7.8 DIAPHRAGM CALIBRATION CURVES SHOWING EFFECT OF PLATE SPACING VARIATION.

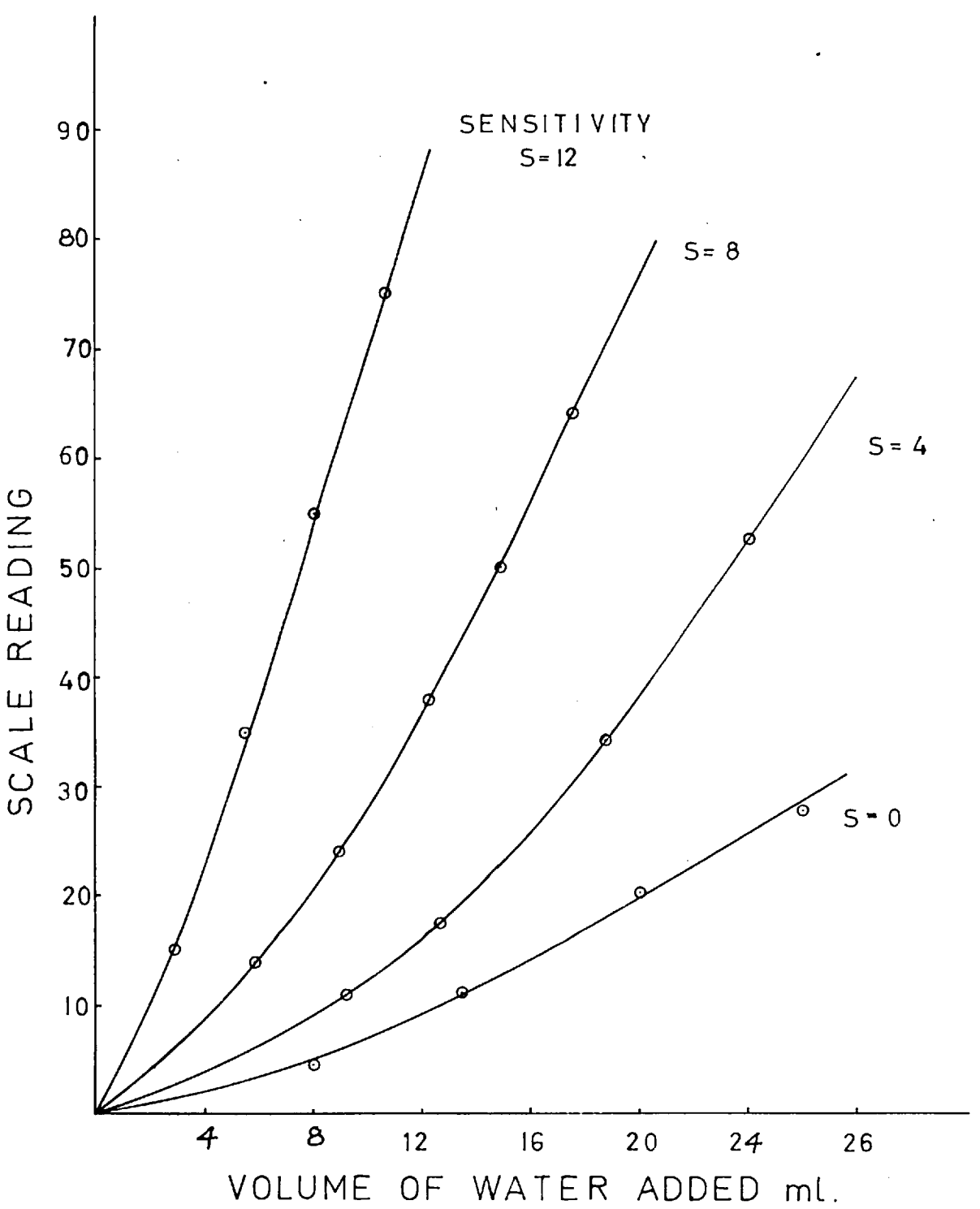

FIG.7.9. DIAPHRAGM CALIBRATION CURVES SHOWING EFFECT OF SENSITIVITY VARIATION.

V_{29} the rate of air flow is limited by the maximum flow rate conditions in the pipe line to F_7 and hence the rate of decrease of bellows loading is slow. Surface evaporation takes place at a slow rate during this period and the maximum pressure difference recorded becomes smaller. The results were reproducible after the bellows hysteresis had been eliminated by the insertion of tension springs.

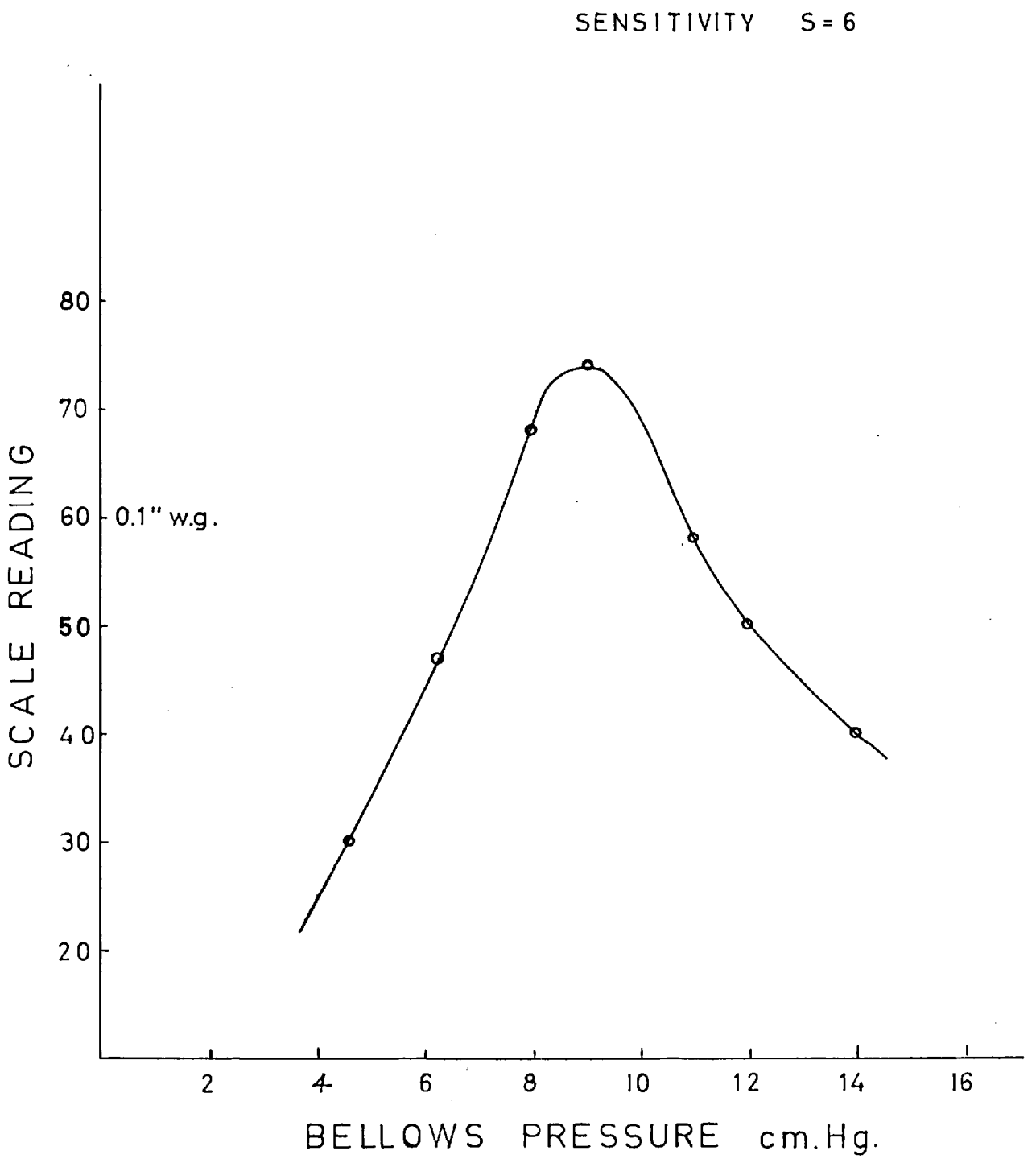

FIG.7.10. BELLOWS CALIBRATION

a)

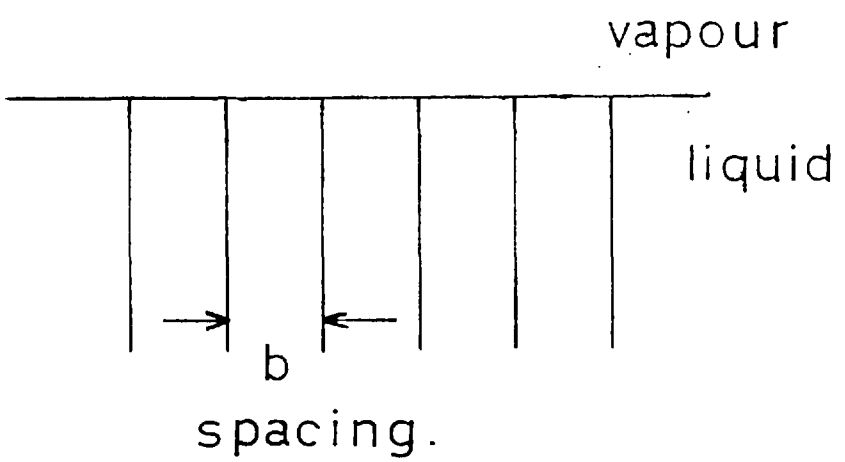

b)

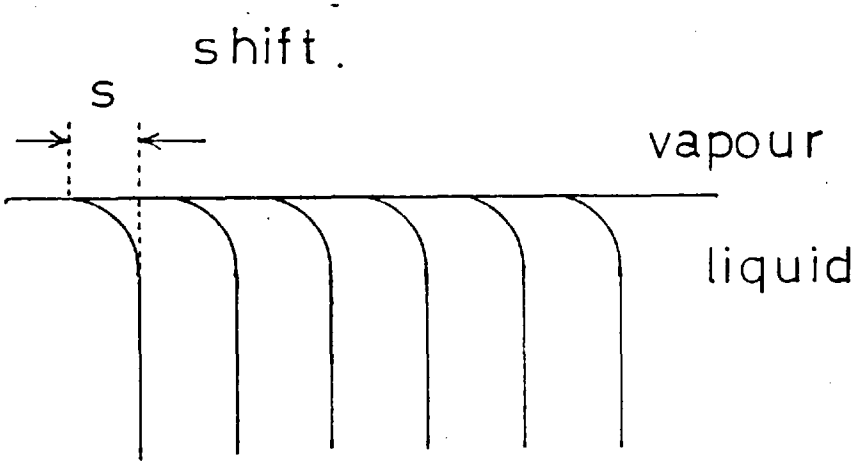

No. OF FRINGE SHIFTS = s/b

FIG. No. 7.11. FRINGE CALIBRATION.

CHAPTER 8.
DISCUSSION.

The programme of runs detailed in 7.4.1. was completed and the experimental data are presented in A.2.1. - 22 as direct measurements from the photographs together with the calculated values of $T^{*}{}'$ and T_s'.

8.1. Evaluation of the Condensation Coefficient by Curve Fitting.

The methods for the calculation of the condensation coefficient have been detailed in chapter 6. It was recognised at the outset that a satisfactory correlation by series would be obtained only if the series converged in a small number of terms. In A.4.1. the curve fits for the data of $T^{*}{}'$ and T_s' are given for a series containing two to five terms describing the results of Run No. 8. It is apparent from these series that rapid convergence does not occur. The number of data points available for curve fitting is restricted since interpolation must be avoided; if the number of terms in the series approaches the number of data points the calculated curve will be irregular in shape to accommodate the individual errors[58]. The root mean square deviation will decrease for each increase in series length, but as the rate of decrease falls with series length there is an optimum length. It has been suggested by Angus[2] that the optimum fit (acceptable residuals of a series with the least number of terms) may be determined by plotting the experimental values against the residuals for each series. A satisfactory fit is said to be that for which the distribution on the graph is random; if the distribution shows some regularity or recognizable shape a better fit will be achieved by including more terms in the series. The distribution was found to be random for all the series considered but for the series of two terms the magnitude of the maximum redisual often exceeded 15% of the experimental value.

a) From Surface Temperature Measurements.

The calculated values of α_n found by the method of art. 6.3.b. are given in A.3.4. and A.4.1. - 4., and are summarised in Table 8.1.. A sample calculation is given in A.3.4.. It can be seen from the table that the constants for any one series differ according to the number of terms taken, and that sometimes negative values are obtained. Although the coefficients for Run No. 1 vary, the average values are of the order of magnitude which would agree with the results of previous workers. The occurrence of negative values for the coefficients for Run Nos. 8 and 49 may be due to gross experimental error or excessive sensitivity to small errors.

b) Temperature Profile Measurement.

The values of α_n calculated using the fringe profiles are given in A.4.6. and a sample calculation in A.3.5.. The temperature - time data was correlated and the values of b_n deduced from the calculated values of c_n. The final stage of the calculation was as before. The values of the coefficient vary with the term of the series and the order of the fit, and as before negative values occur. It had been anticipated that this technique would provide a check on the accuracy of surface temperature measurement, as used in the first method, but owing to the inadequacy of both methods no reliance can be placed on either.

Table 8.1.

Run No.	No. of terms in series	α_n n = 1	2	3	4	5
1.						
Water cond.	2		0.0457	0.0132		
	3		0.1831	0.0376	0.0073	
8.						
Water Cond^n	2	0.0274	0.0112			
	3		0.0643	0.0281	0.0078	
	4	0.0477	0.0091	0.0017	-0.0016	
	5	0.0036	-0.0098	-0.0165	0.8350	0.0052
36.						
Water evap^n	2		0.0830	0.0160		
	3			0.1730	0.0325	0.0085
47						
N.NaCl Cond^n	2		0.0332	0.0315		
	3	0.0379	0.0087	0.0025		
	3		0.0376	0.0240	0.0066	
49.						
N.NaCl Evap^n	2		0.0893	-0.0042		
	3	0.1880	0.0208	0.0054		
	3		0.0938	0.0392	0.0073	

8.2. Experimental Errors.

The values of the coefficients calculated from both curve fitting techniques show a large variation, indicating a fault in

the theory. However, before modifying the analytical methods or original premises it is appropriate to consider the experimental errors and their effect upon the measured variables.

a) Trace analysis.

No provision was made on the oscilloscope for modulation of beam intensity with trace amplitude. At high beam intensities light scattering occurred on the face of the oscilloscope tube and this caused appreciable errors at small beam amplitudes. The intensity was chosen to reduce the scattering to a minimum but to be sufficient to give an acceptable trace density at large amplitudes. Traces of small width were measured accurately, using a travelling microscope but at large amplitudes the definition was not sufficient for this method. Comparable accuracy was obtained for the traces of width greater than 0.75 cms. by using a magnifying glass and scale graduated in divisions of 0.2 mm..

It proved impossible to eliminate all 'mains ripple' from the trace and this error was estimated at $\pm$ 2% of the trace width. Calibrations of the diaphragm were made before each run to eliminate the effect of creep, liquid level and meter drift. The method of calibration by injection of fluid into the cell proved successful but may be used over only a small pressure range, because of the physical limitations of the cell. Over the small range of liquid levels used the variation in cross sectional area of the cell was negligible.

b) Cine film analysis.

Several methods have been used for the analysis of interferograms and these may be classified according to the method of fringe centre location:-

i) Centre location by photometer.

Binnersley[8] used a Hilger and Watts photometer to produce profiles of light intensity from which he estimated the position of the fringe centres. He found it necessary to orientate the fringe axis perpendicular to the photometer traverse; this required frequent adjustment of the

interferogram when the radius of curvature of the fringe was small. In the present work the high film magnification necessary emphasises the grain of the film and it was found that the photometer responded to the individual agglomerates of emulsion. No major trough or peak occured on the trace to locate the fringe centre.

ii) Centre location by eye.

The eye can detect smaller contrasts in an image seen by transmitted rather than reflected light. A high magnification was used in this work from film to screen and it was decided to trace the fringe centre loci on a transparent screen. Measurements from the tracings gave fringe shifts which were reproducible to $\pm$ 5% at low shifts and the accuracy improved with the magnitude of the shift.

c) Time Scales.

The measurement of temperature profiles from the interferograms and of vapour pressure from the oscilloscope trace were not made from a common datum. A light flash would have given a time marker on the cine film but a pressure pulse on the diaphragm would have been difficult to achieve without disturbing the test conditions. However, since the start of the transient conditions was well marked, it was assumed in the calculations that the measurements were made from a common datum, the zero on the oscilloscope trace being well defined, but an error of up to one frame being necessarily incurred on the cine film. Calculations for Run No. 8 are given in A.4.5. and show the effect of zero error. The correction was considered up to a maximum of four frames, and if this error was significant the calculated values of the condensation coefficient should have converged within one frame correction. No convergence was achieved but as would be expected the absolute values of the coefficient diminished since the rate of mass transfer was decreased. The time scale of the oscilloscope trace was recalibrated for each run, but the speed of the cine film was assumed constant over the whole series of runs. This was confirmed

by a final recalibration which agreed to within ½% with that prior to Run No. 1.

d) Surface alignment and refraction

If the system was ideal the light beam would remain parallel to the surface during its passage through the liquid. In a practical system the beam is refracted by the menisci and by the temperature gradient in the liquid. All liquids studied in this work have positive contact angles at the air glass interface; liquids exhibiting negative contact angles would require the light beam adjacent to the surface to be transmitted through an air layer with the accompanying refraction.

The optical flats are easily set perpendicular to the incident light beam but unless the flats can be set accurately in the vertical plane there is no certainty that the light beam is parallel to the liquid surface. Surface alignment by the technique of Howes and Buchle[37] (art. 4.2.e.) was straightforward but tedious because a sequence of adjustments had to be adopted. The beam of light is refracted by its passage perpendicular to a refractive index gradient. This error is minimised by arranging the fringe plane at D/3 from the exit window. The problem is more serious in aerodynamics where higher gradients of refractive index are encountered.

e) Pressure measurement.

The pressure transducer was described in art. 7.2.c. and its calibration detailed an art. 7.5.e. The calibration of the diaphragm by head of liquid was accurate to less than 2% error, but the drift of the proximity meter and errors from the oscilloscope trace gave an overall maximum error of $\pm$ 5%. The static calibration was assumed to be directly applicable to the dynamic performance of the diaphragm. This appears to be not strictly correct but a very good approximation. The diaphragm will respond more rapidly to a rise rather than to a fall in pressure because of the head of liquid above it. The anomalous pressure difference readings recorded for the evaporation of pure water are

discussed in art. 7.4.a.

The magnitude of the experimental errors has been discussed and it is concluded that the variation in calculated values of the condensation coefficients cannot be wholly attributable to this source. Spurious values for the condensation coefficients were obtained for all runs calculated from the series fits of four or more terms and it was concluded that the fitting of a curve to a few experimental points containing small errors results in series coefficients which are not characteristic of the data. A smooth curve was obtained from fitting the data to a series of few terms but the magnitude of the residuals was high.

8.3. Modification of the Analysis to Calculate the Average Value of α up to Time ϑ.

Consider fig 8.1. in which $T^{\infty\prime}$ and T_s' are plotted against ϑ. It can be seen that the first part of the curve of $T^{\infty\prime}$ is proportional to ϑ to a power of about unity. But, as is shown by the analysis art. 6.2., it then follows that T_s' should be proportional to ϑ to a power of about 1.5; and that this is evidently not so is seen in fig. 8.4..

By the original assumptions the only factor which should depend on time and which effects the rate of heat or mass transfer across the interface is $(T^{\infty\prime} - T_s')$:

$$\bar{N}\,\bar{N} = \alpha\phi\beta\,(T^{\infty\prime} - T_s') \qquad (6.5.)$$

if $(T^{\infty\prime} - T_s')$ is plotted against ϑ, as in fig 8.2., whilst the driving force is low, T_s', the resulting temperature, rises quickly in spite of the fact that heat is conducted initially at a high rate into the bulk of the liquid. However when $(T^{\infty\prime} - T_s')$ has increased, the rate of rise of T_s' falls off. A conclusion which can straightway be drawn from this behaviour is that the proportionality constant in equat. 6.5. is a function of time, and consequently that the condensation coefficient depends on the rate

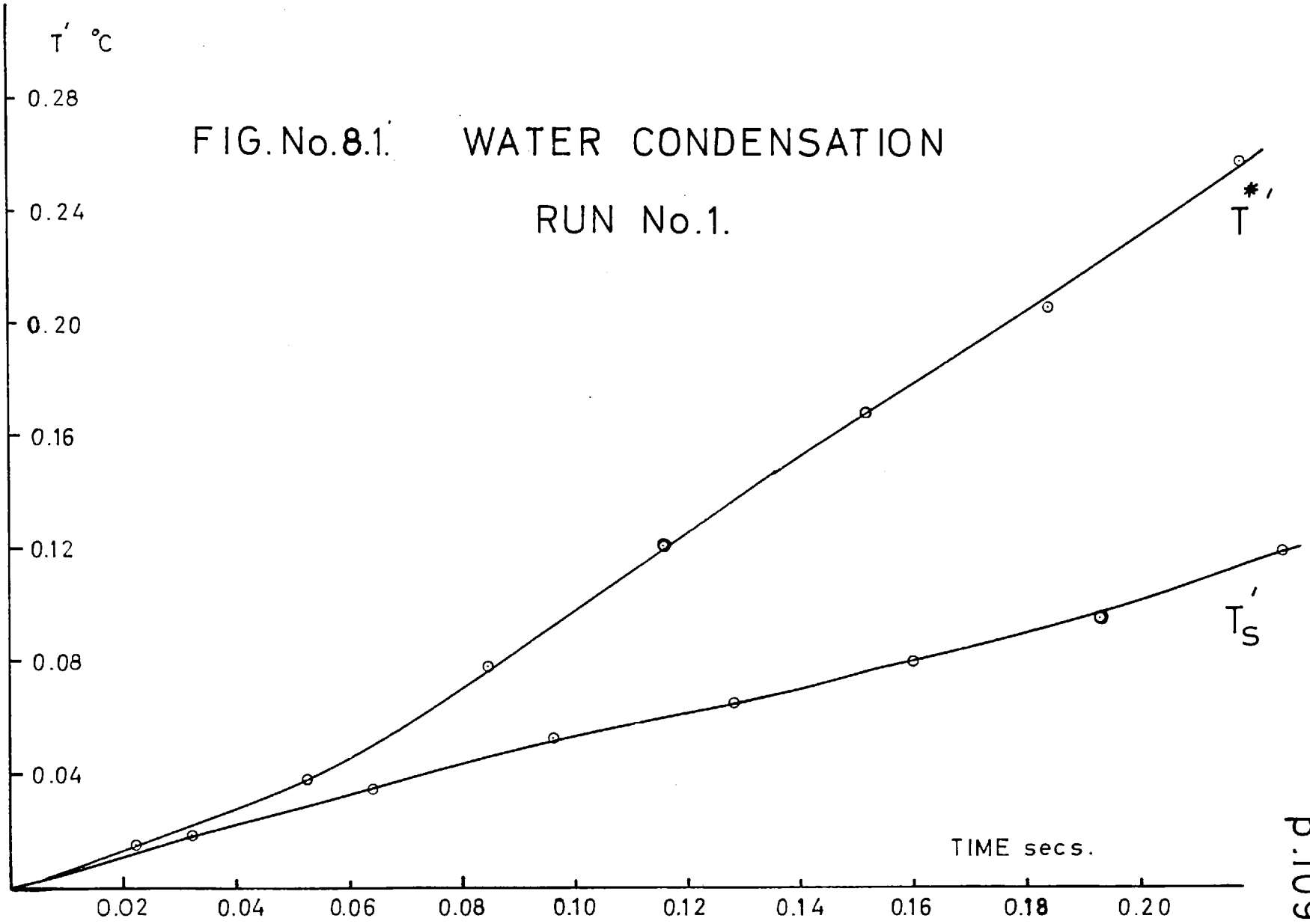

FIG. No. 8.1. WATER CONDENSATION

RUN No. 1.

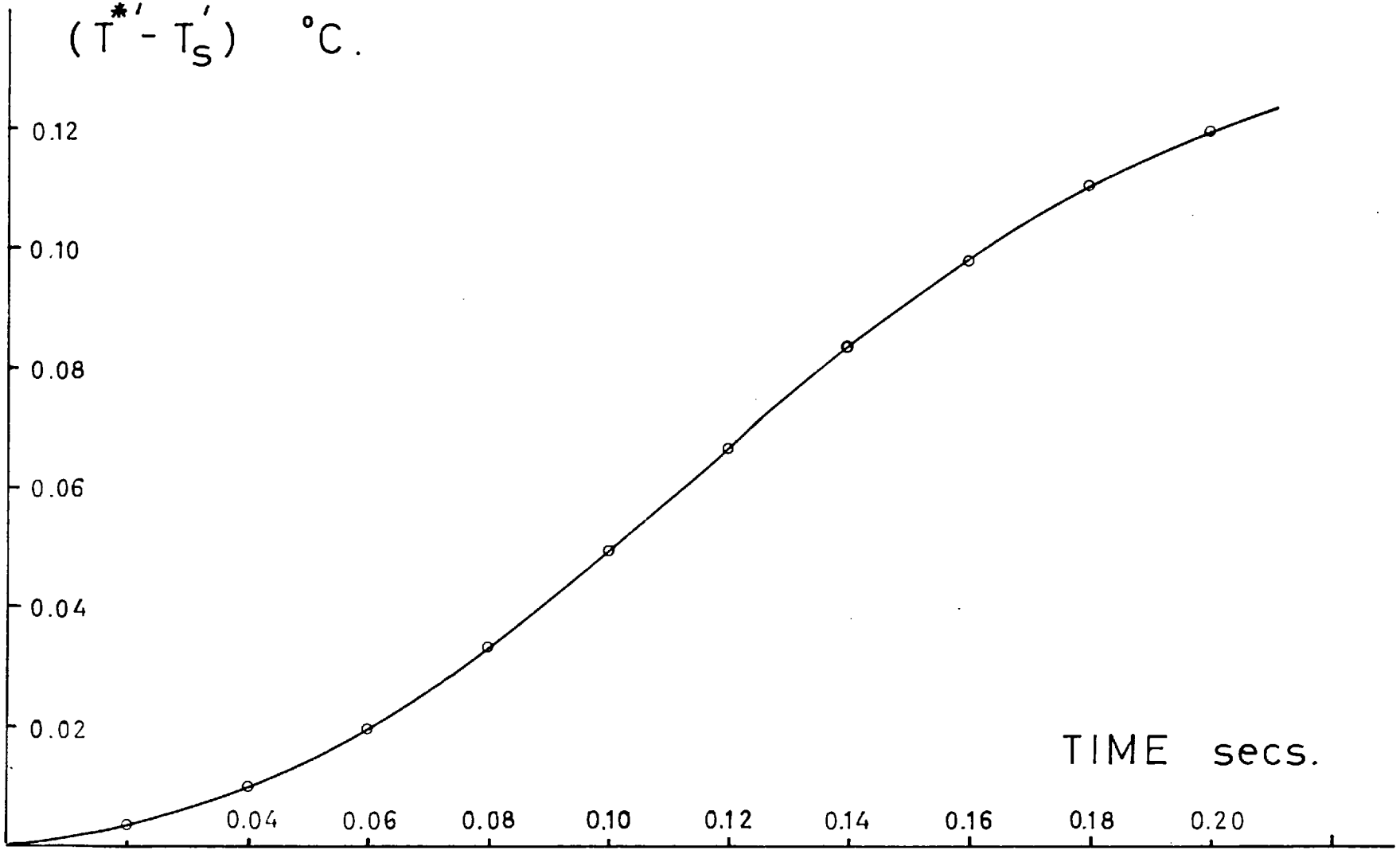

FIG. No. 8.2. WATER CONDENSATION RUN No. 1.

of condensation or surface age. We therefore modify our analysis to take this into account and to calculate average values of the condensation coefficient.

From equation 6.10.

Heat flux through the surface $= -k \left(\frac{\delta T}{\delta x}\right)_s$

$= +k \cdot \gamma \cdot \Delta T'$

$= f(\vartheta)$

where $\Delta T = (T^{\text{at}'} - T_s')$ is measured and is a function of time ϑ. As before temperature distribution in the liquid is governed by a solution of

$$\frac{\delta T}{\delta \vartheta} = K \frac{\delta^2 T}{\delta x^2} \qquad (6.11.)$$

and Carslaw and Jaegar[12] show that the solution of this equation, when the heat flux is a function of time, is given by

$$T' = \frac{K^{\frac{1}{2}}}{k.\pi^{\frac{1}{2}}} \cdot \int_0^{\theta} f(\theta - \gamma)\gamma^{-\frac{1}{2}}\, d\gamma \qquad (8.1.)$$ *

At a surface where $x = 0$

$$T_s' = \frac{K^{\frac{1}{2}}}{k.\pi^{\frac{1}{2}}} \int_0^{\theta} f(\theta - \gamma)\gamma^{-\frac{1}{2}}\, d\gamma \qquad (8.2.)$$

Put $y = (\vartheta - \gamma)$

then $$T_s' = \frac{K^{\frac{1}{2}}}{k.\pi^{\frac{1}{2}}} \int_{\theta}^{0} f(y).(\vartheta - y)^{-\frac{1}{2}}.(-dy)$$

$$= \frac{K^{\frac{1}{2}}.\gamma}{\pi^{\frac{1}{2}}} \int_0^{\theta} \Delta T(y).(\vartheta - y)^{-\frac{1}{2}}.dy \qquad (8.3.)$$

* see ERRATA.

The value of α calculated from this equation will be the mean value over the time interval $\vartheta = 0$ to $\vartheta = \vartheta$, and if the coefficient is a constant, the calculated coefficients will be equal for all time intervals.

The value of the integral at $y = 0$ is infinite and in order to integrate the function using the experimental values of ΔT, we must split the limits of the integral:

$$T_s' = R' \cdot \int_0^{\vartheta-\epsilon} \psi \, dy + R' \int_{\vartheta-\epsilon}^{\vartheta} \psi \, dy \qquad (8.4.)$$

where $R' = K^{\frac{1}{2}} \cdot \gamma \cdot \pi^{-\frac{1}{2}}$ and $\psi = \Delta T(y) \cdot (\vartheta - y)^{-\frac{1}{2}}$.

The value of ϵ is chosen such that over the time range $(\vartheta - \epsilon)$ to ϑ the value of the function ΔT may be considered constant and equal to C_1. For convenience ϵ was set equal to 0.001 secs. for each run.

The detailed calculations for Run No. 1 up to time $\vartheta = 0.12$ secs. are as follows. From the data in A.2.1. graphs of $T^{*}{}'$ and T_s' against ϑ are plotted and, selecting identical abcissae, the temperature difference $(T^{*}{}' - T_s')$ may be tabulated directly as a function of time ϑ. This data is plotted on fig 8.2.. Values of ψ were calculated as follows:-

Table 8.2.

y secs.	ΔT ^{o}C	$(\vartheta - y)$	$(\vartheta - y)^{+\frac{1}{2}}$	ψ
0	0	0.12	0.346	0
0.03	0.0061	0.09	0.300	0.020
0.06	0.0198	0.06	0.245	0.081
0.08	0.0329	0.04	0.200	0.161
0.10	0.0491	0.02	0.143	0.343
0.1095	0.0573	0.0105	0.1025	0.558
0.1190	0.0655	0.0010	0.0316	2.070

The first part of the integral is given by the area under the curve between $y = 0$ and $y = (\vartheta - \epsilon)$. This may be measured graphically, but it was found more convenient to use Simpson's rule, which states that the area under the curve $\Psi(y)$ between y_1 and y_3 is given by

$$\frac{1}{6}(y_3 - y_1)(\Psi_1 + 4\Psi_2 + \Psi_3)$$

where Ψ_2 is the mid ordinate. The expression is exact only when the function is a cubic, but the error caused by using Simpson's rule is less than the error in the data. By careful selection of the abcissae in the calculation of Ψ we may avoid plotting the curve of Ψ versus ϑ. Thus:

Table 8.3.

Time interval.	0 - 0.06	0.06 - 0.10	0.10 - 0.119
Ψ_1	0	0.0809	0.343
$4\Psi_2$	0.080	0.646	2.232
Ψ_3	0.081	0.343	2.070
$\Sigma\Psi$	0.1609	1.0699	4.654
y/6	0.01	0.00667	0.00318
A	0.00161	0.00712	0.01475

Total area = 0.0235

The second part of the integral may be integrated explicitly

$$R' \int_{\theta-\epsilon}^{\theta} \Psi \, dy = R' \int_{\theta-\epsilon}^{\theta} C_1(\vartheta - y)^{-\frac{1}{2}} \, dy.$$

$$= -2.R'.C_1.\left[(\vartheta - y)^{\frac{1}{2}}\right]_{\vartheta-\epsilon}^{\vartheta}$$

$$= 2.R'.C_1.\sqrt{}$$

$$= 0.0632\ R'.C_1$$

For Run No.1. at $\vartheta = 0.12$ $C_1 = 0.0660$ and $T_s' = 0.0610$

Therefore by adding the two areas we obtain

$$T_s' = R'(0.0235 + 0.0632 \times 0.0660)$$

$$= R' \times 0.0277$$

$$= 0.0610$$

$$\text{therefore } R = 2.20$$

From equation 6.9.

$$\alpha = \frac{k\ \delta}{H.\beta.\phi}$$

$$= \frac{k}{H.\ \beta.\phi} \cdot \frac{\pi^{\frac{1}{2}}}{K^{\frac{1}{2}}} \cdot R'$$

$$\text{and } \bar{\alpha} = 0.0148$$

*.

This is the average value of the condensation over the range $\vartheta = 0$ to $\vartheta = 0.12$. A similar calculation was carried out at other values for the same experiment and $\bar{\alpha}$ is plotted against ϑ in fig 8.3..

Figs A.4.1 – 12 show plots of $\bar{\alpha}$ versus ϑ for all runs.

It is more useful to plot point values of the condensation coefficient (as opposed to average valuos over a time interval ϑ) against point values of tne rate of mass transfer. The average value of a variable $\dot{Z}$ over a time interval $\Delta\vartheta = \vartheta_1 - \vartheta_2$ may be calculated if average values $\bar{Z}$ are available over the time

* see ERRATA

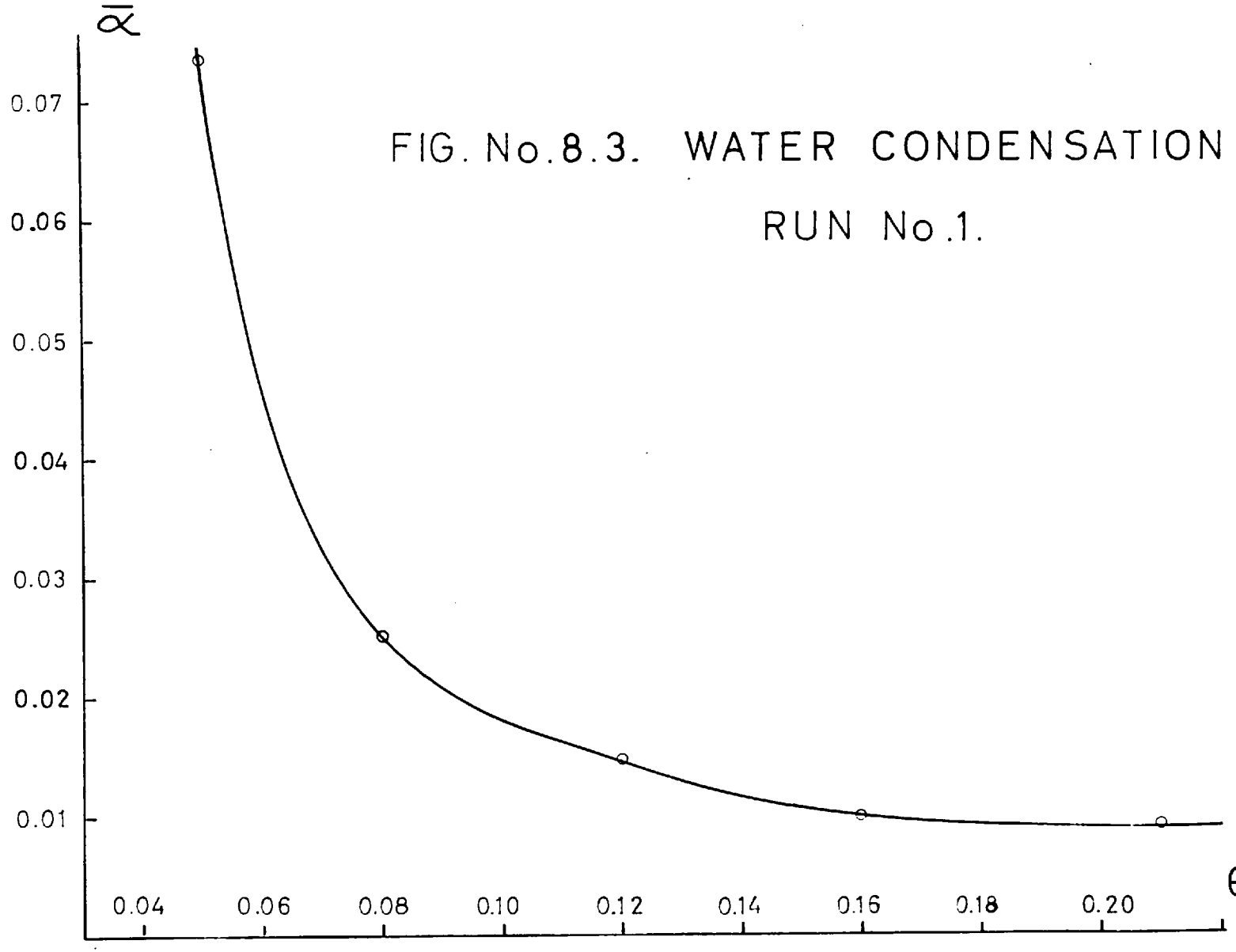

FIG. No.8.3. WATER CONDENSATION

RUN No.1.

intervals $0 - \vartheta_1$ and $0 - \vartheta_2$ from the formula

$$\dot{Z} = \frac{\bar{Z}_2 . \vartheta_2 - \bar{Z}_1 . \vartheta_1}{\vartheta_2 - \vartheta_1} \qquad (8.6.)$$

By choosing the values of $\Delta\vartheta$ as low as possible, the value of $\dot{Z}$ will tend to a point value, but difficulty in accurately determining the numerator reduces the value of the formula. Point values of the condensation coefficient were calculated for Run Nos 5 and 11 using a value of $\Delta\vartheta = 0.01$ secs., the results are plotted in figs. A;4.13. and A.4.14.. However, point values of the rate of mass transfer can be calculated from this data only by using the measured values of the condensation coefficient. A correlation based upon these values would not reflect the true variation and would be sensitive to errors in α^{59}.

8.4. Interpretation of the Results.

All previous workers have assumed that the condensation coefficient is a constant at a given temperature and not a function of the rate of mass transfer. It has been found that * the coefficient for all liquids studied decreased on account of a reduced driving force, the average values of the condensation coefficient approached a constant value.

When comparing coefficients for condensation and evaporation, the different rates of mass transfer must be considered. Also, during evaporation the surface temperature will be lower than the bulk and natural convection will take place in the liquid. The temperature differences were always small ($< 0.2^{\circ}C$) and during the maximum time interval of 0.25 secs. no disturbances which might have been attributable to convection were observed on the interferograms.

* see ERRATA.

8.4.a. Pure Water.

The experiments on the condensation of water all gave similar results. The average coefficients at short times were greater than 0.07 whereas at longer times the curves tended to constant values between 0.0145 and 0.0090 .

No previous data is available on water condensation and it was hoped to compare and contrast the results with those for evaporation. The experimental results of $T^{*'}$ and T'_s for the runs on water evaporation when plotted against time ϑ show that at low val ues of ϑ, T'_s was greater than $T^{*'}$, indicating a negative driving force. Although slow diaphragm response would give low values of $T^{*'}$, this was not the case in experiments om the evaporation of other liquids and solutions which gave positive driving forces at all times. No physical changes were made in the apparatus between carrying out these sets of runs and these anomolous results remain unexplained. A graph of $(T^{*'} - T'_s)$ versus ϑ is given in fig.A.4.2. for the positive portion of the data for Run No. 36. on the evaporation of water. If we assume that the driving force has been underestimated, calculated values of the coefficient will err on the high side.

Run No.	ϑ	$\bar{\alpha}$
36	0.24	0.00754
37	0.24	0.00516
39	0.24	0.00725

These values are suprisingly low and owing to t he uncertainty of driving force measurement little reliance should be placed on them.

In both condensation and evaporation the scatter of points on the plots of α versus ϑ was high and the majority of runs were typified by the data of Run No.5. as plotted on Fig.A.4.13.. The results of Run No.1 4. proved exceptional and are plotted on Fig. A.4.14.; this data emphasises the difference between point

and average values of the coefficient. It is unlikely that the average values truely become constant for in this case the point values pass through a minimum. Previously determined coefficients for water evaporation, which are described in art. 5.2., vary appreciably with the experimental method used. For the rate of mass transfer to remain constant, the surface temperature, supply of heat and degree of undersaturation must not vary. Few of the methods satisfy these criterea and hencewill yield average rather than point values of the condensation coefficient.

8.4.b. Propyl Alcohol.

The temperature refractive index coefficient of propyl alcohol is four times that of water and the interferometric method of measurement will be proportionately more sensitive. Fringe shifts of a similar magnitude to those for water were observed for propyl alcohol and these correspondingly low values of T_s' together with different physical properties (see A.1.) gave values of α in the range of 4 to 8 x 10^{-4} at high values of ϑ. The values for condensation are higher than those for evaporation, but this difference is possibly caused by the higher rate of mass transfer.

The only other published value is that of Baraneav[7] (α = 0.037) for the evaporation of alcohol of unspecified purity. In the present experiments 'general purpose reagent' purity was used, the impurities present being limited to 0.01% of aldehydes and ketones of similar boiling point and less than 0.001% of involatile matter. Dow-Corning high vacuum grease was used for the ground glass vacuum joints, since it has been reported that this is completely insoluble in the lower alcohols[51]. No softening of the PVC tubing occurred during extended tests and it was concluded that there would be little contamination from this source.

8.4.c. Normal Sodium Chloride Solution.

Whenever a substance is dissolved in a liquid the vapour

pressure of the latter is lowered which results in an elevation of boiling point at the ambient pressure. This phenomena is one of a group of colligative properties of solutions[24], all of which depend upon the number and not the nature of the molecules present. The law of Raoult[62] is obeyed by most dilute solutions viz

$$\frac{p^o - p}{p^o} = x$$

where p^o = vapour pressure of the pure solvent,
p = vapour pressure of the solution,
x = mole fraction of the solute.

For a molar solution of common salt in water at 21°C

$$p^o - p = 18.56 \times 0.018 = 0.335 \text{ mm of mercury}$$

this slight reduction in vapour pressure will not affect the coefficient but it was thought that the different interfacial structure may inhibit condensation.

The average values of α are plotted against time in fig. A.4.9. and A.4.10.. The calculated coefficients for condensation and evaporation are less than those for pure water: the curves tend to a value of 0.004 - 0.006 at long time intervals. It is probable that the coefficient for dilute solutions progressively approaches that for pure water.

8.4.d. Water Containing Surface - Active Agents.

The experiments using small traces of sodium lauryl sulphate, a surfactive agent, gave values of 0.003 for the coefficient at high rates of mass transfer. At lower rates the coefficient approaches that of pure water. The sodium lauryl sulphate was introduced into the de-aeration flask F_2 to give 3.10^{-5} normal

solution. Much of thisagent would be lost to other surfaces during solution transfer to the test cell and no measurements of surface tension could be made in the cell itself. Hence the results cannot be related to a particular concentration of surface active agent. Davis and Rideal[15] state that α may be lowered by as much as x 10^{-4} by addition of surfactive agent, but other workers suggest that a factor of 2 to 10 would be more realistic[48]. In the present work it could not be tested whether a monolayer was achieved and no comparable results for sodium lauryl sulphate are available.

The liquid surface was stationary and the reduction in the condensation coefficient must be due to concentration of surfactive agent at the interface. The agent will obscure possible areas for interchange of molecules between liquid and vapour and, if present in sufficient quantity, will cover the whole surface with a monolayer. The blocking of the interface was suggested by Harvey[29] to explain results of absorption experiments. The long hydrophobic portions of the molecules, which are orientated perpendicular to the true liquid interface, permit only those vapour molecules which approach within a limited solid angle to strike the surface.

Long chain acids and alcohols have been used to reduce evaporation by 30 - 40%. Suitable compounds for this purpose should have a high surface pressure to spread over a maximum surface area and must be permeable to oxygen molecules to avoid water stagnation.

8.5. Mass Transfer in the presence of a Non-condensable Gas.

The problems and techniques of degassing were discussed in art. 7.3.b.. Any air which remains in the cell or enters through the leaks will affect the rate of transfer and the measured pressures. The diaphragm responds to changes in total pressure above it and if air is present the partial pressure of the vapour and thus the calculated value of T^{**} will be low. This error will be numerically small unless the percentage of air present in the vapour space exceeds 10%, a condition which would be readily

noticeable in practice on the manometer.

During condensation any small quantity of air, at first evenly distributed in the gas phase, may become progressively concentrated at the interface owing to bulk movement of gas and removal of condensable vapour. Baer and McKelvey[5] have studied the influence of non-condensables upon the coefficient for methanol. Their method, which was very simple and yielded consistent results, showed a decrease in α, during condensation, for increasing percentages of air They found that α was reduced by a factor of 20 by the presence of 1% of air. Also, in the presence of air, the absolute value of α decreased with reduction of temperature. This does not agree with the observations of Delaney who correlated the coefficient for water evaporation as a function of temperature using the equation $\alpha = Ae^{-E/RT}$ and found that E = -1,523 cals/mole. Baer and McKelvey calculated that the coefficient for methanol at 300°K was 0.016 when all air hadbeen purged from the cell; no data was presented for other systems. They showed that diffusion through the inert gas (air) should have a negligible effect upon α. From their data it appears that the reduced coefficients in the presence of inert gas are due to a blocking of the interface.

In the present work coefficients were found to decrease with increase in rate of mass transfer during both condensation and evaporation. The reduction in coefficients during condensation may be explained by postulating the build up of air at the interface but during evaporation the bulk flow will be away from the interface and it might be expected that the interface would be progressively cleared of inerts and the value of α increased. In practice the opposite occurs.

CHAPTER 9.
CONCLUSIONS.

1) A Mach - Zehnder interferometer has been constructed with 8" optical plates arranged on a 60° parallelogram. The instrument has been used to study the temperature gradients existing in a liquid during interphase mass transfer.

2) Values of the condensation coefficient calculated theoretically from half-power series representations of the experimental data give inconsistent results. This is attributed to non-convergence of the series and sensitivity of the values of the series coefficients to experimental error when longer series were employed.

3) A study of the experimental data suggested that the condensation coefficient varies with the rate of mass transfer. The calculated average values for the condensation coefficient decrease with the increase in rate of mass transfer.

4) Values for water condensation at low rates of mass transfer are higher than those previously reported for evaporation from a quiescent surface.

5) Expressions for the rate of mass transfer necessarily include the calculated coefficients and no true correlation can be presented.

6) The variation of the condensation coefficient with rate of transfer may in some but not all cases be attributed to the small percentages of air present in the cell. It is suggested that air molecules will block the interface, rather than that

diffusion through air is limiting the rate.

7) Evaporation and condensation of the fluids gave similar results. The values for propyl alcohol are about one twentieth of those for water.

8) The addition of sodium chloride or surfactive agents to water also reduce the condensation coefficients.

A P P E N D I C E S .

APPENDIX 1.

PHYSICAL AND DERIVED CONSTANTS.

	WATER	N.NaCl SOLUTION	PROPYL ALCOHOL
Density ρ_L (grams/cc.)	1.000	1.038	0.807
Specific Heat c_L (cal/gram °C.)	1.000	0.931	0.585
Latent Heat L (cal/gram mole)	10,520	10,520	12,000
Thermal Conductivity (cal/cm.sec.°C.)	0.001418	0.001418	0.000413
Temperature Coefficient Refractive Index /°C	82.5×10^{-6}	114×10^{-6}	380×10^{-6} (at 15°C)
$\phi.10^6$ (gram mole/(ergs.cm)$^{\frac{1}{2}}$)	0.598	0.598	0.328
$K^{\frac{1}{2}}$ (cm/sec$^{\frac{1}{2}}$)	0.0385	0.0382	0.0296
β (dynes/cm^2 °C)	20°C 0.00145 21°C 0.00153 22°C 0.00161	21.5°C 0.00152	20°C 0.00165
$k/H\beta\phi$ (cm.)	20°C 0.000162 21°C 0.000154 22°C 0.000146	21.5°C 0.000147	20°C 0.0000634

Constants for the surfactive solution were taken to be identical to pure water. The main sources of data were the 'International Critical Tables'(38), 'Properties of Organic Compounds' by Timmermans(73) and the American Chemical Society monograph on sodium chloride(42).

A.2.1. Run 1. Water Condensation.

a) Cine Film Data.

TIME. secs.	FRAME NUMBER	FRINGE SHIFT AT SURFACE X_s cms.	T_s' ^oC
0	0	0	0
0.0321	2	1.00	0.0196
0.0642	4	1.76	0.0343
0.0963	6	2.73	0.0532
0.1284	8	3.22	0.0628
0.1605	10	4.12	0.0803
0.1926	12	4.85	0.0946
0.2247	14	6.05	0.1180
0.2568	16	6.74	0.1315

b) Trace Data.

TIME secs.	DISTANCE ALONG TRACE AXIS cms.	TRACE WIDTH cms.	Δp 1/10" wg.	T^{*} ^oC
0	0	0.055	0	0
0.0217	0.36	0.11	0.093	0.0145
0.0525	0.87	0.22	0.247	0.0385
0.0845	1.40	0.43	0.504	0.0786
0.1160	1.92	0.67	0.773	0.1208
0.1520	2.52	0.97	1.078	0.1682
0.1845	3.06	1.22	1.316	0.2055
0.2185	3.62	1.44	1.520	0.2370
0.2500	4.15	1.56	1.640	0.2560

Fluid bulk temperature = 21.8°C.

Average speed of trace = 16.56 cm/sec.

Fringe spacing = 2.74 cms.

= 0.053°C.

Magnification: fringe plane - screen = 87.5

A.2.2. Run 5. Water Condensation.

a) Cine Film Data.

TIME: secs.	FRAME NUMBER	FRINGE SHIFT AT SURFACE X_s cms.	T_s' °C.
0	0	0	0
0.0321	2	0.80	0.02905
0.0642	4	1.32	0.04790
0.0963	6	1.55	0.05630
0.1284	8	2.10	0.07620
0.1605	10	2.35	0.08540
0.1926	12	2.85	0.1035
0.2247	14	3.10	0.1090
0.2568	16	3.25	0.1180

b) Trace Data

TIME secs.	DISTANCE ALONG TRACE AXIS cms.	TRACE WIDTH cms.	Δp 1/10" wg.	T^{*}, °C.
0	0	0.063	0	0
0.0304	0.5	0.171	0.156	0.0228
0.0608	1.0	0.376	0.418	0.0612
0.0912	1.5	0.696	0.775	0.1130
0.1216	2.0	0.935	1.045	0.1520
0.1520	2.5	1.188	1.310	0.1910
0.1824	3.0	1.291	1.415	0.2063
0.2128	3.5	1.363	1.495	0.2180
0.2432	4.0	1.327	1.455	0.2120

Fluid bulk temperature = 21.6°C.

Average speed of trace = 16.60 cms/sec.

Fringe spacing = 1.46 cms.

= 0.053°C.

Magnification: fringe plane - screen = 80.6

A.2.3. Run 8. Water Condensation.

a) Cine Film Data.

TIME secs.	FRAME NUMBER	FRINGE SHIFT AT SURFACE X_s cms.	T_s' °C
0	0	0	0
0.032	2	0.72	0.037
0.064	4	1.15	0.050(5)
0.096	6	1.42	0.062
0.128	8	1.65	0.072
0.160	10	1.85	0.081
0.193	12	2.13	0.094
0.225	14	2.31	0.101(5)
0.257	16	2.55	0.112

b) Trace data.

TIME secs.	DISTANCE ALONG TRACE AXIS. cms.	TRACE WIDTH cms.	Δp 1/10" wg.	T^{**}, °C
0	0	0.088	-	0
0.0304	0.5	0.219	0.255	0.0398
0.0608	1.0	0.368	0.475	0.0741
0.0912	1.5	0.545	0.697	0.1088
0.1216	2.0	0.677	0.865	0.1350
0.1520	2.5	0.820	1.040	0.1622
0.1824	3.0	0.874	1.100	0.1715
0.2128	3.5	0.891	1.118	0.1733
0.2432	4.0	0.896	1.125	0.1755

Fluid bulk temperature = 21.7°C.

Average speed of trace = 16.26 cm/sec.

Fringe spacing = 1.216 cms.

= 0.053°C.

Magnification = 69.2

A.2.4. Run 11. Water Condensation.

a) Cine film data.

TIME secs.	FRAME NUMBER	FRINGE SHIFT AT SURFACE X_s cms.	T_s' °C
0	0	0	0
0.032	2	0.62	0.0286
0.064	4	1.00	0.0461
0.096	6	1.20	0.0553
0.128	8	1.50	0.0691
0.160	10	1.65	0.0760
0.192	12	1.90	0.0876
0.224	14	2.20	0.1015
0.256	16	2.20	0.1015

b) Trace data.

TIME secs.	DISTANCE ALONG TRACE AXIS cms.	TRACE WIDTH cms.	Δp 1/10" wg.	T^{*}, °C
0	0	0.103	-	0
0.0305	0.5	0.195	0.210	0.0314
0.0610	1.0	0.328	0.430	0.0642
0.0915	1.5	0.452	0.602	0.0898
0.1220	2.0	0.619	0.792	0.1182
0.1525	2.5	0.740	0.925	0.1381
0.1830	3.0	0.866	1.025	0.1530
0.2135	3.5	0.860	1.075	0.1605
0.2440	4.0	0.895	1.097	0.1638

Fluid bulk temperature = 21.9°C

Average speed of trace = 16.42 cm/sec.

Fringe spacing = 1.158 cms.

= 0.053°C

Magnification = 68.7

A.2.5. Run 33. Water Evaporation.

a) Cine film data.

TIME secs.	FRAME NUMBER	FRINGE SHIFT AT SURFACE X_s cms.	T_s' °C
0	0	0	0
0.032	2	0.32	0.0111
0.064	4	0.61	0.0211
0.096	6	0.82	0.0284
0.144	9	1.40	0.0434
0.192	12	1.55	0.0537
0.228	14	1.65	0.0571
0.256	16	1.70	0.0589

b) Trace Data.

TIME secs.	DISTANCE ALONG TRACE AXIS cms.	TRACE WIDTH cms.	Δp 1/10" wg.	T', °C
0	0	0.085	0	0
0.038	0.625	0.100	0.021	0.0036
0.075	1.220	0.145	0.066	0.0136
0.107	1.730	0.230	0.150	0.0258
0.144	2.340	0.370	0.271	0.0467
0.177	2.890	0.590	0.475	0.0818
0.206	3.910	0.730	0.630	0.1085
0.241	4.435	0.870	0.780	0.1342

Fluid bulk temperature = 20.0

Average speed of trace = 16.20 cms/sec.

Fringe spacing = 1.53 cms.

Magnification = 78.5

A.2.6. Run 34. Water Evaporation.

a) Cine film data.

TIME secs.	FRAME NUMBER	FRINGE SHIFT AT SURFACE X_s cms.	T_s' °C
0	0	0	0
0.048	3	0.58	0.0229
0.080	5	1.00	0.0396
0.112	7	1.35	0.0534
0.160	10	1.70	0.0673
0.192	12	1.80	0.0713
0.256	16	1.80	0.0713

b) Trace data.

TIME secs.	DISTANCE ALONG TRACE AXIS cms.	TRACE WIDTH cms.	Δp 1/10" wg.	T^{**}, °C
0	0	0.085	0	0
0.065	0.92	0.130	0.052	0.0089
0.107	1.72	0.160	0.083	0.0142
0.154	2.49	0.280	0.197	0.0337
0.192	3.10	0.535	0.391	0.0669
0.234	3.78	0.740	0.640	0.1090
0.280	4.52	0.920	0.840	0.1438

Fluid bulk temperature = 20.1

Average speed of trace = 16.10 cm/sec.

Fringe spacing = 1.34 cm. = 0.053°C

Magnification = 70.1

A.2.7. Run 35. Water Evaporation.

a) Cine film data.

TIME secs.	FRAME NUMBER	FRINGE SHIFT AT SURFACE X_s cms	T_s' °C
0	0	0	0
0.048	3	0.85	0.0254
0.080	5	1.40	0.0419
0.112	7	1.70	0.0509
0.144	9	1.80	0.0539
0.176	11	1.92	0.0575
0.208	13	2.00	0.0599
0.240	15	2.10	0.0628
0.272	18	1.80	0.0539

b) Trace data.

TIME secs.	DISTANCE ALONG TRACE AXIS cms.	TRACE WIDTH cms.	Δp 1/10" wg.	$T^{3\epsilon}$ °C
0	0	0.070	0	0
0.041	0.67	0.110	0.045	0.0080
0.077	1.28	0.145	0.080	0.0144
0.117	1.94	0.210	0.143	0.0256
0.160	2.65	0.400	0.326	0.0585
0.189	3.14	0.610	0.535	0.0960
0.225	3.75	0.710	0.638	0.1147
0.262	4.33	0.720	0.700	0.1258

Fluid bulk temperature = 19.20

Average speed of trace = 16.64 cms/sec.

Fringe spacing = 1.77 cm.

= 0.053°C

Magnification = 70.1

A.2.8. Run 36. Water Evaporation.

a) Cine film data.

TIME secs.	FRAME NUMBER	FRINGE SHIFT AT SURFACE X_s cms.	T_s' °C
0	0	0	0
0.032	2	0.30	0.0103
0.064	4	0.60	0.0203
0.096	6	0.80	0.0270
0.144	9	1.10	0.0372
0.192	12	1.32	0.0446
0.256	16	1.60	0.0541
0.288	18	1.70	0.0575

b) Trace data.

TIME secs.	DISTANCE ALONG TRACE AXIS cms.	TRACE WIDTH cms.	Δp 1/10" wg.	T^*, °C
0	0	0.080	0	0
0.032	0.53	0.120	0.050	0.0089
0.069	1.13	0.150	0.105	0.0187
0.104	1.70	0.260	0.198	0.0352
0.138	2.26	0.470	0.420	0.0747
0.171	2.80	0.620	0.575	0.1022
0.203	3.33	0.750	0.710	0.1262
0.237	3.88	0.850	0.815	0.1449
0.272	4.46	0.910	0.878	0.1561

Fluid bulk temperature = 19.4°C

Average speed of trace = 16.42 cm/sec.

Fringe spacing = 1.58 cms.

= 0.053°C

Magnification = 74.7

A.2.9. Run 37. Water Evaporation.

a) Cine film data.

TIME secs.	FRAME NUMBER	FRINGE SHIFT AT SURFACE X_s cms.	T_s' °C
0	0	0	0
0.032	2	0.40	0.0159
0.064	4	0.62	0.0247
0.096	6	0.82	0.0331
0.144	9	1.00	0.0399
0.176	11	1.10	0.0438
0.192	12	1.10	0.0438
0.224	14	1.20	0.0478
0.272	17	1.25	0.0498

b) Trace data.

TIME secs.	DISTANCE ALONG TRACE AXIS cms.	TRACE WIDTH cms.	Δp 1/10" wg.	T^{3E}, °C
0	0	0.08	0	0
0.035	0.56	0.10	0.023	0.0041
0.077	1.24	0.17	0.110	0.0197
0.120	1.92	0.33	0.312	0.0559
0.165	2.64	0.60	0.651	0.1168
0.207	3.32	0.78	0.895	0.1607
0.248	3.98	0.89	1.050	0.1884
0.292	4.68	1.03	1.250	0.2241

Fluid bulk temperature = 19.1°C

Average speed of trace = 16.16 cm/sec.

Fringe spacing = 1.34 cms.

= 0.053°C

Magnification = 74.7

A.2.10. Run 38. Water Evaporation.

a) Cine film data.

TIME secs.	FRAME NUMBER	FRINGE SHIFT AT SURFACE X_s cms.	T_s' °C
0	0	0	0
0.032	2	0.52	0.0151
0.080	5	0.90	0.0261
0.112	7	1.13	0.0327
0.144	9	1.20	0.0348
0.176	11	1.37	0.0397
0.224	14	1.60	0.0464
0.272	17	1.80	0.0522

b) Trace data.

TIME secs.	DISTANCE ALONG TRACE AXIS cms.	TRACE WIDTH cms.	Δp 1/10" wg.	T^* °C
0	0	0.070	0	0
0.034	0.55	0.090	0.010	0.0018
0.073	1.17	0.140	0.045	0.0080
0.116	1.87	0.240	0.120	0.0213
0.156	2.50	0.420	0.260	0.0462
0.188	3.02	0.710	0.482	0.0856
0.225	3.61	0.950	0.695	0.1235
0.261	4.18	1.100	0.840	0.1492

Fluid bulk temperature = 19.4°C

Average speed of trace = 16.24 cms/sec.

Fringe spacing = 1.84 secs.

= 0.053°C

Magnification = 74.7

A.2.11. Run 39. Water Evaporation.

a) Cine film data.

TIME secs.	FRAME NUMBER	FRINGE SHIFT AT SURFACE X_s cms.	T_s' °C
0	0	0	0
0.048	3	0.40	0.0107
0.080	5	0.56	0.0149
0.112	7	0.90	0.0240
0.144	9	1.12	0.0299
0.176	11	1.22	0.0326
0.208	13	1.40	0.0374
0.240	15	1.60	0.0427
0.272	17	1.80	0.0480

b) Trace data.

TIME secs.	DISTANCE ALONG TRACE AXIS cms.	TRACE WIDTH cms.	Δp 1/10" wg.	T^{**} °C
0	0	0.080	0	0
0.028	0.45	0.110	0.039	0.0069
0.060	0.98	0.155	0.075	0.0133
0.091	1.48	0.190	0.105	0.0186
0.123	2.01	0.230	0.160	0.0283
0.152	2.47	0.410	0.294	0.0520
0.188	3.06	0.600	0.472	0.0835
0.221	3.60	0.780	0.656	0.1160
0.265	4.15	1.000	0.920	0.1628

Fluid bulk temperature = 19.5°C

Average speed of trace = 16.32 cms/sec.

Fringe spacing = 2.01 cms.

= 0.053°C

Magnification = 74.7

A.2.12. Run 42. $\overline{\text{Pr}}$OH Condensation.

a) Cine film data.

TIME secs.	FRAME NUMBER	FRINGE SHIFT AT SURFACE X_s cms.	T_s' °C
0	0	0	0
0.048	3	0.59	0.0038
0.096	6	1.10	0.0071
0.128	8	1.32	0.0086
0.160	10	1.41	0.0091
0.192	12	1.68	0.0109
0.224	14	1.98	0.0128
0.256	16	2.15	0.0139
0.288	18	2.15	0.0139

b) Trace data.

TIME secs.	DISTANCE ALONG TRACE AXIS cms.	TRACE WIDTH cms.	Δp 1/10" wg.	T^{**}, °C
0	0	0.065	0	0
0.023	0.38	0.110	0.030	0.0045
0.053	0.86	0.200	0.088	0.0133
0.081	1.31	0.350	0.182	0.0274
0.106	1.72	0.501	0.276	0.0417
0.134	2.16	0.670	0.380	0.0574
0.155	2.51	0.880	0.480	0.0724
0.186	3.00	0.990	0.575	0.0867
0.215	3.48	1.230	0.695	0.1048
0.253	4.12	1.440	0.809	0.1220

Fluid bulk temperature = 20.0°C

Average speed of trace = 16.24 cms/sec.

Fringe spacing = 1.765 cms.

= 0.0114°C

Magnification = 74.7

A.2.13. Run 43. $\overline{Pr}OH$ Evaporation.

a) Cine Film Data.

TIME secs.	FRAME NUMBER	FRINGE SHIFT AT SURFACE X_s cms.	T_s' ^oC
0	0	0	0
0.032	2	0.41	0.0029
0.064	4	0.67	0.0047
0.080	5	0.82	0.0058
0.096	6	1.06	0.0075
0.112	7	1.18	0.0083
0.128	8	1.36	0.0096
0.144	9	1.53	0.0108
0.160	10	1.72	0.0122
0.176	11	1.90	0.0134
0.192	12	2.05	0.0145

b) Trace data.

TIME secs.	DISTANCE ALONG TRACE AXIS cms.	TRACE WIDTH cms.	Δp 1/10" wg.	T^{35}' ^oC
0	0	0.057	0	0
0.023	0.370	0.170	0.098	0.0148
0.051	0.820	0.320	0.215	0.0324
0.073	1.185	0.510	0.346	0.0522
0.098	1.58	0.770	0.510	0.0744
0.121	1.96	0.935	0.627	0.0946
0.146	2.35	1.240	0.828	0.1250
0.172	2.78	1.480	0.975	0.1470
0.198	3.20	1.800	1.175	0.1722

Fluid bulk temperature = 20.1°C

Average speed of trace = 16.26 cms/sec.

Fringe spacing = 1.620 cms.

= 0.0114°C

Magnification = 74.7

A.2.14. Run 44. PrOH Evaporation.

a) Cine film data.

TIME secs.	FRAME NUMBER	FRINGE SHIFT AT SURFACE X_s cms.	T_s' °C
0	0	0	0
0.048	3	0.45	0.0030
0.064	4	0.56	0.0037
0.080	5	0.73	0.0048
0.096	6	0.86	0.0057
0.112	7	1.00	0.0066
0.144	9	1.23	0.0081
0.160	10	1.43	0.0094
0.176	11	1.52	0.0100

b) Trace data.

TIME secs.	DISTANCE ALONG TRACE AXIS cms.	TRACE WIDTH cms.	Δp 1/10" wg.	T^{**}, °C
0	0	0.085	0	0
0.023	0.38	0.150	0.050	0.0075
0.035	0.57	0.220	0.107	0.0161
0.054	0.88	0.350	0.210	0.0317
0.074	1.22	0.490	0.337	0.0508
0.093	1.48	0.635	0.477	0.0719
0.112	1.83	0.790	0.665	0.1020
0.130	2.12	0.900	0.807	0.1217
0.149	2.44	0.990	0.930	0.1403
0.167	2.74	1.080	1.050	0.1585
0.185	3.03	1.190	1.205	0.1720

Fluid bulk temperature = 18.2°C

Average speed of trace = 16.40 cms/sec.

Fringe spacing = 1.74 cms.

= 0.0114°C

Magnification = 74.7

A.2.15. Run 46. PrOH Evaporation.

a) Cine film data.

TIME secs.	FRAME NUMBER	FRINGE SHIFT AT SURFACE X_s cms.	T_s' °C
0	0	0	0
0.048	3	0.30	0.00180
0.064	4	0.62	0.00250
0.096	6	0.78	0.00371
0.112	7	0.74	0.00441
0.144	9	0.92	0.00550
0.160	10	1.02	0.00605
0.192	12	1.25	0.00742
0.208	13	1.32	0.00783

b) Trace data.

TIME secs.	DISTANCE ALONG TRACE AXIS cms.	TRACE WIDTH cms.	Δp 1/10" wg.	$T^{3\epsilon}$ ' °C
0	0	0.090	0	0
0.013	0.21	0.100	0.025	0.0038
0.024	0.40	0.140	0.058	0.0087
0.040	0.65	0.220	0.125	0.0189
0.054	0.89	0.270	0.165	0.0249
0.070	1.14	0.380	0.256	0.0386
0.084	1.37	0.470	0.332	0.0501
0.100	1.62	0.570	0.416	0.0627
0.112	1.83	0.720	0.542	0.0817
0.124	2.02	0.790	0.610	0.0920
0.133	2.27	0.910	0.720	0.1087
0.1548	2.530	1.000	0.804	0.1212
0.1725	2.820	1.110	0.900	0.1358
0.1870	3.060	1.220	1.014	0.1530
0.2030	3.320	1.330	1.120	0.1690
0.2185	3.575	1.410	1.196	0.1803

Fluid bulk temperature = 21.0°C

Average speed of trace = 16.44 cms/sec.

Fringe spacing = 1.93 cms

= 0.0114°C

Magnification = 74.7

A.2.16. Run 47. N.NaCl Solution Condens tion

a) Cine film data.

TIME secs.	FRAME NUMBER	FRINGE SHIFT AT SURFACE X_s cms.	T_s' °C
0	0	0	0
0.032	2	0.310	0.0064
0.064	4	0.610	0.0126
0.080	5	0.710	0.0147
0.112	7	1.000	0.0207
0.128	8	1.160	0.0240
0.160	10	1.520	0.0315
0.176	11	1.780	0.0369
0.192	12	1.900	0.0394
0.208	13	2.000	0.0415

b) Trace data.

TIME secs.	DISTANCE ALONG TRACE AXIS cms.	TRACE WIDTH cms.	Δp 1/10" wg.	T^{36} ' °C
0	0	0.080	0	0
0.031	0.510	0.150	0.082	0.0134
0.060	0.975	0.245	0.173	0.0282
0.090	1.460	0.360	0.270	0.0441
0.121	1.980	0.550	0.410	0.0669
0.152	2.485	0.780	0.572	0.0933
0.184	3.000	1.020	0.738	0.1207
0.215	3.505	1.260	0.900	0.1470
0.246	4.020	1.550	1.087	0.1772

Fluid bulk temperature = 21.3

Average speed of trace = 16.36 cms/sec.

Fringe spacing = 1.915 cms.

= 0.0397°C

Magnification = 74.7

A.2.17. Run 48. N.NaCl Solution Evaporation

a) Cine film data.

TIME secs.	FRAME NUMBER	FRINGE SHIFT AT SURFACE X_s cms.	T_s' °C
0	0	0	0
0.032	2	0.41	0.0059
0.080	5	1.00	0.0143
0.096	6	1.16	0.0166
0.112	7	1.32	0.0189
0.144	9	1.70	0.0243
0.160	10	1.90	0.0272
0.192	12	2.42	0.0346
0.224	14	2.97	0.0425

b) Trace data.

TIME secs.	DISTANCE ALONG TRACE AXIS cms.	TRACE WIDTH cms.	Δp 1/10" WG.	T^{*}, °C
0	0	0.080	0	0
0.033	0.53	0.140	0.073	0.0119
0.051	0.83	0.180	0.112	0.0183
0.068	1.10	0.255	0.183	0.0299
0.085	1.37	0.335	0.250	0.0408
0.103	1.66	0.440	0.331	0.0540
0.121	1.96	0.550	0.409	0.0668
0.140	2.26	0.660	0.505	0.0824
0.160	2.58	0.840	0.612	0.0999
0.178	2.88	0.990	0.716	0.1169
0.196	3.16	1.170	0.840	0.1371
0.212	3.42	1.325	0.942	0.1538
0.230	3.71	1.480	1.043	0.1706
0.248	4.01	1.590	1.101	0.1820

Fluid bulk temperature = 21.3°C

Average speed of trace = 16.25 cms/sec.

Fringe spacing = 2.78 cms. = 0.0397°C

Magnification = 74.7

A.2.18. Run 49.N.NaCl Solution.. Evapora·ion.

a) Cine film data.

TIME secs.	FRAME NUMBER	FRINGE SHIFT AT SURFACE X_s cms.	T_s' °C
0	0	0	0
0.048	3	0.32	0.0059
0.096	5	0.61	0.0113
0.128	8	0.90	0.0166
0.160	10	1.28	0.0236
0.176	11	1.46	0.0269
0.192	12	1.80	0.0332
0.224	14	2.32	0.0429
0.256	16	3.10	0.0573

b) Trace data.

TIME secs.	DISTANCE ALONG TRACE AXIS cms.	TRACE WIDTH cms.	Δp 1/10" wg.	T^{**}, °C
0	0	0.060	0	0
0.026	0.42	0.110	0.032	0.0052
0.039	0.62	0.130	0.050	0.0081
0.050	0.80	0.170	0.058	0.0093
0.074	1.18	0.200	0.122	0.0196
0.091	1.46	0.245	0.157	0.0253
0.110	1.76	0.335	0.232	0.0374
0.129	2.06	0.440	0.300	0.0483
0.150	2.40	0.490	0.365	0.0588
0.169	2.71	0.565	0.431	0.0694
0.188	3.02	0.670	0.528	0.0852
0.206	3.31	0.745	0.600	0.0967
0.246	3.95	0.910	0.764	0.1231
0.226	3.63	0.810	0.665	0.1072

Fluid bulk temperature = 21.5°C

Average speed of trace = 16.18 cms/sec.

Fringe spacing = 2.15 cms.

= 0.0397°C

Magnification = 74.7

A.2.19. Run 52. Water + Surfactive Agent. Condensation.

a) Cine film data.

TIME secs.	FRAME NUMBER .	FRINGE SHIFT AT SURFACE X_s cms.	T_s' ^oC
0	0	0	0
0.032	2	0.40	0.0113
0.048	3	0.57	0.0162
0.064	4	0.68	0.0193
0.080	5	0.90	0.0255
0.112	7	1.13	0.0320
0.144	9	1.47	0.0417
0.160	10	1.64	0.0466
0.176	11	1.67	0.0474
0.192	12	1.72	0.0488

b) Trace data.

TIME secs.	DISTANCE ALONG TRACE AXIS cms.	TRACE WIDTH cms.	Δp 1/10" wg.	T^{**}, ^oC
0	0	0.070	0	0
0.027	0.445	0.130	0.076	0.0123
0.041	0.660	0.160	0.110	0.0178
0.058	0.930	0.210	0.168	0.0272
0.072	1.160	0.270	0.236	0.0381
0.087	1.410	0.365	0.343	0.0564
0.102	1.640	0.467	0.450	0.0727
0.116	1.880	0.585	0.573	0.0927
0.131	2.120	0.695	0.693	0.1121
0.143	2.315	0.810	0.813	0.1315
0.157	2.540	0.950	0.959	0.1550
0.167	2.695	1.060	1.068	0.1735
0.181	2.920	1.200	1.209	0.1952
0.193	3.125	1.350	1.360	0.2198

Fluid bulk temperature = 21.2°C.

Average speed of trace = 16.26 cms/sec.

Fringe spacing = 1.88 cms.

= 0.0533°C

Magnification = 74.7

A.2. 20. Run 53. Water + Surfactive Agents. Condensation.

a) Cine film data.

TIME secs.	FRAME NUMBER .	FRINGE SHIFT AT SURFACE X_s cms.	T_s' °C
0	0	0	0
0.032	2	0.400	0.0095
0.064	4	0.620	0.0148
0.080	5	0.750	0.0178
0.096	6	0.810	0.0193
0.128	8	0.95	0.0226
0.160	10	1.050	0.0250
0.176	11	1.250	0.0297
0.208	13	1.550	0.0369
0.224	14	1.650	0.0393

b) Trace data.

TIME secs.	DISTANCE ALONG TRACE AXIS cms.	TRACE WIDTH cms.	Δp 1/10" wg.	T^*, °C
0	0	0.065	0	0
0.026	0.425	0.120	0.075	0.0121
0.048	0.790	0.150	0.108	0.0174
0.070	1.165	0.240	0.190	0.0307
0.095	1.580	0.280	0.290	0.0468
0.121	2.000	0.430	0.422	0.0681
0.149	2.460	0.595	0.595	0.0962
0.177	2.935	0.820	0.832	0.1345
0.201	3.330	1.000	1.020	0.1648
0.239	3.960	1.260	1.285	0.2077

Fluid bulk temperature = 21.2°C

Average speed of trace = 16.66 cms/sec.

Fringe spacing = 2.24 cms.

= 0.0533°C

Magnification = 74.7

A.2.21. Run 54. Water + Surfactive Agen . Evaporation.

a) Cine film data.

TIME secs.	FRAME NUMBER	FRINGE SHIFT AT SURFACE X_s cms.	T_s' °C
0	0	0	0
0.032	2	0.30	0.0079
0.064	4	0.55	0.0145
0.080	5	0.70	0.0185
0.096	6	0.80	0.0211
0.112	7	1.00	0.0264
0.144	9	1.30	0.0343
0.160	10	1.40	0.0370
0.176	11	1.50	0.0396
0.192	12	1.61	0.0425

b) Trace data.

TIME secs.	DISTANCE ALONG TRACE AXIS cms.	TRACE WIDTH cms.	Δp 1/10" wg.	$T^{\#}$ ' °C
0	0	0.02	0	0
0.017	0.290	0.070	0.060	0.0095
0.037	0.620	0.180	0.140	0.0222
0.052	0.870	0.240	0.235	0.0373
0.065	1.080	0.265	0.280	0.0444
0.081	1.350	0.370	0.390	0.0618
0.094	1.570	0.500	0.496	0.0787
0.107	1.790	0.580	0.587	0.0932
0.119	1.995	0.685	0.710	0.1128
0.133	2.220	0.770	0.818	0.1300
0.148	2.475	0.860	0.938	0.1490
0.163	2.720	0.950	1.068	0.1697
0.177	2.960	1.070	1.155	0.1835
0.190	3.180	1.080	1.260	0.2000

Bulk fluid temperature = 21.4°C

Average speed of trace = 16.70 cms/sec.

Fringe spacing = 2.02 cms.

= 0.0533°C

Magnification = 74.7

A.2.22. Run 55. Water + Surfactive Agent Evaporation.

a) Eine Film Data.

TIME secs.	FRAME NUMBER	FRINGE SHIFT AT SURFACE X_s cms.	T_s' ^oC
0	0	0	0
0.048	3	0.35	0.0038
0.080	5	0.42	0.0055
0.112	7	0.52	0.0080
0.144	9	0.71	0.0123
0.160	10	0.80	0.0151
0.192	12	1.09	0.0224
0.224	14	1.30	0.0276
0.256	16	1.65	0.0364

b) Trace data.

TIME secs.	DISTANCE ALONG TRACE AXIS cms.	TRACE WIDTH cms.	Δp 1/10" wg.	T^{**}, ^oC
0	0	0.025	0	0
0.015	0.240	0.060	0.060	0.0094
0.032	0.525	0.140	0.132	0.0208
0.046	0.755	0.220	0.200	0.0315
0.063	1.030	0.250	0.245	0.0386
0.076	1.240	0.310	0.316	0.0482
0.093	1.502	0.410	0.405	0.0637
0.106	1.725	0.502	0.502	0.0788
0.122	1.980	0.580	0.585	0.0921
0.139	2.260	0.630	0.705	0.1110
0.157	2.550	0.810	0.870	0.1400
0.172	2.790	0.900	0.992	0.1562
0.187	3.040	0.920	1.080	0.1700
0.204	3.315	1.020	1.170	0.1842
0.219	3.560	1.090	1.276	0.2008
0.236	3.840	1.170	1.303	0.2050
0.256	4.150	1.260	1.462	0.2302

Bulk fluid temperature = 21.6°C

Average speed of trace = 16.38 cms/sec.

Fringe spacing = 2.10 cms.

= 0.0533°C

Magnification = 74.7

APPENDIX 3.

SAMPLE CALCULATIONS.

A.3.1. Calculation of temperatures T_s' and T_x' as functions of time from the cine film.

Techniques of fringe evaluation are discussed in the text (art.7.2.b.): the method chosen was that of fringe tracing. Every frame was not analysed in order to reduce the amount of data to be processed; a sufficient number of frames were selected to define the curves of fringe displacement versus time as plotted in fig. A.3.1. and A.3.2.. The curves shown of fringe displacement at different depths as functions of time were not used in calculations, but are presented to illustrate the profiles. The fringe spacing over the width of the emulsion was measured on the projected image and an average value calculated. It was assumed that the error introduced by taking the average spacing over the whole of the interferogram would be less than that of a single measurement adjacent to the fringe being studied. The temperature of the fluid was calculated from the reading of the thermocouple in the cell and the correspondeing value of $\frac{d\mu}{dT}$ selected. The temperature change necessary to cause a shift of one fringe width was then computed as shown in art. 6.5.d. using the equation

$$\Delta T = \frac{\lambda}{D. \; d\mu/dT}$$

where D is the geometric length of the fluid plate in the test section.

For Run No. 1.

$$\Delta T = \frac{54.6 \times 10^{-6}}{4.875 \times 2.54 \times 82.5 \times 10^{-6}}$$

$$= 0.0533^{\circ}C$$

As shown in art. 6.5.a. the camera speed may be assumed constant for the duration of a run and equal to 62.5 frames/sec.

FRINGE SHIFT
m.m.

'X' is the depth below the liquid surface.

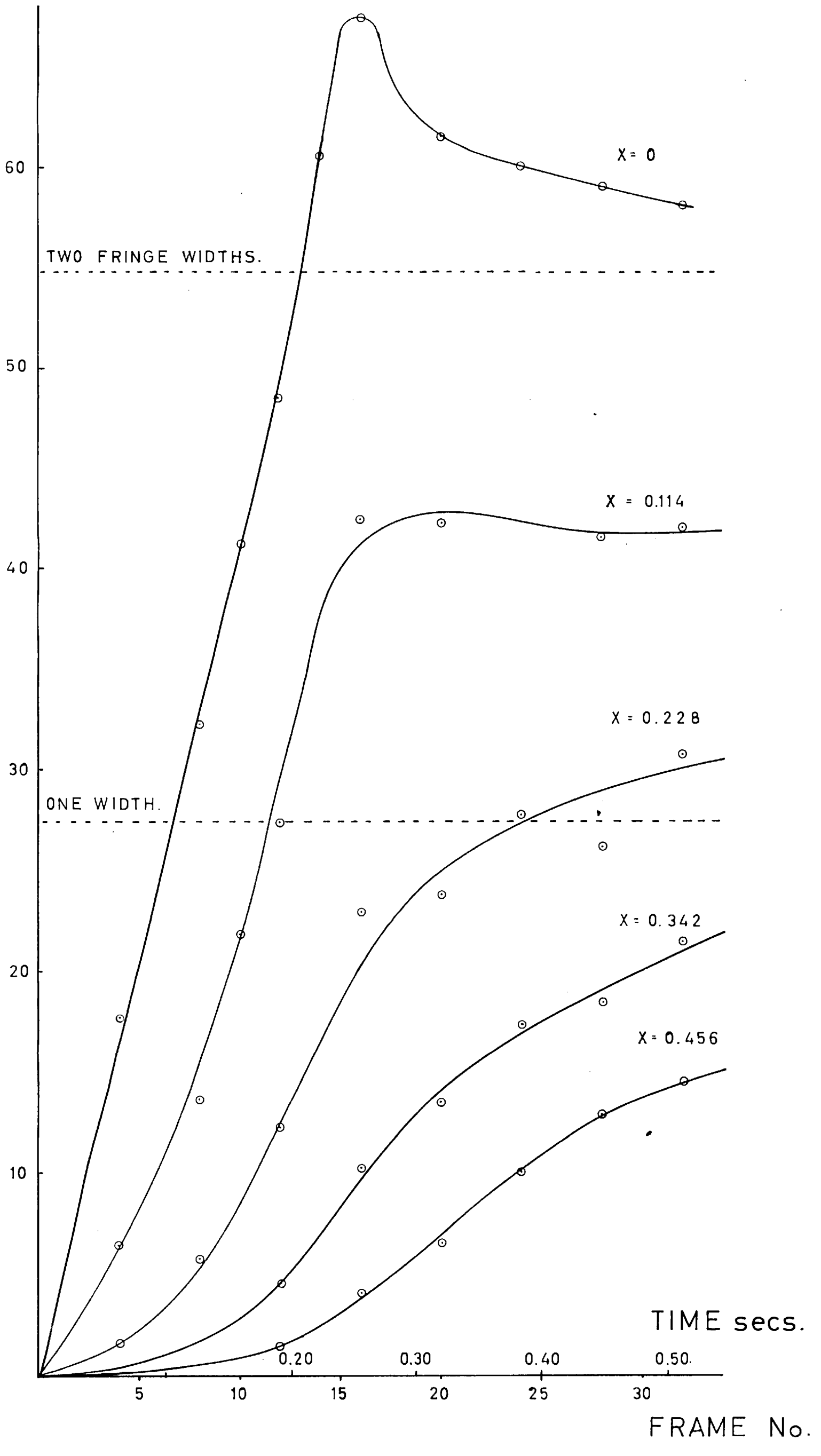

FIG. No. A.3.1. FRINGE PROFILES RUN No.1.

P.150.

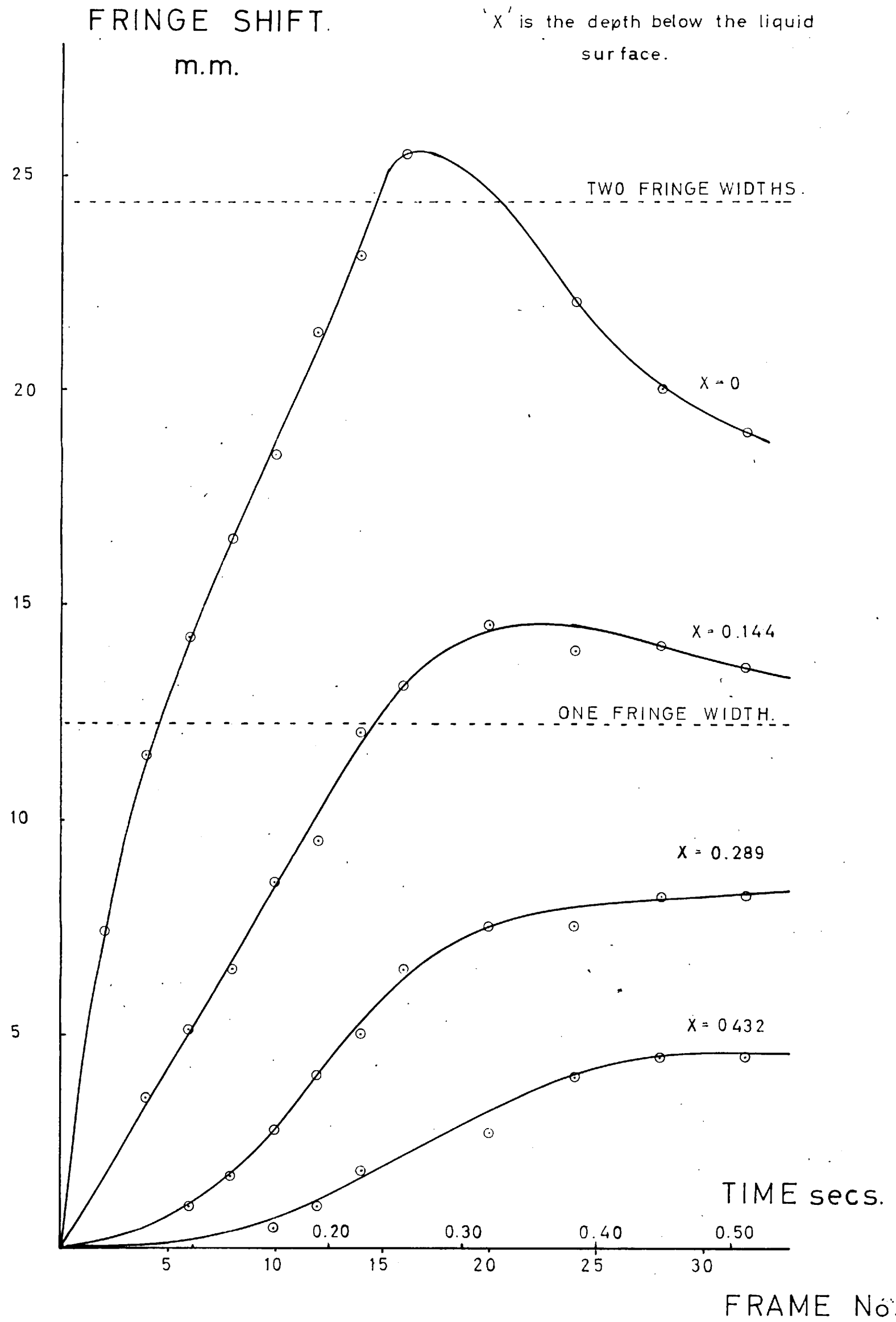

FIG. No. A.3.2. FRINGE PROFILES RUN No.8.

= 0.016 sec/frame. The magnification of the fringe pattern was then calculated by measuring on the projected image the width of a known slit placed in the fringe plane. The data was then plotted as graphs of $T_x' - \vartheta$ (fig A.3.1. and A.3.2.). The data was analysed to a value of $\vartheta = 0.25$ secs., above this value the transducer pressures were frequently off scale and as ϑ approached 0.50 secs. the surface temperature fell as a fresh equilibrium was established.

A.3.2. Calculation of the temperature $T^{\mathfrak{M}}$ as a function of time from the oscilloscope trace.

The pressure calibration of the diaphragm was checked before each run by introducing known pressure differences and recording the change in band width on the oscilloscope trace, as described in article 6.5.e.. The calibration curve for run 1. is given in fig. A.3.3. The cross sectional area of the cell at the optical flat mid-point is 84.44 cm^2 and the addition of 1 ml. of liquid of density ρ_L will result in an increase in pressure on the diaphragm given by

$$\Delta p = \frac{1}{2.54 \times 84.44} \cdot \rho_L$$

$$= 0.00467 \ \rho_L \quad \text{in.w.g.}$$

Definition of the oscilloscope trace at large amplitudes was poor owing to the necessity of reducing over exposure at small amplitudes. Thus it was not always possible to use a travelling microscope to measure width. Measurements made at large amplitudes with a ruler and magnifying glass were accurate to within $\pm$ 1%. The time calibration of the oscilloscope trace was calculated from the separation of the 'blip' time markers. Owing to the flexible pulley drive of the camera drum and system backlash, variations occurred in drum speed. These were small, but any general trend could be detected by plotting the speeds for each section.

FIG. No. A.3.3. DIAPHRAGM CALIBRATION

RUN No. 1.

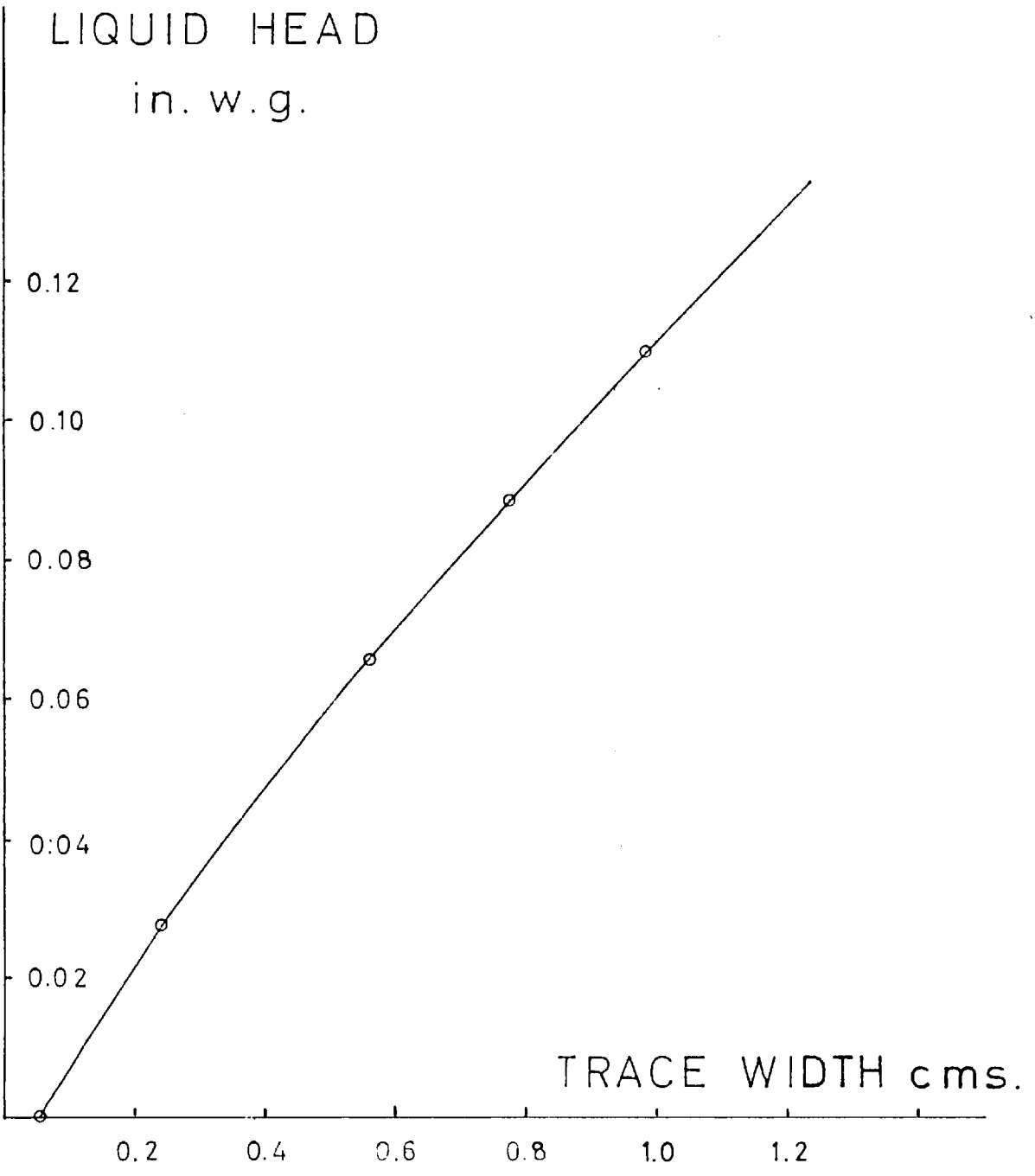

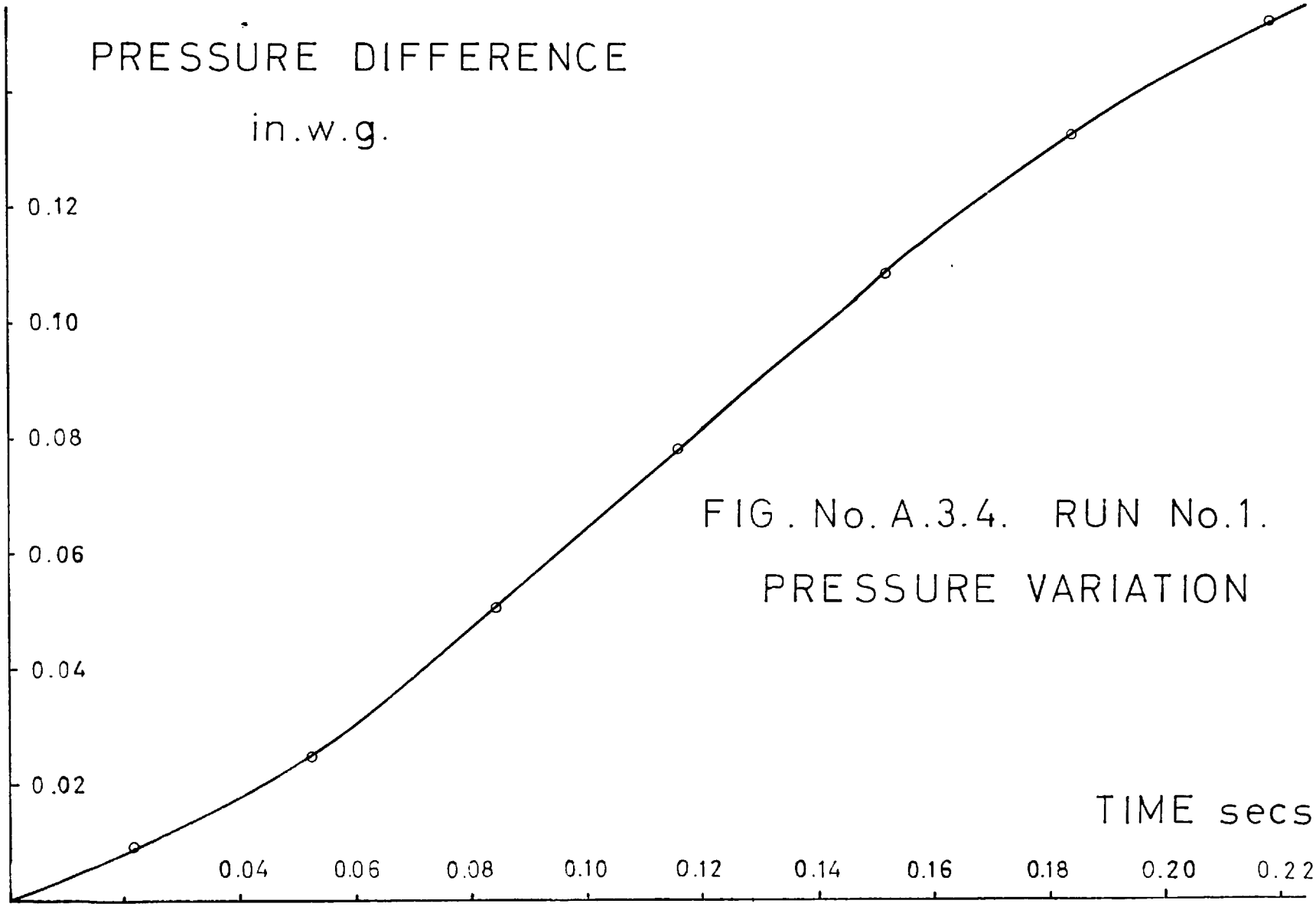

FIG. No. A.3.4. RUN No.1.
PRESSURE VARIATION

For run No. 1 over the test interval the time marker separation was 8.28 cms.

Therefore 1 mm. on the trace = $\frac{0.5007}{8.28}$

= 0.0060 secs.

In 6.3.b. we define $T^{*'} = T^{*} - T_o$

Also from the vapour pressure curve, $p = \beta T + \mu$

Hence $T^{*'} = \frac{p - p_o}{\beta}$

For water at the bulk fluid temperature of 21.8°C, β = 0.645 in.w.g./°C

Therefore $T^{*'} = 1.55\ (p - p_o)$°C

The data for this run No. 1. are tabulated in A.2.1. and the plot of $(p - p_o)$ versus ϑ is shown in fig. A.3.4.

A.3.3. Curve fitting by Least Squares.

The curve fitting was carried out using the University of London Mercury computer. The Library Program 1000, written by J.H. Caldwell of RAE Farnborough, computed the coefficients in the series

$$F(z) = a_o + a_1 z + a_2 z^2 + \ldots\ldots\ldots\ldots + a_n z^n$$

for a list of m pairs of data, using the test condition of obtaining the least sum of the squares of the residuals.

The data input requires the specification of several parameters in addition to the pairs of data. These describe the order of fit required, the relative importance of the pairs of data and the output style. The program offers the facility of alternative print styles:

a) coefficients of all the series up to power 'n' plus the values of the maximum residual of each series.

b) the above data together with the predicted values and the residuals.

As in all computers the output phase of the operation is far slower than the calculation steps and hence in order to use the

minimum computer time, the complete output was used only for test purposes. In order to use this program to fit a half - power series it was necessary to change the variable; for run No. 1., where the coefficients of the series

$$T^{\ast\prime} = a_1\vartheta^{\frac{1}{2}} + a_2\vartheta + a_3\vartheta^{3/2} + \ldots\ldots\ldots + a_n\vartheta^{n/2}$$

were required, the transformation $Z = \frac{T^{\ast\prime}}{\vartheta^{1/2}}$, $Y = \vartheta^{\frac{1}{2}}$ was used.

A similar substitution was used for series starting at the second or third term.

A.3.4. Calculation of the Condensation coefficient from the correlation of surface temperature T_s' with time.

Firstly the data of $T^{\ast\prime}$ versus ϑ was correlated in a half power series, using the computer program as described in A.3.3.. Coefficients were calculated for the series which commenced at $n = 1(\vartheta^{\frac{1}{2}})$ and $n = 2(\vartheta^1)$ and are tabulated below.

For the series $T' = a_1\vartheta^{\frac{1}{2}} + a_2\vartheta^1 + a_3\vartheta^{3/2} + a_4\vartheta^2$

Coefficients for Run No. 1.

Two term series	$a_1 = -0.9931$	and	$a_1 = 0$
	$a_2 = +1.295$		$a_2 = +0.4679$
			$a_3 = +1.469$
Three term series	$a_1 = -0.167$	and	$a_1 = 0$
	$a_2 = +1.768$		$a_2 = +0.2094$
	$a_3 = -0.7213$		$a_3 = +3.274$
			$a_4 = -2.755$

The first coefficient in each of the series starting at $\vartheta^{\frac{1}{2}}$ is negative and this would result in a negative value for the condensation coefficient α_1 from equation 6.24.. Series starting at ϑ^1 have positive first coefficients. The power series fits for T_s' commence at one higher term, namely b_3 in the second case:

$$T_s' = b_3\theta^{3/2} + b_4\theta^2 + b_5\theta^{5/2}$$

Two term series $b_3 = +4.236$ Three term series $b_3 = +7.598$

$b_4 = -7.029$ $b_4 = -28.55$

$b_5 = +31.13$

The constant f_{n+1} as in equation 6.23. was defined by equation 6.17.

$$f_n = \frac{\Gamma(n/2 + 1)}{\sqrt{K}.\ \Gamma\left(\frac{n+1}{2}\right)}$$

where $$\Gamma(n) = \int_0^\infty t^{n-1}.\ e^{-t}\ dt.$$

From mathematical tables

x	1.5	2.0	2.5	3.0	3.5	4.0	4.5
Γx	0.8802	1.0	1.329	2.00	3.23	6.00	11.63

Hence

$f_2\sqrt{K} = 1.135$ $f_4\sqrt{K} = 1.502$ $f_6\sqrt{K} = 1.855$

$f_3\sqrt{K} = 1.329$ $f_5\sqrt{K} = 1.615$ $f_6\sqrt{K} = 1.946$

The values of α_n, the condensation coefficient, were then caloulated as follows:-

n	b_{n+1}	$f_{n+1}\sqrt{K}$	$b_{n+1}.f_{n+1}.\sqrt{K}$	a_n	b_n	$(a_n - b_n)$	$\sqrt{K}.\delta_n$	α_n
2	4.236	1.329	5.620	0.468	-	0.468	12.07	0.0457
3	-7.209	1.502	-9.750	1.469	4.625	-2.796	3.49	0.0132
2	7.598	1.329	10.10	0.209	-	0.209	48.3	0.1831
3	-28.55	1.502	-42.8	+3.274	7.598	-4.32	+9.92	0.0376
4	31.13	1.615	50.02	-2.755	-28.55	25.80	1.94	0.0073

α_n is calculated from equation 6. 23..

The value of α_n should, of course, be independent of n. The constants used in calculating α_n are given in A.1..

A.3.5. Calculation of the Condensation Coefficient from the correlation of fringe shift at depth x, (T_x') with time ϑ.

A description of the method is given in 6.3.c., the calculations for RUN 8 are given below. The method requires the measurement of the fringe shift at depth x and time ϑ where $x = 2I\sqrt{K\vartheta}$. For convenience I was chosen at 0.50.

Frame No.	Time secs.	$2\sqrt{K\vartheta}$	x' cms.	Fringe shift cms.	T_x' °C
2	0.032	0.0135	0.469	0.510	0.0222
4	0.064	0.0192	0.663	0.770	0.0336
6	0.096	0.0235	0.813	0.820	0.0378
8	0.128	0.0271	0.938	1.000	0.0436
10	0.160	0.0303	1.050	1.100	0.0483
12	0.192	0.0332	1.115	1.200	0.0523
14	0.224	0.0358	1.242	1.350	0.0588

where x' is the measurement on the magnified image (for this run the magnification was 69.2).

This set of data together with data of $T^{\infty}' - \vartheta$ as given in apperdix A.2.3. was correlated using the computer program.

2 term fit: $a_1 = +0.201$ $c_2 = +0.901$

$a_2 = +0.429$ $c_3 = -1.459$

3 term fit: $a_2 = +1.152$ $c_3 = +10.61$

$a_3 = +1.687$ $c_4 = -46.82$

$a_4 = -5.145$ $c_5 = +54.57$

From equation 6.26.

$$b_n = \frac{o_n}{\Gamma\left(\frac{n}{2}+1\right).\ 2^n.\ i^n\ \mathrm{erfc}\ L.}$$

the coefficients b_n were calculated using the c_n data as shown below.

n	$\Gamma\left(\frac{n}{2}+1\right)$	2^n	L	i^n erfc 0.5	c_n	b_n
2	1.00	4	0.5	0.0666	+0.901	+3.39
3	1.239	8	0.5	0.0216	-1.459	-6.37
3	1.329	8	0.5	0.0216	+10.61	+46.4
4	2.000	16	0.5	0.0060	-46.82	-244.0
5	3.230	32	0.5	0.0016	+54.57	+329.0

Values of i^n. erfc L were taken from Carslaw and Jaegar[7]. From these values of a_n and b_n, condensation coefficients α_n were calculated using the relation of equation 6.23.

n	b_{n+1}	f_{n+1}	$b_{n+1}.f_{n+1}$	a_n	b_n	$a_r - b_n$	$\sqrt{K.\gamma_n}$	α_n
2	+3.39	1.135	+3.85	0.201	-	0.209	+18.45	0.07
3	-6.37	1.329	-8.46	0.429	3.39	2.90	+2.90	0.0113
2	46.4	1.329	61.7	1.520	-	1.520	+40.6	+0.1568
3	-244.0	1.502	-367.0	1.687	46.4	-44.7	+8.20	+0.0317
4	329.0	1.615	531.0	-5.145	-244.0	239.0	+2.22	+0.0036

A.4.1. Run 8. Coefficients from surface temperature correlation.

5 term series

				$\gamma_n\sqrt{K}$	α_n
a_1	= +0.6150	b_2	= +0.5070	+0.934	+0.0036
a_2	= -6.766	b_3	= +11.38	-2.530	-0.0098
a_3	= +37.44	b_4	= +73.72	-4.260	-0.0165
a_4	= -72.92	b_5	= +161.2	+322.0	+0.8350
a_5	= +45.91	b_6	= -120.0	+1.345	+0.0052

4 term series

				$\gamma_n\sqrt{K}$	α_n
a_1	= +0.1656	b_2	= +1.614	+12.35	+0.0477
a_2	= -0.6118	b_3	= -3.883	+2.35	+0.0091
a_3	= +7.495	b_4	= +1.517	+0.444	+0.0017
a_4	= -11.14	b_5	= +3.227	-0.413	-0.0016

3 term series

a_2	= +1.152	b_3	= +14.40	+16.60	+0.0643
a_3	= +1.687	b_4	= -61.33	+7.26	+0.0281
a_4	= -5.145	b_5	= +70.30	+2.02	+0.0078

2 term series

a_1	= +0.2007	b_2	= +1.251	+7.07	+0.0274
a_2	= +0.4290	b_3	= -1.797	+2.90	+0.0112

A.4.2. Run 36. Water Evaporation

2 term series

				$\gamma_n\sqrt{K}$	α_n
a_2	= +0.152	b_3	= -2.257	+19.76	+0.0830
a_3	= +0.803	b_4	= -3.696	+3.81	0.0160

3 term series

				$\gamma_n\sqrt{K}$	α_n
a_3	= +0.842	b_4	= +22.98	+41.2	+0.1730
a_4	= +3.730	b_5	= -92.43	+7.74	+0.0325
a_5	= -6.120	b_6	= +94.86	+2.035	+0.0085

A.4.3. Run 47. N.NaCl Condensation.

2 term series

a_2	= +0.219	b_3	= +1.422	+8.64	+0.0332
a_3	= +0.999	b_4	= -2.311	+8.18	+0.0315

3 term series

				$\gamma_n\sqrt{K}$	α_n
a_1	= +0.036	b_2	= +0.265	+9.84	+0.0379
a_2	= -0.029	b_3	= -0.501	+2.27	+0.0087
a_3	= +1.390	b_4	= +0.824	+0.656	+0.0025

				$\gamma_n\sqrt{K}$	α_n
a_2	= +0.352	b_3	= +2.59	+9.78	+0.0376
a_3	= +0.154	b_4	= -10.15	+6.24	+0.0240
a_4	= +1.23	b_5	= 12.11	+1.72	+0.0066

A.4.4. Run 49. N.NaCl. Evaporation.

2 term series

			$\gamma_n\sqrt{K}$	α_n
a_2 = +0.0314	b_3 = +0.548		+23.2	+0.0893
a_3 = +0.935	b_4 = −0.355		−1.09	−0.0042

3 term series

			$\gamma_n\sqrt{K}$	α_n
a_1 = +0.0064	b_2 = +0.275		+48.8	+0.1880
a_2 = −0.039	b_3 = −1.140		+5.41	+0.0208
a_3 = +1.06	b_4 = +2.050		+1.40	+0.0054

			$\gamma_n\sqrt{K}$	α_n
a_2 = +0.076	b_3 = +1.594		+24.4	+0.0938
a_3 = +0.606	b_4 = −5.330		+10.2	+0.0392
a_4 = +0.512	b_5 = +6.860		+1.90	+0.0073

A.4.5. Calculation of the effect of zero error in the time scale of T_s'.

It was assumed that at time ϑ the true time was $(\vartheta + \pi)$ from the initiation of the condensation. Data fits were made for two term series and values of $\sqrt{K}.\ \gamma_n$ were calculated for Run 8.

π	b_{n+1}	$f_{n+1}.\sqrt{K}$	a_n	b_n	$a_n - b_n$	$\sqrt{K}.\gamma_n$
0	+1.433	1.135	0.201	-	0.201	+7.44
	-1.862	1.329	0.429	-1.48	-1.05	+2.35
0.5	+1.175	1.135	0.201	-	0.201	+6.64
	-1.206	1.329	0.429	-1.17	-0.74	+2.16
1.0	+0.974	1.135	0.203	-	0.201	+5.50
	-0.829	1.329	0.429	-0.974	-0.54	+2.04
1.5	+0.821	1.135	+0.201	-	0.201	+4.64
	-0.532	1.329	0.429	-0.821	-0.39	+1.81
2.0	0 731	1.135	0.201	-	0.201	+3.98
	-0.318	1.329	0.429	-0.703	-0.27	+1.50
3.0	+0.508	1.135	0.207	-	0.201	+2.87
	+0.021	1.329	0.429	-0.508	-0.078	-0.351
4.0	0.360	1.135	0.201	-	0.201	+2.03
	+0.249	1.329	0.429	-0.360	+0.069	+0.48

A.4.6. Calculation of α_n from fringe shift measurements at depth T_x' as a function of time for R. 1.

Run 1. L = 0.60 Water Condensation

FRAME	ϑ	$2\sqrt{K\vartheta}$	x'	Fringe shift	T_s'
2	0.032	0.01356	0.712	0.460	0.00889
4	0.064	0.01918	1.008	0.900	0.0174.
6	0.096	0.02348	1.232	1.23	0.0238
8	0.128	0.02700	1.422	1.46	0.0282
10	0.160	0.03035	1.592	1.58	0.0306
12	0.192	0.03322	1.740	2.22	0.0429
14	0.224	0.03515	1.881	2.75	0.0532
16	0.256	0.03840	2.016	3.12	0.0604

n	$\Gamma\left(\frac{n}{2}+1\right)$	2^n	$i^n.erfc\ L.$	c_n	b_n
3	1.329	8	0.0166	+1.984	+11.25
4	2.000	16	0.0042	-3.358	-25.10
3	1.329	8	0.0166	+3.602	+20.4
4	2.000	16	0.0042	-13.72	-102.0
5	3.230	32	0.0010	+15.01	+145.0

n	b_{n+1}	$f_{n+1}.\sqrt{K}$	a_n	b_n	$\gamma_n\sqrt{K}$	α_n
2	11.25	1.329	+0.468	0	+0.468	+0.0018
3	-25.10	1.502	+1.469	+11.25	-9.780	-0.0378
2	20.4	1.329	+0.209	0	+0.209	+0.0081
3	-102.0	1.502	+3.274	+20.4	-17.10	-0.0661
4	145.0	1.615	-2.755	-102.0	+99.50	+0.3850

A.4.7. Calculation of α_n from fringe shifts T_x'.

Run 42. L = 0.60 Propyl Alcohol Condensation.

FRAME	ϑ	$2\sqrt{K\vartheta}$	x'	Fringe Shift	T_s'
3	0.048	0.0128	0.574	0.210	0.00136
6	0.096	0.0181	0.812	0.280	0.00182
8	0.128	0.0209	0.938	0.350	0.00227
10	0.160	0.0234	1.050	0.395	0.00256
12	0.192	0.0256	1.150	0.450	0.00292
14	0.228	0.0277	1.241	0.490	0.00318
16	0.256	0.0296	1.329	0.530	0.00344

n	$\Gamma\left(\frac{n}{2}+1\right)$	2^n	$i^n.\mathrm{erfc}\,\Sigma.$	c_n	b_n
3	1.329	8	0.0166	+0.180	+1.022
4	2.000	16	0.0042	-0.330	-2.460
4	2.000	16	0.0042	+2.000	+14.95
5	3.23	32	0.0010	-8.597	-83.00
6	6.00	64	0.0002	+9.482	+98.80

n	b_{n+1}	$f_{n+1}\cdot\sqrt{K}$	a_n	b_n	$\gamma_n\sqrt{K}$	α_n
2	+1.022	1.329	+0.106	0	+12.8	+0.0275
3	-2.460	1.502	+0.795	+1.022	+16.3	+0.0350
3	+14.95	1.502	+1.03	0	+21.8	+0.0468
4	-83.00	1.615	+1.34	+14.95	+9.84	+0.0211
5	+98.80	1.855	-2.81	-83.00	+2.27	+0.0049

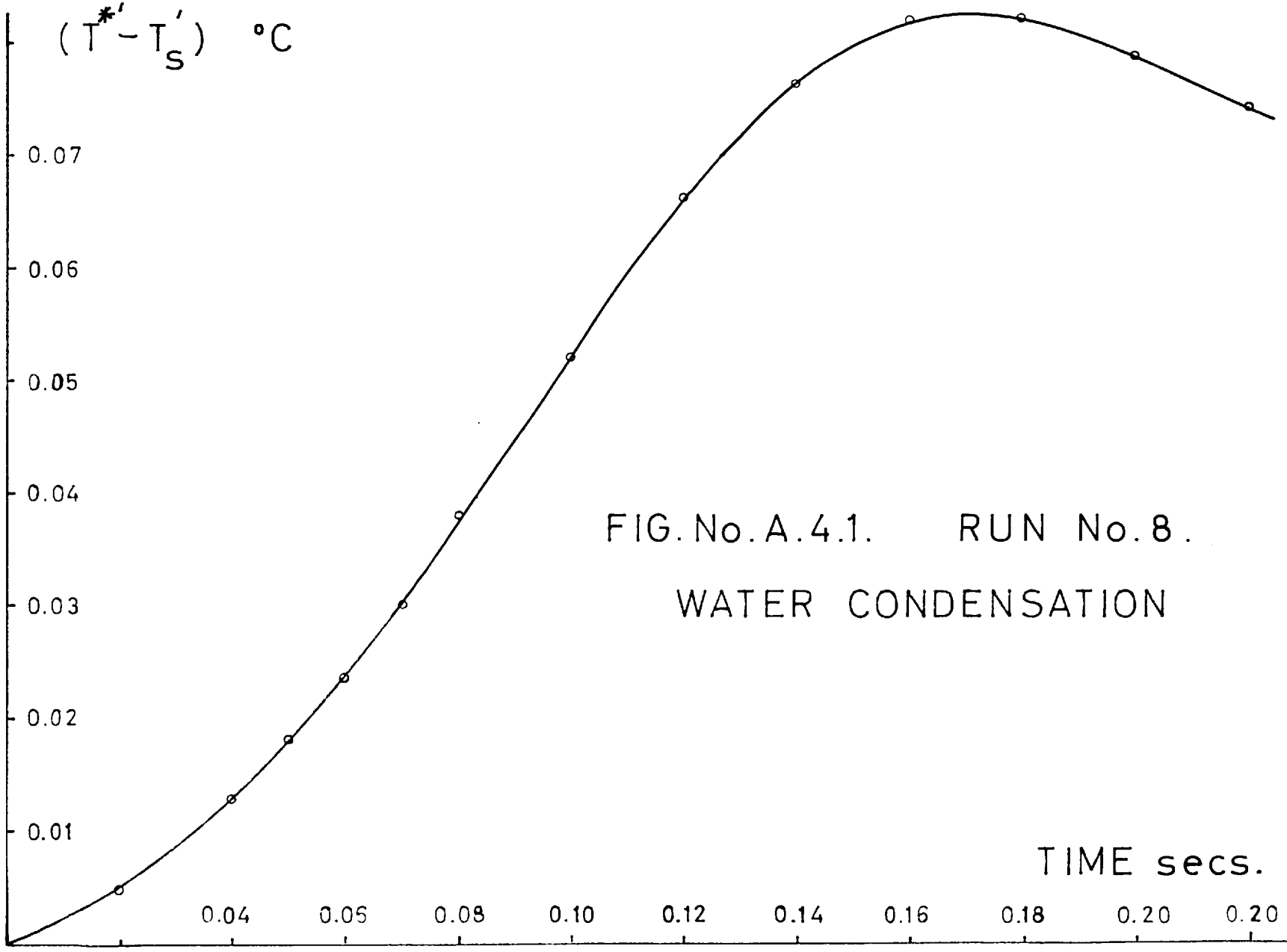

FIG. No. A.4.1. RUN No. 8.

WATER CONDENSATION

FIG. No. A.4.2. WATER EVAPORATION

RUN No. 36.

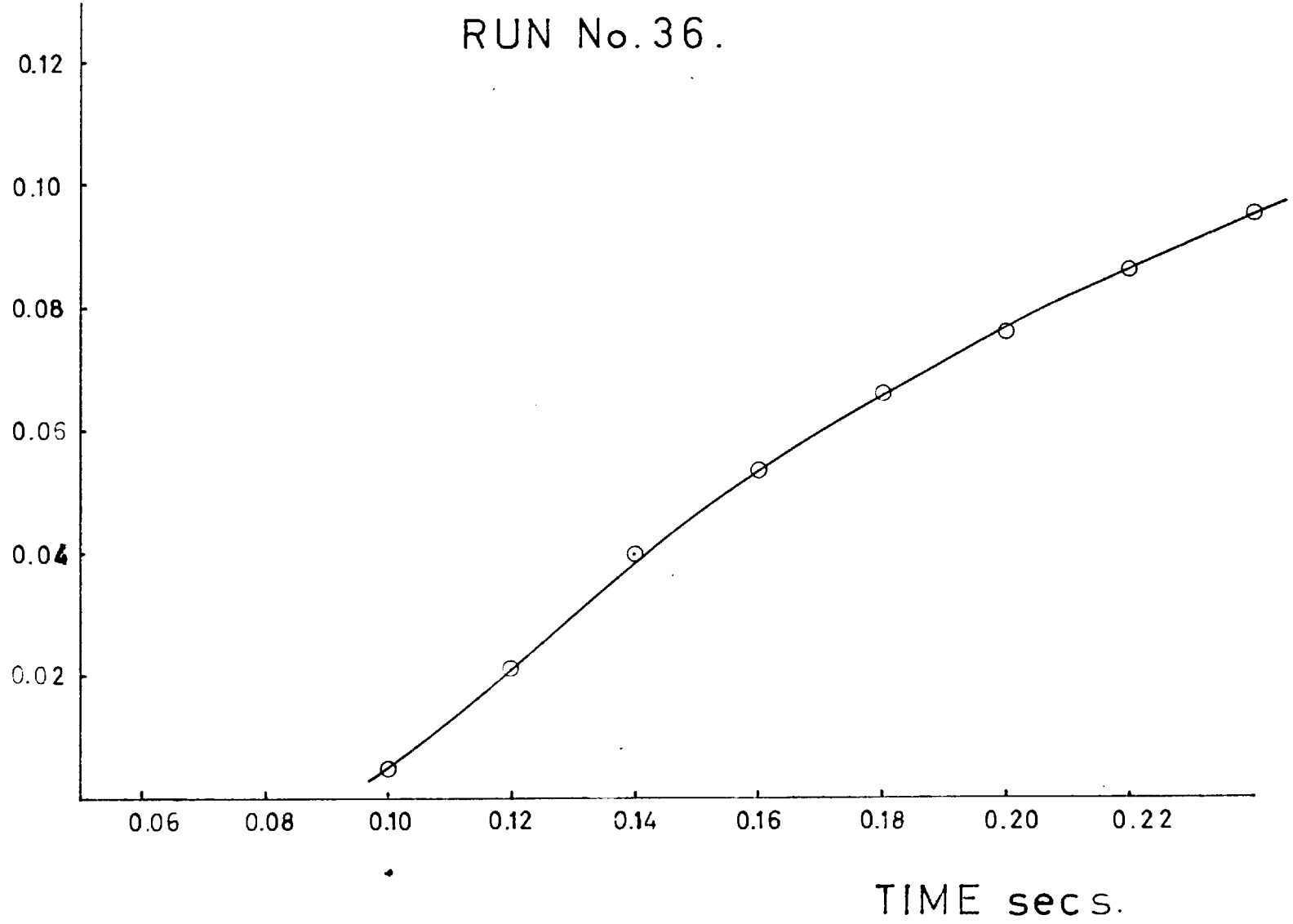

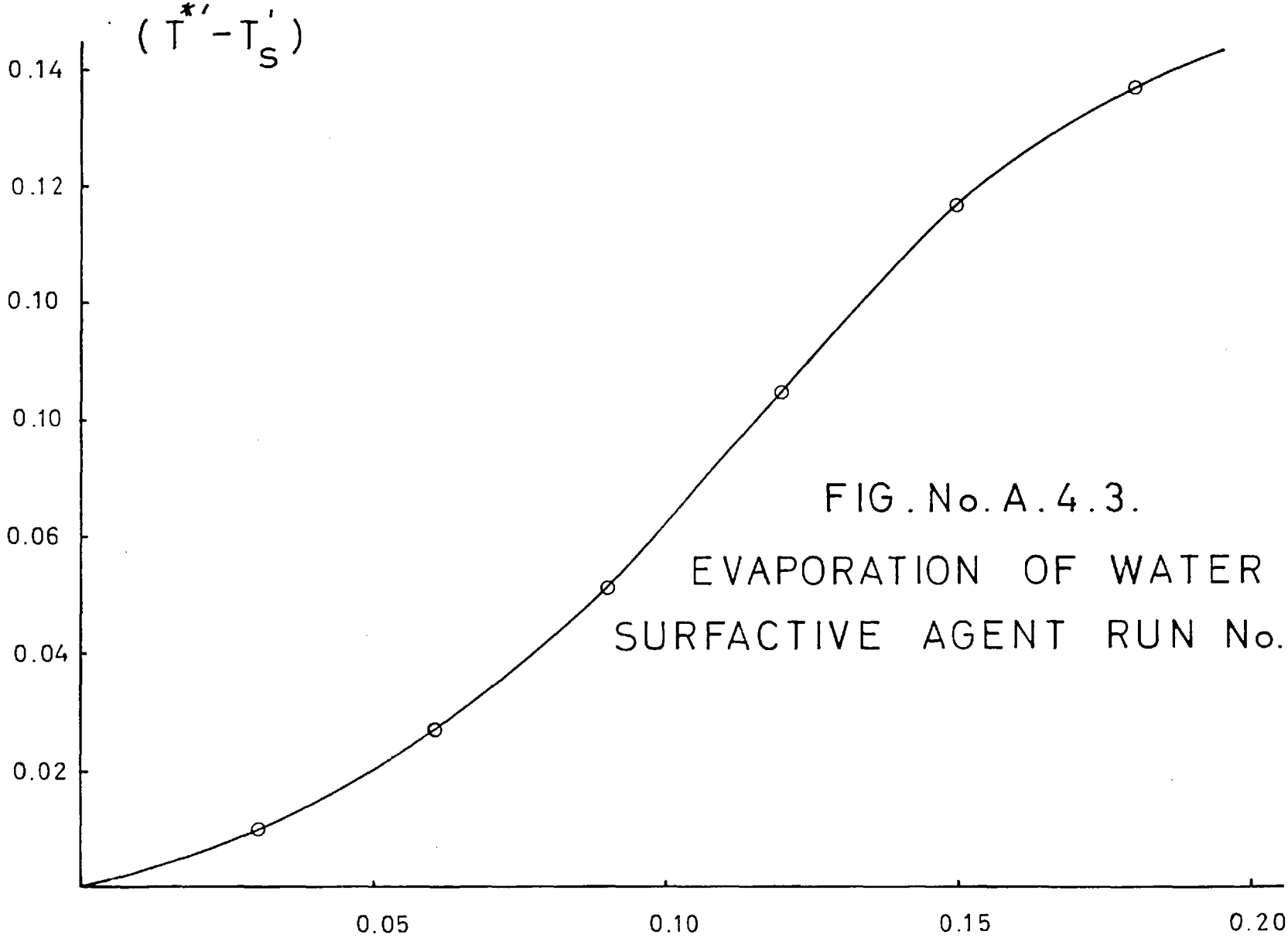

FIG. No. A.4.3.

EVAPORATION OF WATER PLUS SURFACTIVE AGENT RUN No. 54.

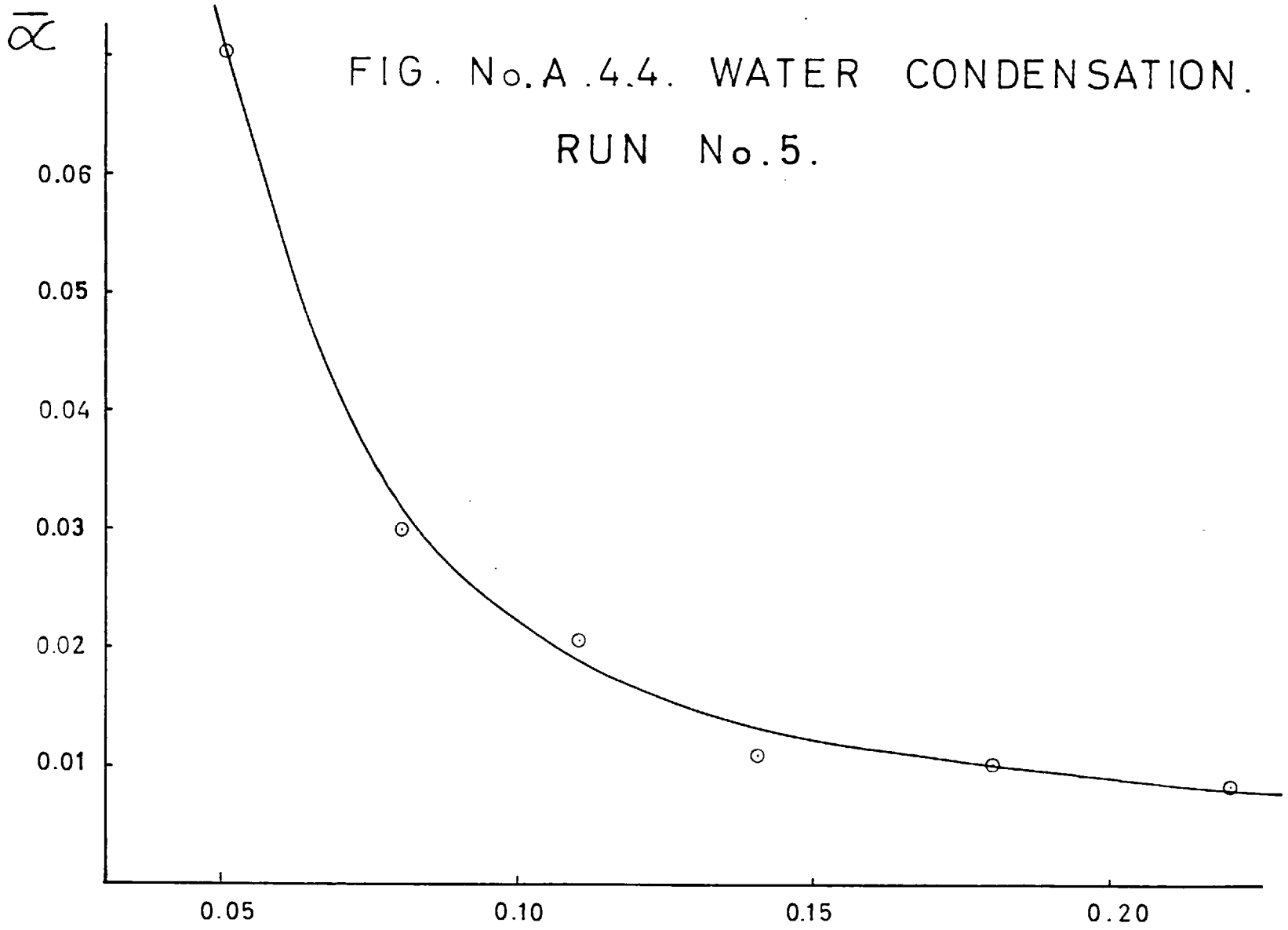

FIG. No.A.4.4. WATER CONDENSATION.
RUN No.5.

FIG. No. A.4.5. WATER CONDENSATION.

RUN No. 8.

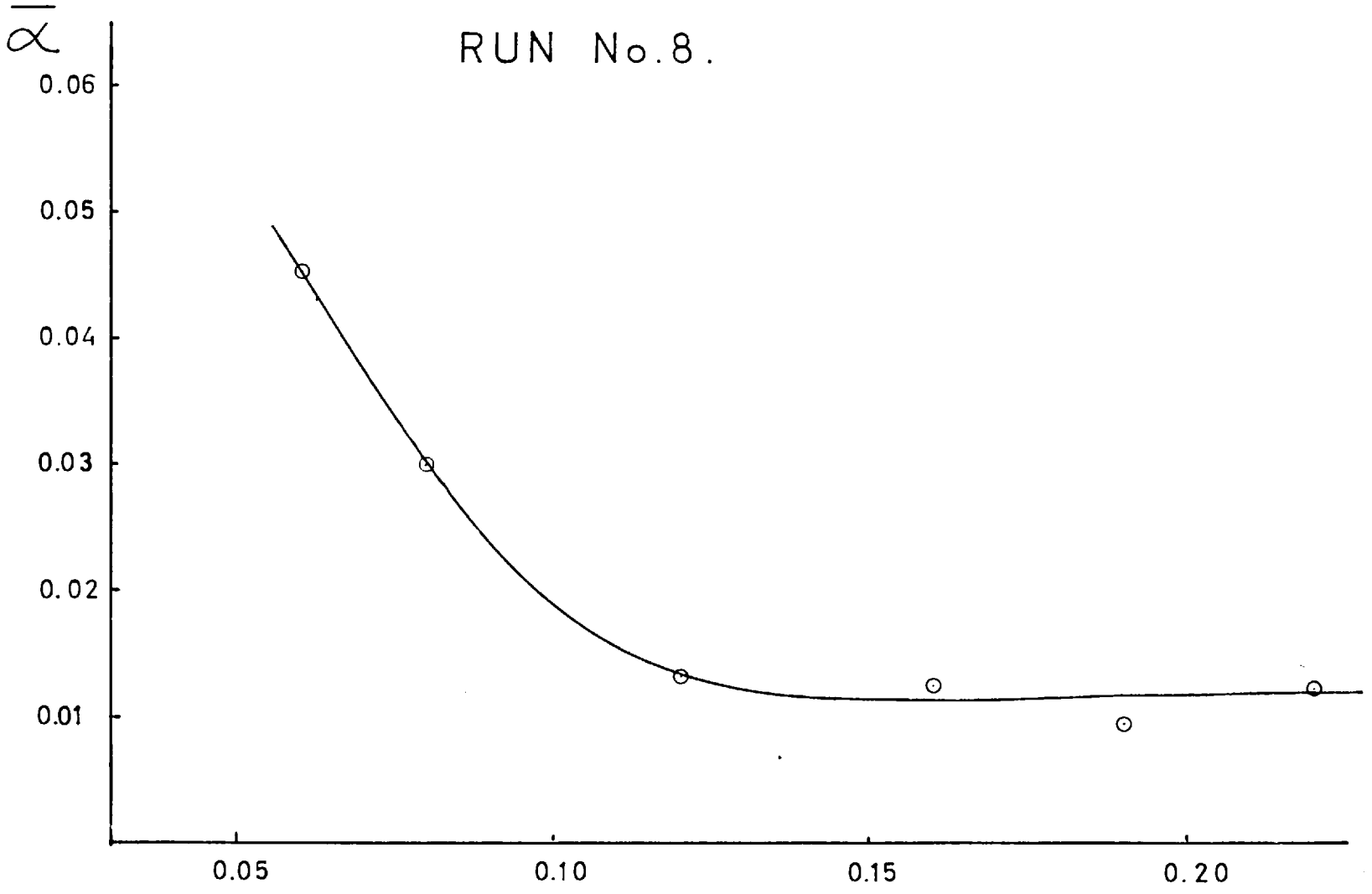

FIG. No. A.4.6. WATER CONDENSATION.

RUN No.11.

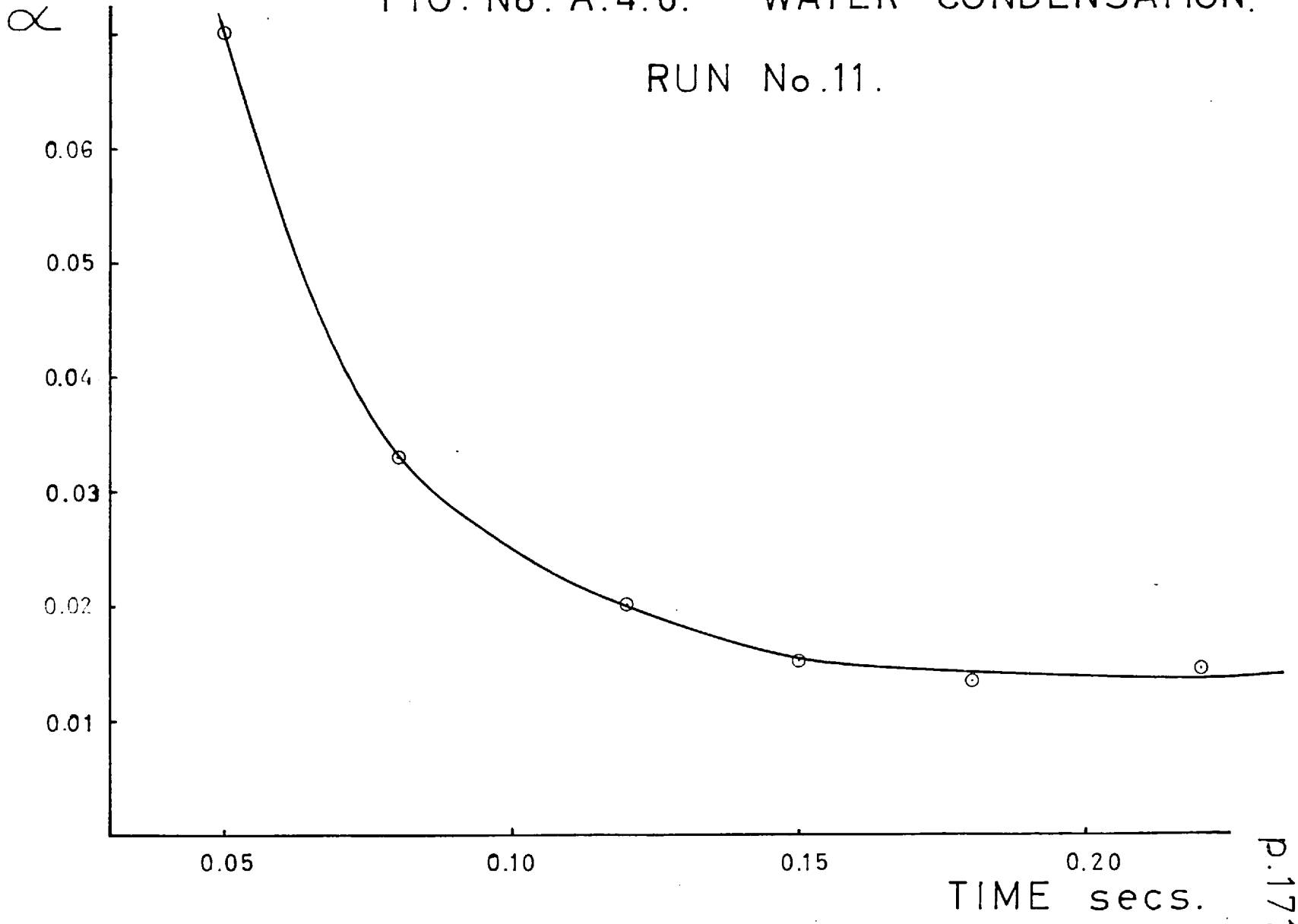

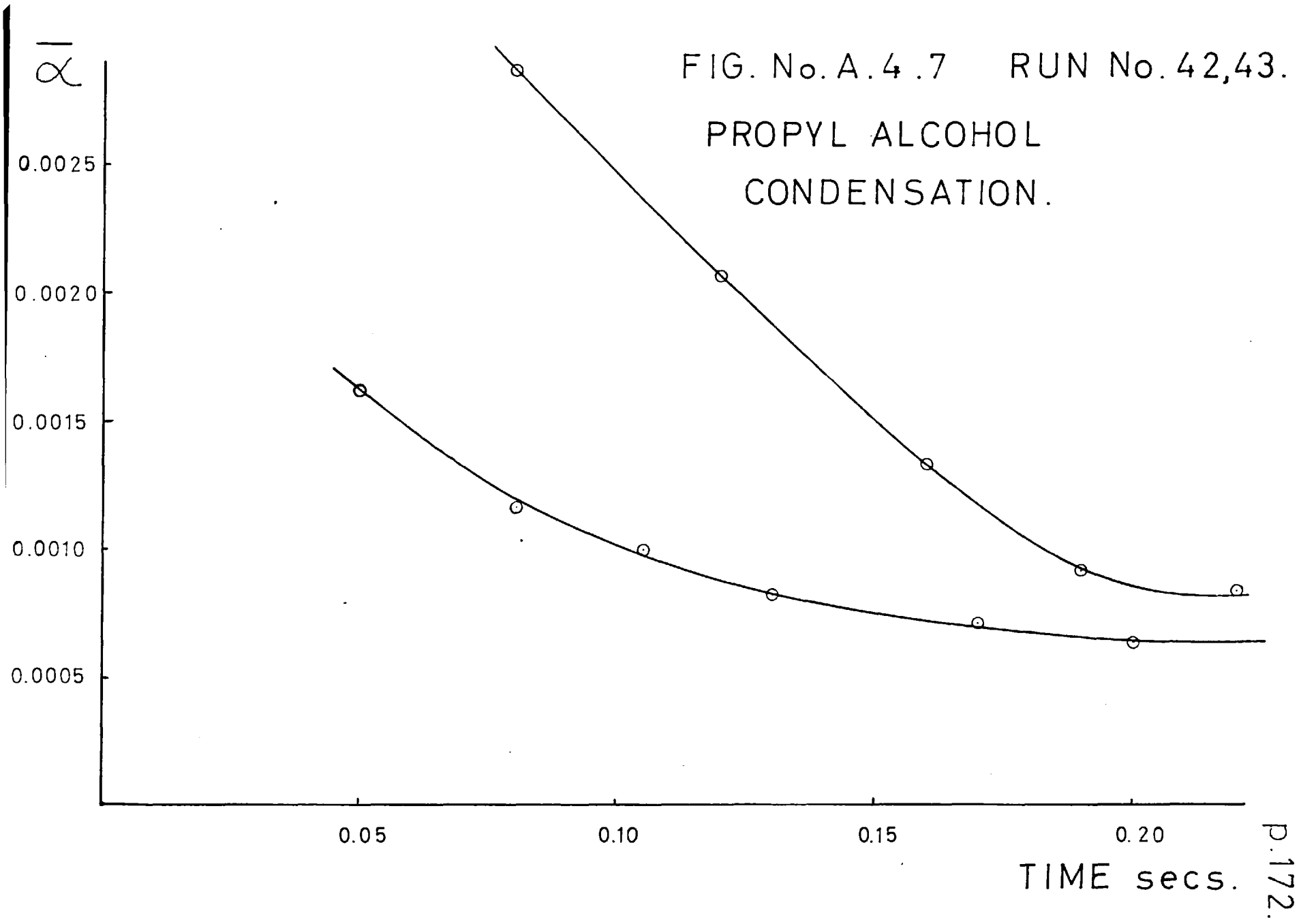

FIG. No. A.4.7 RUN No. 42,43.

PROPYL ALCOHOL

CONDENSATION.

FIG. No.A.4.8. PROPYL ALCOHOL EVAPORATION.

RUN Nos. 44 and 46.

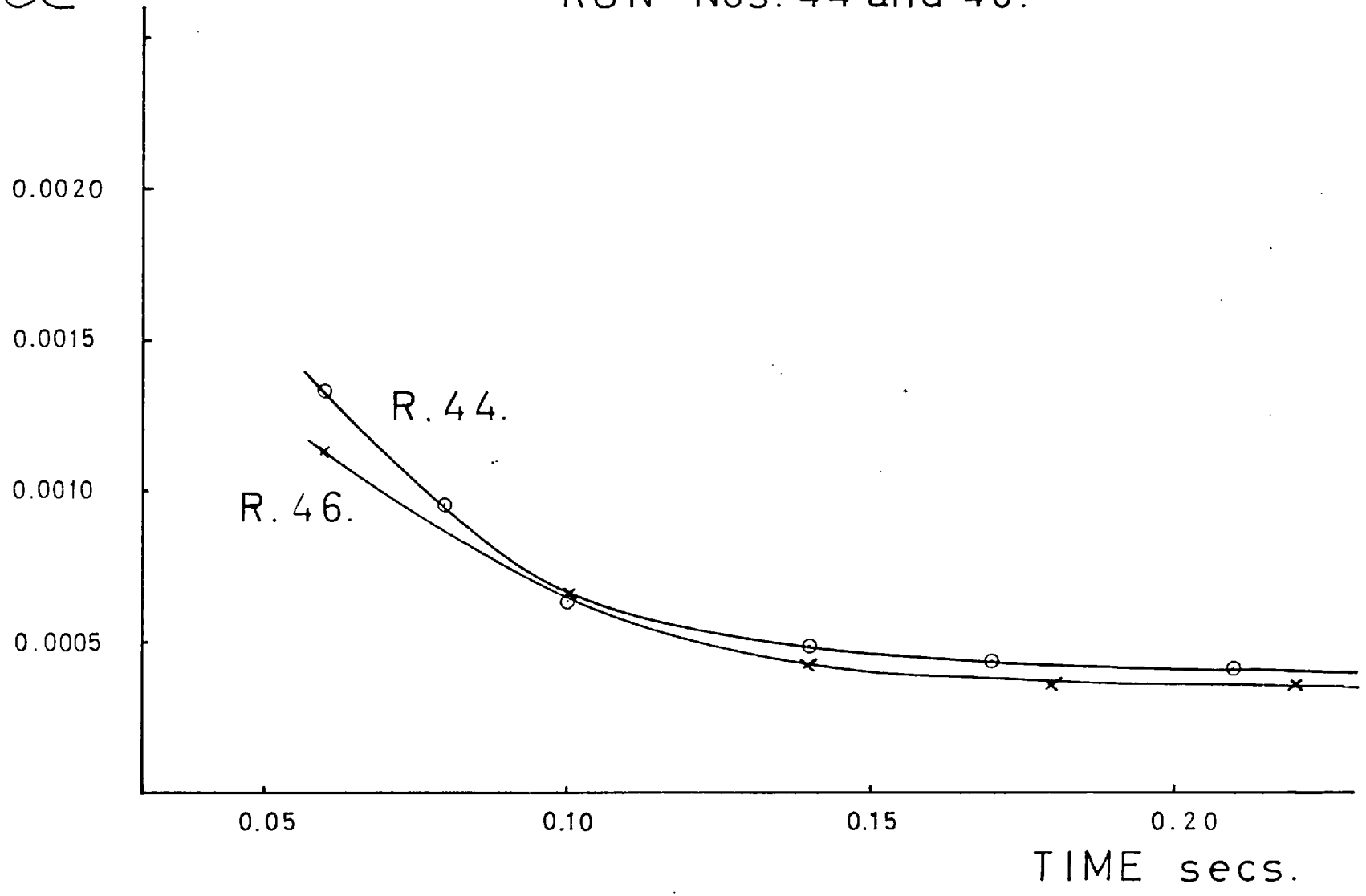

FIG. No. A. 4.9. CONDENSATION ONTO NORMAL NaCl SOLUTION RUN No. 47.

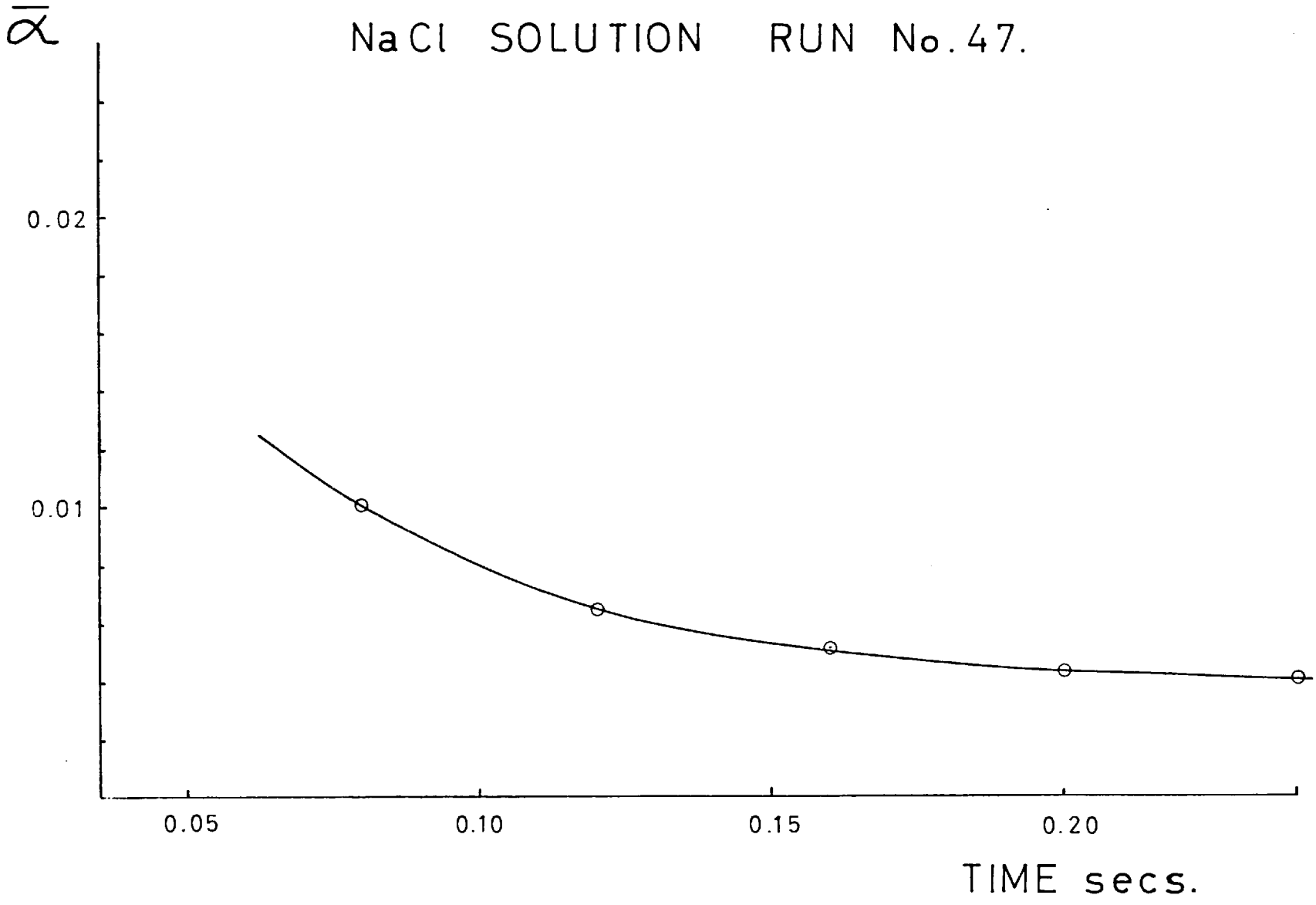

FIG. No. A. 4.10. EVAPORATION FROM NORMAL SODIUM CHLORIDE SOLN.

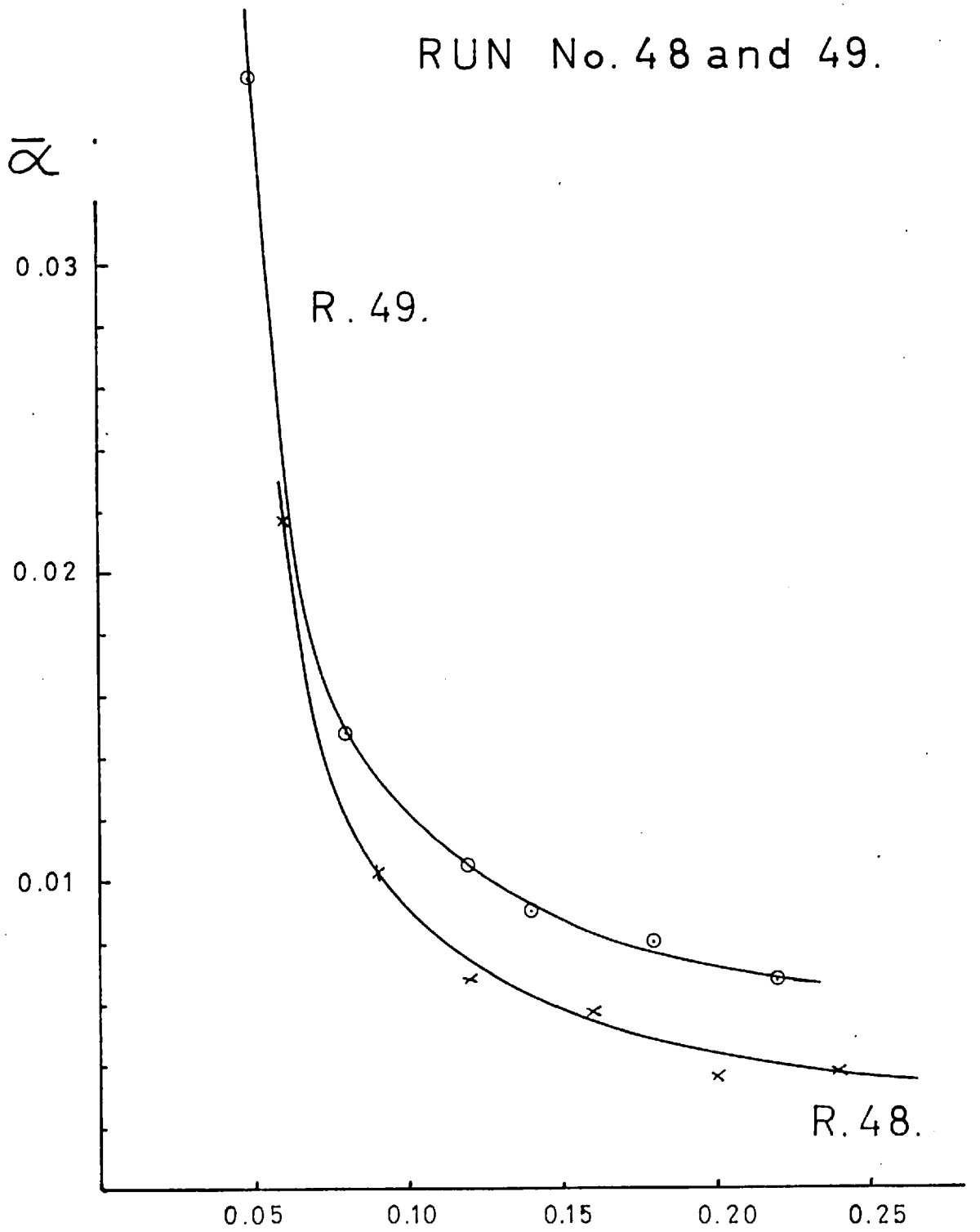

FIG. No. A. 4.11. CONDENSATION ONTO WATER PLUS SURFACTIVE AGENT RUN No. 52 and 53.

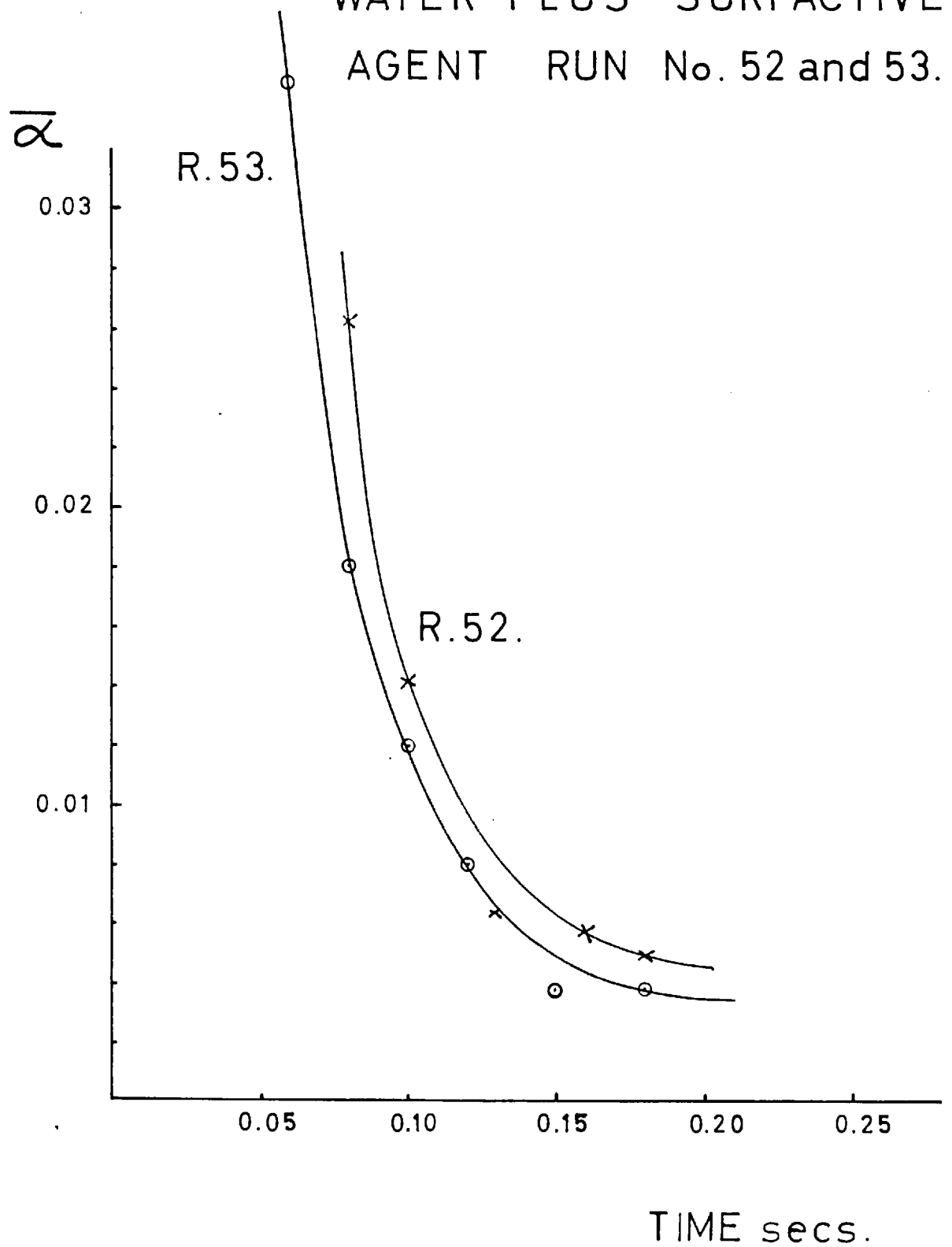

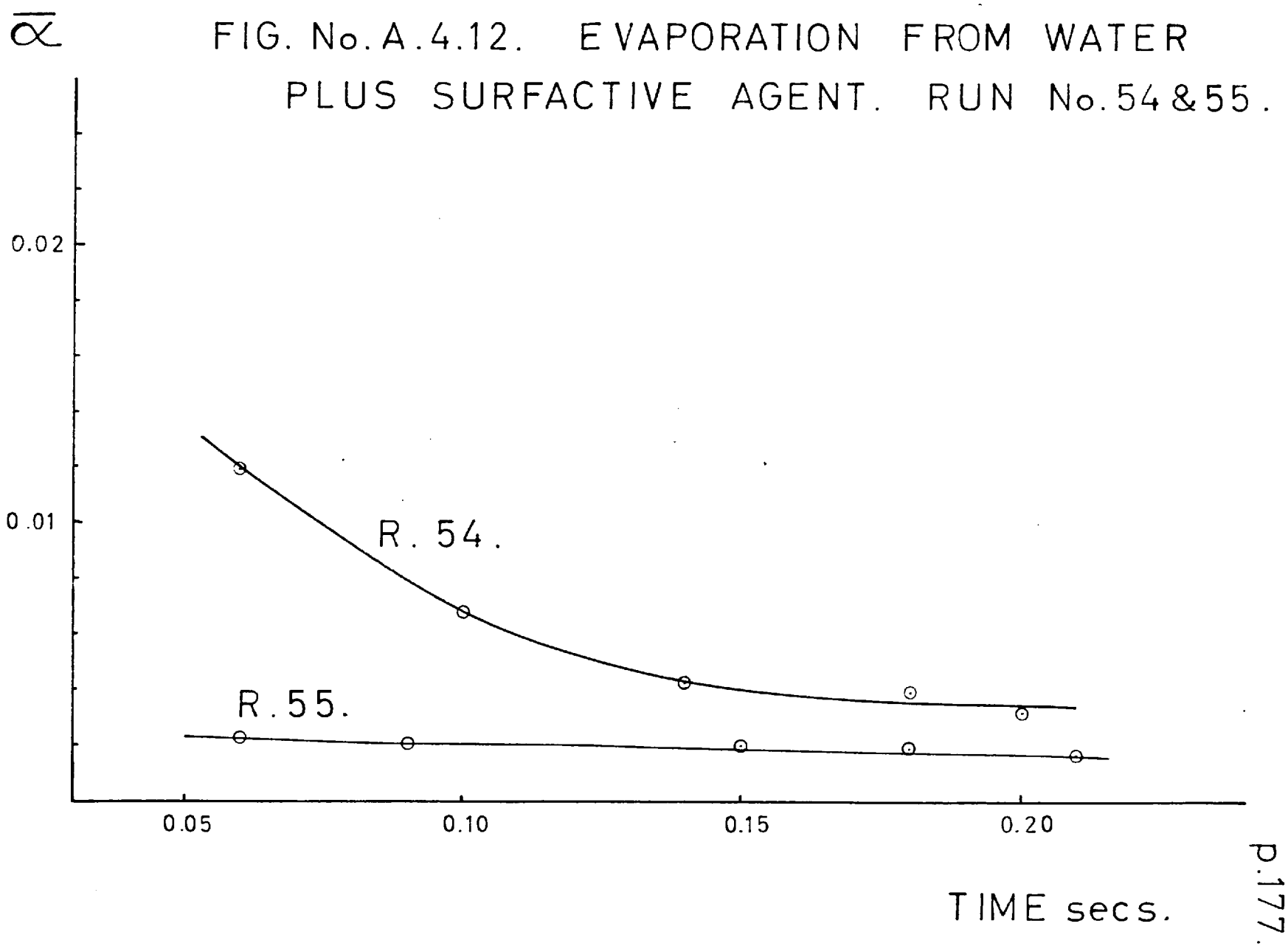
$\overline{\alpha}$
FIG. No. A. 4.12. EVAPORATION FROM WATER PLUS SURFACTIVE AGENT. RUN No. 54 & 55.
0.02
0.01
R. 54.
R. 55.
0.05
0.10
0.15
0.20
TIME secs.

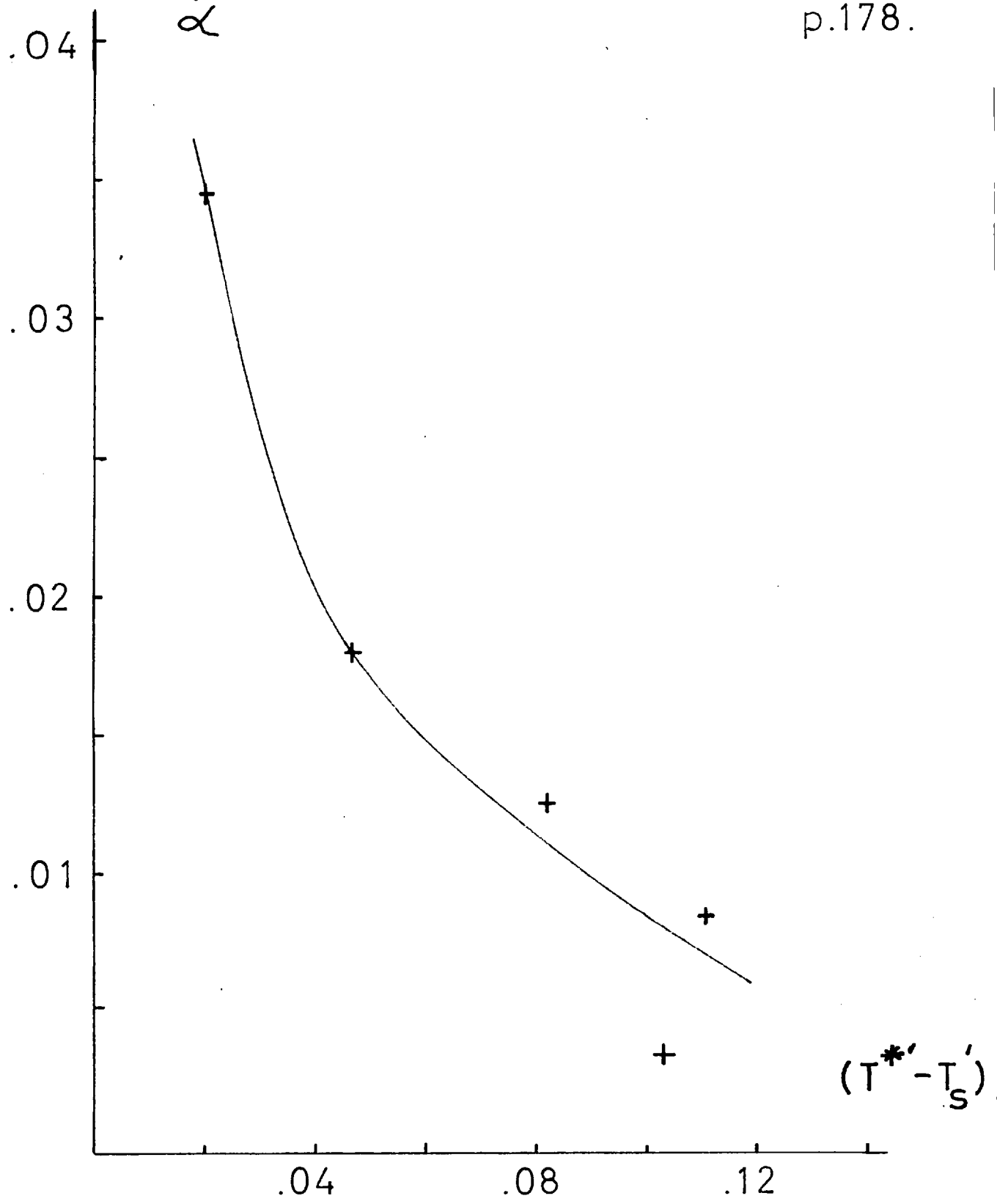

FIG. No. A. 4.13. RUN No. 5. WATER CONDENSATION.

FIG. No. A. 4.14. RUN No. 11.

WATER CONDENSATION.

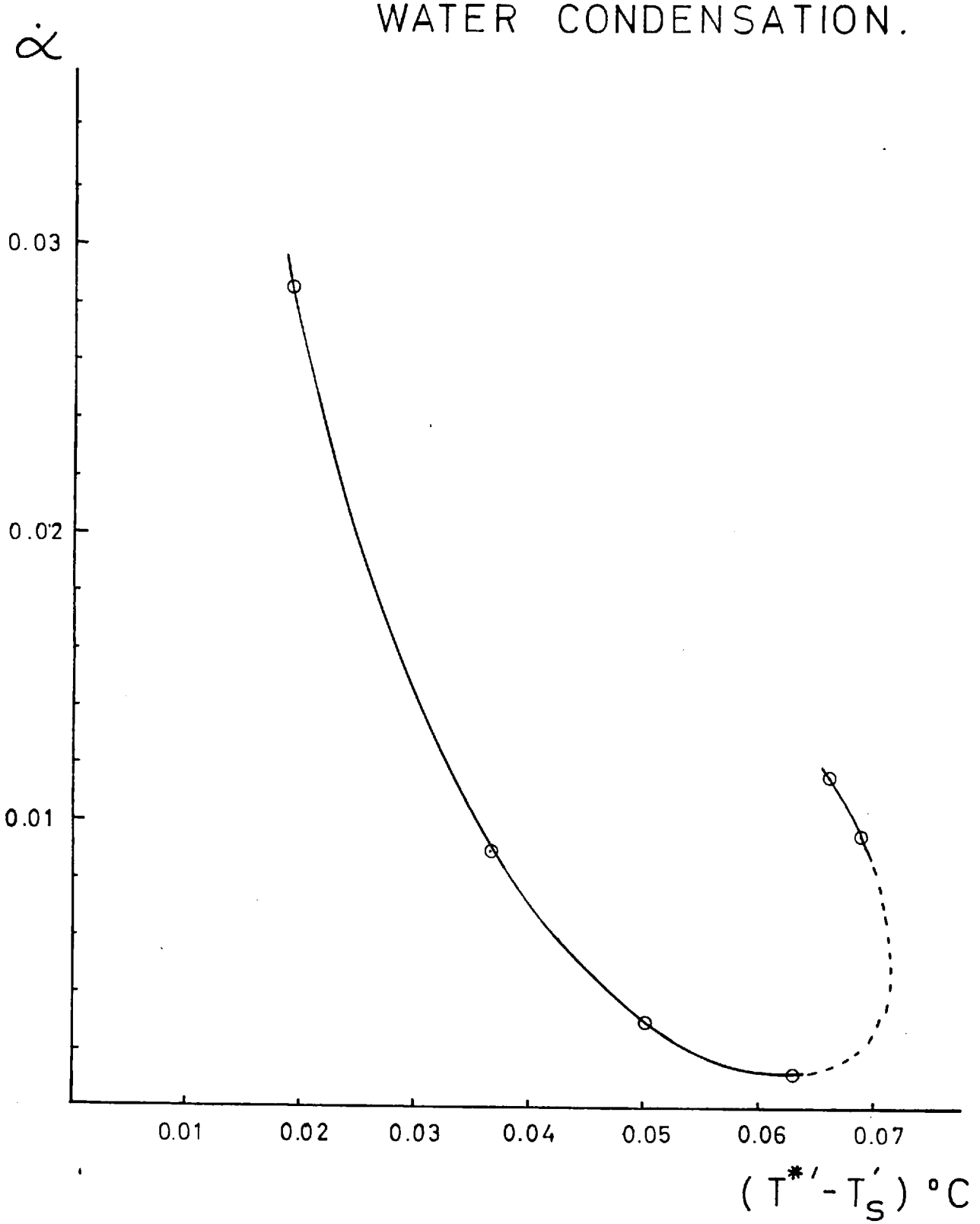

A.5. Bibliography.

1. ALTY. T. Phil. Mag. 15, (1933), 82.
Proc. Roy. Soc. A131, (1931), 554.
Proc. Roy. Soc. A149, (1935), 104.
2. ANGUS. S. Private communication, Imperial College Chemical Engineering Dept..
3. ASHKENAS. California Inst. Tech. Ph.D. Thesis (1949).
4. ASHKENAS and BRYSON. Jnl. Aero. Sci. 18, (1951), 82.

5. BAER and MACKELVEY. A.I.Ch.E.Jnl. 4, (1958), 218.
6. BAILEY, BARRY and De FRATE. Meteor Report No.51. M.I.T.
7. BARANEAV. J. Phys. Chem. USSR 13, (1939), 1635.
8. BINNERSLEY. Univ. of Leeds Ph.D. Thesis (1961).
9. BOGDANDY*KLEIST and KNACKE. Z. Electrochem. 59, (1955), 460.
10. BRUCE, MACINANTE and KELLY. Aust. Jnl. Appl. Sci. 4, (1953), 28.
11. BUCKA. H. Z. Phys. Chem. 195, (1950), 260.

12. CARSLAW and JAEGAR. 'Conduction of Heat in Solids' Clarendon Press. (1959).
13. COURTENEY. Jnl. American. Rocket Soc. (1961), 751.
14. CREDE. C.E. 'Vibration and Shock Isolation' Chapman and Hall. (1951).

15. DAVIS and RIDEAL. 'Interfacial Phenomena' Academic Press. (1961)
16. DELANEY L.J. Univ. of Pensylvannia Ph.D. Thesis (1961).
17. DEVER, et al. J. Phy. Chem. 59, (1955), 668.

18. EAST and KHAN. Jnl. Sci. Inst. 23, (1946), 185
19. EBERT. Weid. Ann. 36, (1889), 466.
20. ECKERT, DRAKE and SOCHNGEN. USAF Report No.TR5721 (1948).
21. EYRING and KINCARD. J. Chem. Phys. 6, (1938) 620.

22. FOX and WEINBERG. Proc. Roy. Soc. A268, (1962), 222
23. PRESNELL. Oevnes Tom.i. 330.

24. GLASSTONE. S. Textbook of Phys. Chem. 623.
25. GOLTZ and SAWISTOWSKI. Imp.Coll.Chem.Eng. Jnl. 12, (1958),40.

26. HALL. J.G. Univ. of Toronto Inst. of Aerophysics. Report No. 27 (1954).
27. HAMMEKE and KAPPLER. Z. Geophysik (Sonderband) (1953), 181.
28. Den HARTAG. 'Mechanical Vibrations' McGraw Hill (1956).
29. HARVEY. E.A. Univ of London Ph.D. Thesis (1958)
30. HAWARD. R.N. Trans. Far. Soc. 35, (1939), 1401.
31. HEIDGER and BOUDART. Chem. Eng. Sci, 17, (1962), 1.
32. HEIDINGER. W.J. Univ. of Princeton Ph.D. Thesis (1958).
33. HERTZ. H. Ann. Phys(Leipzig). 17, (1882), 177
34. HICKMAN. Ind. Eng. Chem. 46, (1954), 1442.
35. HICKMAN and TREVOY. Ind. Eng. Chem, 44, (1952), 1882.
36. HOLDER and NORTH. Agardograph 23. NATO ARDC. (1956).
37. HOWES and BUCHELE. NACA TN. 3507, (1955).

38. INTERNATIONAL CRITICAL TABLES. Vols. 3 and 7.

39. JAMIN. Ann. Chem. Phys. 52, (1958).
40. JARVIS. Jnl. of Colloid Science 17, (1962), 512.
41. JARVIS and KAGARISE. Jnl. of Colloid Science 17, (1962), 501.

42. KAUFMANN. Amer. Chem. Soc. Monograph No.145 (1960).
43. KINDER. Optik l.b., (1946).
44. KNACKE and STRANSKI. Prog. Metal Physics. 6, (1956), 181.
45. KNUDSEN. M. Ann. Phys.(Leipzig) 47, (1915), 697.
46. KRAMERS and STEMERDING. Appl. Sci. Res. 3A, (1953), 73.

47. LEE. J.D. Univ of Toronto Inst. of Aerophysics Report No. 20 (1952).

48. LINTON and SUTHERLAND. Aust. Jnl. Appl. Sci. 9, (1958), 18.

49. LLOYDS. Trans Roy. Irish Acad. 17, (1834).

50. McARTHUR and DURHAM. Proc 2nd. Int. Conf. Surf. Activity 1, (1957), 259.

51. McGREGOR. R.R. 'Silicones and their uses.' McGraw Hill (1954).

52. McINANTE. Nat. Standards Lab. of Aust. Report No.10. (1958).

53. MACH. L. Weiner Bericht 101, (1892), 5.
102, (1893), 1035.

54. MATTHEWS. J.H. Private communication, Imperial College Chemical Eng. Dept..

55. MARKSTEIN. G.H. 6th Int. Combustion Symp. (1957), 387.

56. MARTIN and WHITE. 7th Int. Combustion Symp. (1958), 865.

57. MICHELSON. Amer. Jnl. Sci, 22, (1881), 120.

58. MICKLEY, SHERWOOD and REED. 'Appl. Mathematics in Chemical Engineering'.

59. OLSEN. H.F. Jnl. Accoustical Soc. America 19, (1947), 307.

60. PRUGER. W. Z. Phys. 115, (1940), 202.

61. RAITC COMPANY of AMERICA. Mechano-electrical transducer No. 5734.

62. RAOULT. Compt. Rend. 103, (1886), 1125.

63. RAYLEIGH. Proc. Roy. Soc. 59, (1896), 201.

64. RIDEAL and WIGGINS. Proc. Roy. Soc. 210A, (1952), 291.

65. RIDEAL and LITTLEWOOD. Trans. Far. Soc. 52, (1956), 1598.

66. SANCIER and RICHESON. Rev. Sci. Insts. 27, (1956), 133.

67. SCHULTZ, GRUNOW and WORTENBURG. Int. Jnl. of Heat and Mass Trans. 2, (1961), 56.

68. SCHRAGE. 'Interphase mass transfer', Univ. Of Columbia (1953).

69. STEVER. Fundamentals of gas dynamics 3, (1958), 526.
70. SVENSSON. Acta. Chem. Scand. 3, (1949), 1170.

71. TANNER. L.H. Aero. Res. Council No. FM 2463 (1956).
72. TANNER. L.H. ibid. FM 2589 (1957).
73. TIMMERMANN. 'Physico-chemical constants of organic compounds.
74. TREVOY. Ind. Eng. Chem. 45, (1953), 2366.
75. TSCHUDIN. Helv. Phys. Acta. 19, (1946), 91.

76. VENKATARMAN. Proc. Ind. Acad. Sci. 10A, (1939) 121.
77. VOLMER and ESTERMANN. Z. Phys. 7, (1921), 1.

78. WASASTJERNA. J.A. Acta. Soc. Sci. Fennicae 50, (1920), 1.
79. WEINBERG and WOOD. Jnl. Sci. Inst. 36, (1959), 227.
80. WEINBERG. 'Optics of Flames'. Butterworths. (1963).
81. WESSEL. G. Z. Phys. 130, (1951), 539.
82. WILSON. Rev. Sci. Insts. 12, (1941), 91.
83. WINKLER. US Naval Lab. Report No. 1077. (1947).
84. WYLLIE. G. Proc. Roy. Soc. A197, (1949), 383.

85. YOUNG. Phil. Trans (1804), 8.

86. ZEHNDER. Zeitschrift fur Instrumenten Kinde 11, (1891), 275.
87. ZOBEL, NACA TN 1184, (1947).

88. PAUL. B. Amer. Rocket Soc. Jnl. (1962), 1321.

APPENDIX 6.

COST OF INTERFEROMETER

ITEM	£
Optical plates	430
Complete mirror mounts	300
Framework and suspension	150
Schlieren mirror and mount	90
Camera and accessories	130
Optical benches, light sources and lenses	100
Traversing mechanism	50
Miscellaneous	50
	£ 1300

Each item includes workshop costs where applicable.

APPENDIX 7.

MATERIALS LIST DRAWING NO. 2.

Item	Description	Material	No. Off
A	Adjustable flat holder	E.M.S.	1
B	Fixed flat holder	E.M.S.	1
C	O - rings	Neoprene	
D	Diaphragm plate.	E.M.S.	1
E	P.T.F.E. Bellows.	P.T.F.E.	1
F	Upper split flange.	Al	1
G	Lower split flange.	Al	1
H	Bellows cover.	M.S.	1
J	Bellows top hat.	E.M.S.	1
K	Securing ring.	Al	1
L	Probe.	E.M.S.	1
M	Blank.	Distrene	1
N	Shaft.	E.M.S.	1
P	Probe cap.	Distrene.	1
Q	Lower cover plate.	Brass	1
R	Neoprene sealing ring.	Neoprene	1
S	Guard ring.	Brass	1
T	Plug.	Distrene	1
U	Tension spring.	Steel	1
V	Compression spring.	Steel	1
W	Diaphragm.	Mo - Cu	1

Thermocouple glands	2	PP51B1	DOWTY Seals.
Fixed flat	1	PP52B1	
Adjustable flat	1	PP52B1	
Flange seals	2	PP52C21	
PTFE Bellows	1	PP52B28	
Diaphragm plate	2	PP52B24	
Vacuum connections	3	PP51B5	

Bellows cover	1	PP49B43
Adjustable flat - balancing cell	1	PP51B30

RINGS MACHINED FROM

GUN METAL CASTINGS.

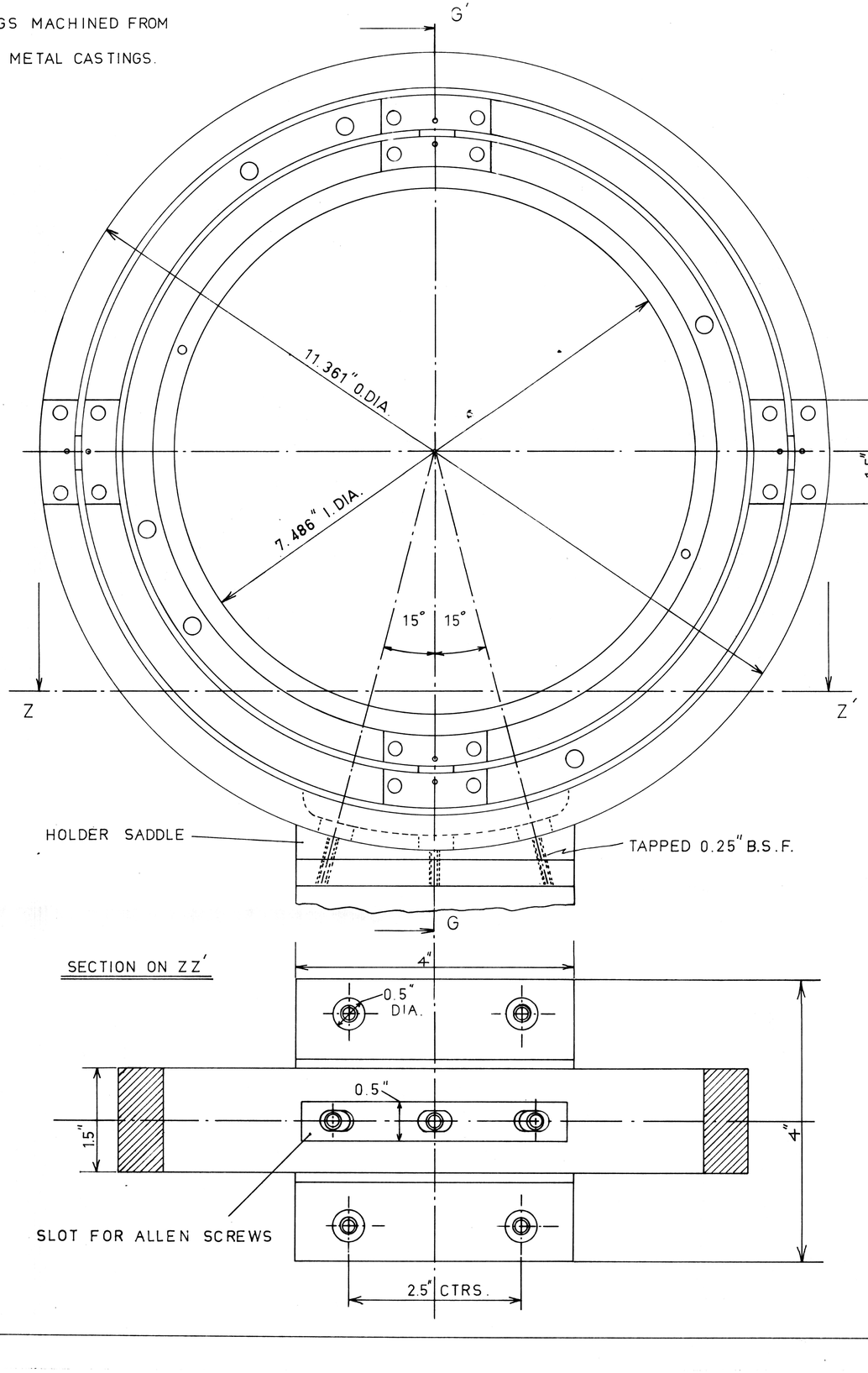

SECTION ON ZZ'

SECTION ON GG'

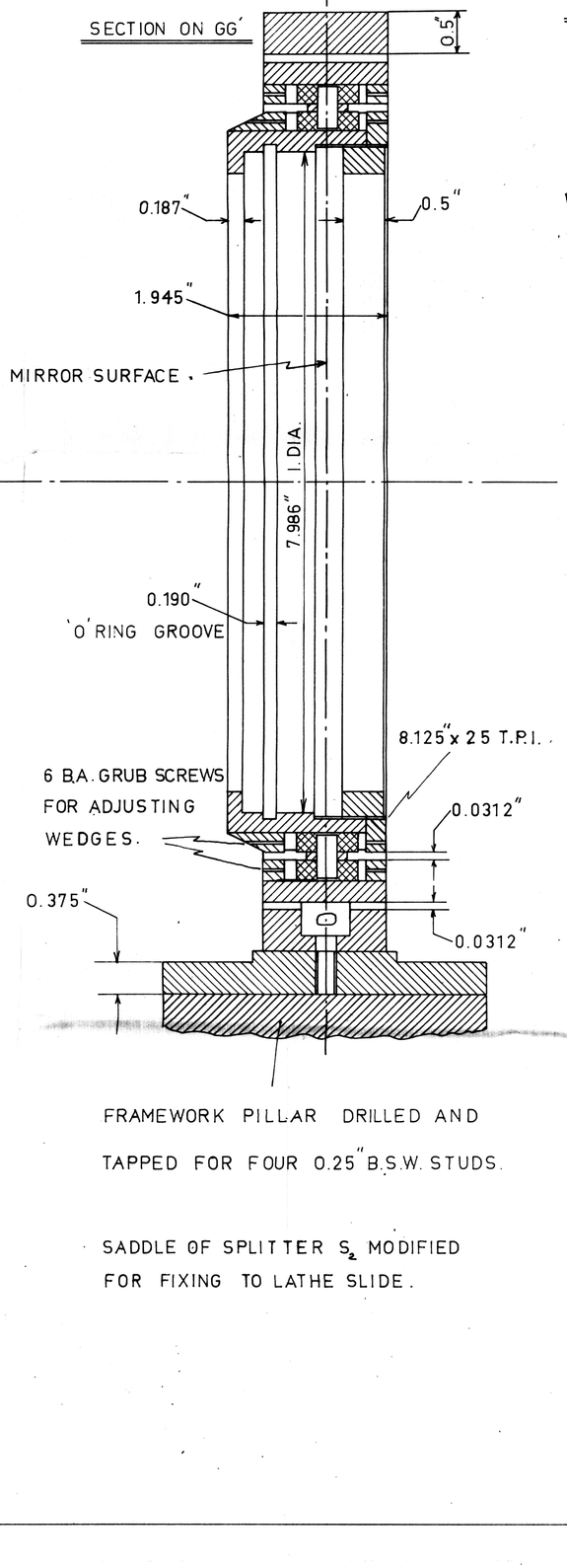

FRAMEWORK PILLAR DRILLED AND TAPPED FOR FOUR 0.25" B.S.W. STUDS.

SADDLE OF SPLITTER S_2 MODIFIED FOR FIXING TO LATHE SLIDE.

BEARING DETAIL

3 x Full Size.

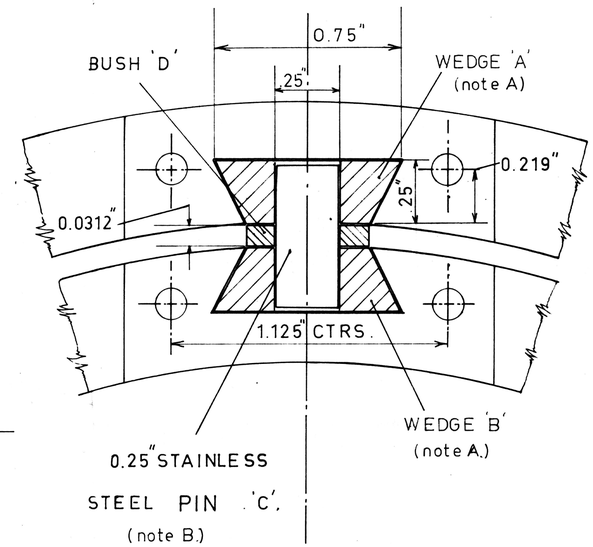

NOTE 'A' WEDGES TO BE SLIDING FIT IN RINGS.

NOTE B PHOSPHOR BRONZE BUSH 'D' TO BE RUNNING FIT ON GYMBAL PIN C.

IMPERIAL COLLEGE
CHEMICAL ENGINEERING DEPARTMENT.

Title:
INTEFEROMETER PLATE HOLDER.

Drawn by:
R.K.M. JOHNSTONE.
12.5.63.

Scale: FULL SIZE.

Drawing No. 1

SECTION ON CC'

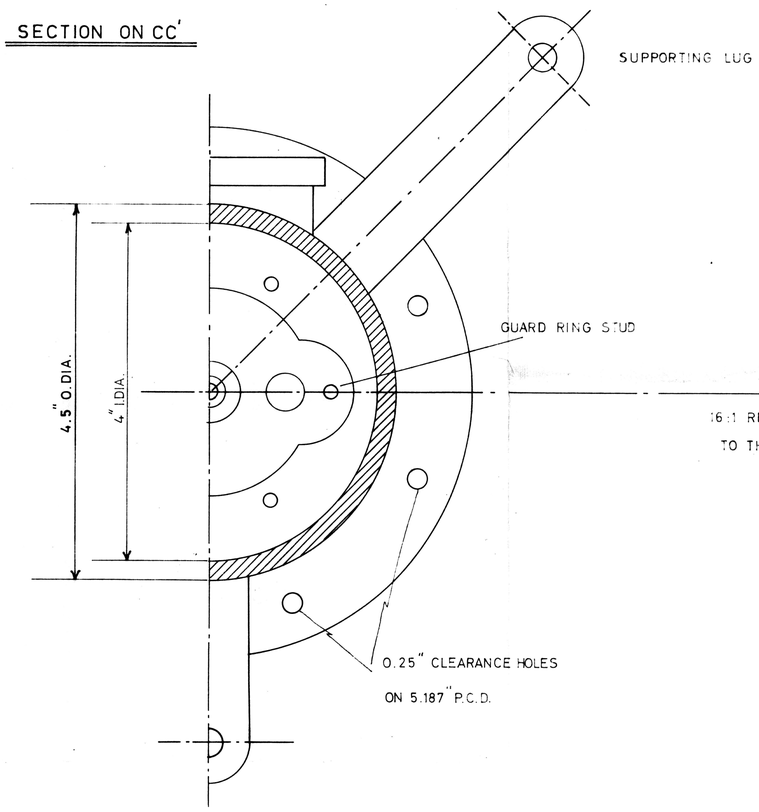

SECTION ON ZZ'

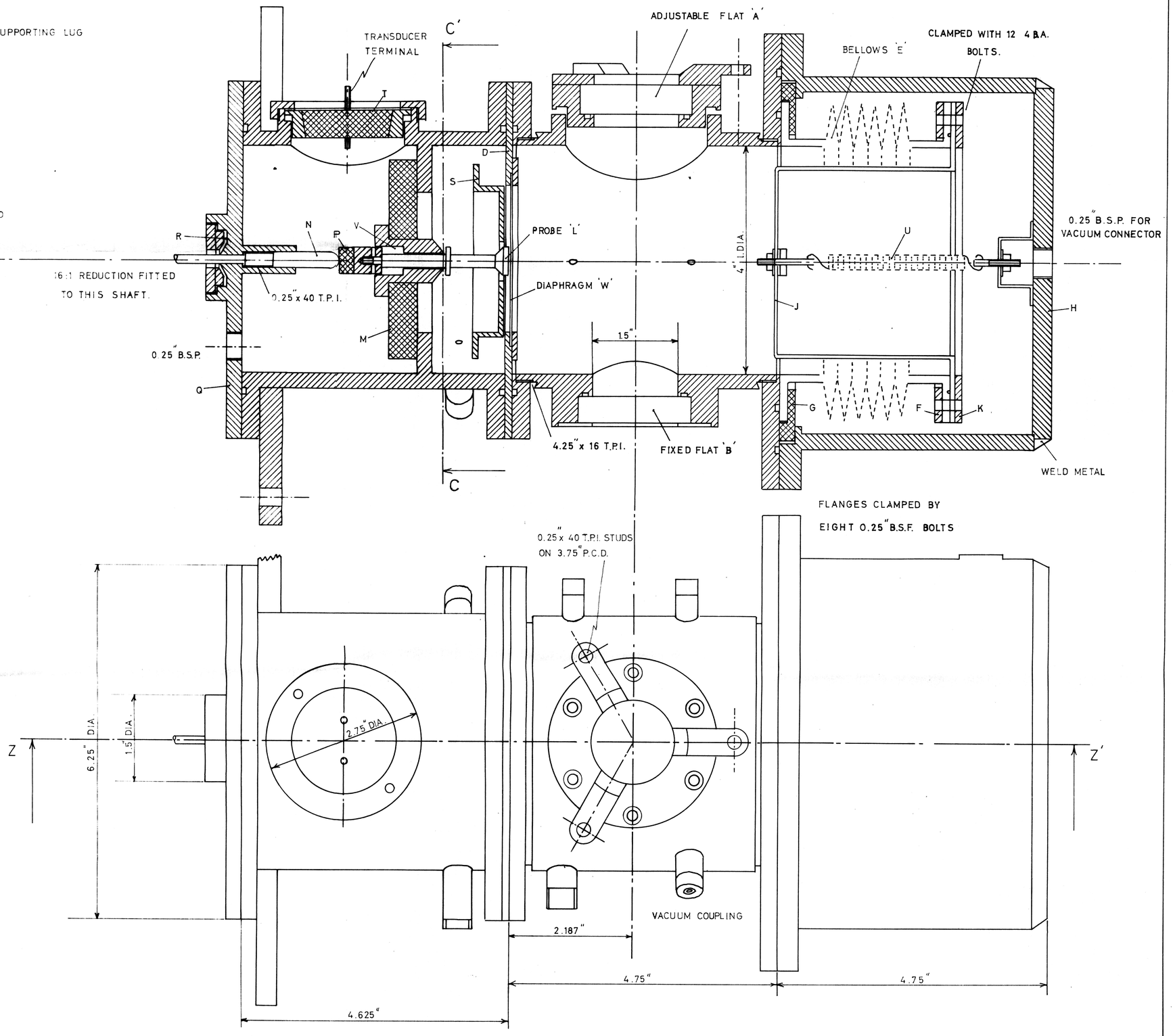

Note A. MATERIALS ON ATTACHED SHEET. A.7.

Note B. O-RINGS NOT SHOWN POSITION. DOWTY REFERENCE NUMBERS GIVEN IN TEXT.

IMPERIAL COLLEGE CHEMICAL ENGINEERING DEPARTMENT	
Title:	CELL ASSEMBLY.
Drawn by:	R.K.M. JOHNSTONE. 12.5.63.
Scale:	FULL SIZE.
Drawing No:	2.